Master of Science in
Electronics and Telecommunication Engineering

Machine Learning Assisted Beam-Steering Microstrip Patch Array Antenna Design

by

Md. Farhad Hossain

ID: 19METE025P

This thesis is submitted in partial fulfillment of the requirement for the degree of MASTER OF SCIENCE IN ELECTRONICS AND TELECOMMUNICATION ENGINEERING

Department of Electronics and Telecommunication Engineering

Chittagong University of Engineering and Technology

Chattogram-4349, Bangladesh.

December, 2024

CERTIFICATION

The thesis titled **Machine Learning Assisted Beam-Steering Microstrip Patch Array Antenna Design** submitted by **Md. Farhad Hossain**, Roll No. **19METE025P**, Session **2019-2020** has been accepted as satisfactory in partial fulfillment of the requirement for the degree of **Master of Science in Electronics and Telecommunication Engineering** on **19/12/2024**.

BOARD OF EXAMINERS

1. ______________________________

Dr. Md. Azad Hossain — Chairman (Supervisor)
Professor & Head
Department of Electronics and Telecommunication Engineering
Chittagong University of Engineering & Technology (CUET)
Chittagong-4349

2. ______________________________

Dr. Md. Jahedul Islam — Member
Professor
Department of Electronics and Telecommunication Engineering
Chittagong University of Engineering & Technology (CUET)
Chittagong-4349

3. ______________________________

Dr. Md. Saiful Islam — Member
Associate Professor
Department of Electronics and Telecommunication Engineering
Chittagong University of Engineering & Technology (CUET)
Chittagong-4349

4. ______________________________

Dr. Md. Kamal Hosain — Member (External)
Professor
Department of Electronics & Telecommunication Engineering
Rajshahi University of Engineering & Technology (RUET)
Rajshahi-6204

Author Declaration for Electronic Submission of MRP

I hereby declare that I am the sole author of the MRP. This is a true copy of the MRP, including any final revisions, as accepted by my Examiners.

I hereby also declare that the work contained in this Thesis could be uploaded to the repository of the library, Chittagong University of Engineering and Technology, after 1 year of submission.

I authorize Chittagong University of Engineering and Technology to lend this MRP to other institutions or individuals for the purpose of scholarly research.

I further authorize the Chittagong University of Engineering and Technology to reproduce this MRP by photocopying or by other means, in total or part, at the request of other institutions or individuals for the purpose of scholarly research.

I understand that my MRP may be made electronically available to the public.

Signature of the Candidate

Md. Farhad Hossain
ID: 19METE025P

CANDIDATE'S DECLARATION

It is hereby declared that this thesis or any part of it has not been submitted elsewhere for the award of any degree or diploma.

Signature of the Candidate

Md. Farhad Hossain
ID: 19METE025P

APPROVAL by the SUPERVISOR

This is to certify that MD. FARHAD HOSSAIN has carried out this research work under my supervision and has fulfilled the relevant Academic Ordinance of the Chittagong University of Engineering and Technology so that he is qualified to submit the following Thesis in the application for the degree of MASTER of SCIENCE in ELECTRONICS AND TELECOMMUNICATION ENGINEERING. Furthermore, the Thesis compiles with the PLAGIARISM and ACADEMIC INTEGRITY regulations of CUET.

Signature of the Supervisor

Dr. Md. Azad Hossain
Professor & Head
Department of Electronics and Telecommunication Engineering
Chittagong University of Engineering and Technology
Chittagong-4349

List of Publications

The following publication is a direct consequence of the research carried out during the elaboration of the thesis and gives an idea of the progression that has been achieved.

Journal Articles

1. **Hossain, M. F.**, Das, D., & Hossain, M. A. (2024). A 5G beam-steering microstrip array antenna using both-sided microwave integrated circuit technology. International Journal of Electrical and Computer Engineering (IJECE), 14(1), 457-468.

Conference Procedings

1. **Hossain, M. F.**, Das, D., Sultana, F., Istiaque, A. & Hossain, M. A. (2025, February). Performance Analysis of Machine Learning Models for Predicting Return Loss in 5G Microstrip Patch Array Antenna Design. In 2025 international conference on electrical, computer and communication engineering (ECCE) (pp. 1-6). IEEE.

Dedication

I dedicate this thesis to my beloved son Mohammad Faraz, my supportive wife, and my cherished family—my father, mother, and sister—whose unwavering love, encouragement, and sacrifices have been my greatest strength throughout this journey.

Acknowledgment

I am profoundly grateful to Almighty Allah for granting me strength, guidance, and countless blessings throughout my academic journey. Without His mercy and grace, this achievement would not have been possible.

I extend my heartfelt gratitude to my supervisor, **Dr. Md. Azad Hossain**, Professor and Head of the ETE Department at CUET, for his invaluable mentorship, constant encouragement, and expert guidance. His unwavering support and insightful advice have been instrumental in shaping this research and in motivating my academic growth.

I am profoundly thankful to my wife, Fahin Sultana, a dedicated faculty member of the ETE Department, whose love, understanding, and encouragement have been the bedrock of my achievements. Her unwavering support and boundless patience have been a constant source of inspiration and strength throughout this journey.

My heartfelt gratitude extends to my dear friend, Debprosad Das, for his invaluable assistance, encouragement, and collaborative spirit. His companionship has not only lightened the challenges of this journey but has also enriched it with memorable and meaningful moments.

I am equally grateful to my friends, colleagues, and the esteemed faculty members of the ETE Department. Their willingness to share knowledge and their camaraderie have created an inspiring and dynamic environment that has greatly contributed to my personal and academic growth.

Finally, I would like to express my deepest appreciation to my beloved family. Their unconditional love, unwavering support, and countless sacrifices have been the cornerstone of my success. Their belief in me has been a driving force behind every milestone I have achieved.

Abstract

The rapid evolution of wireless communication technologies, notably the transition from 4G to 5G, has driven the need for advanced antenna systems to meet growing demands for seamless connectivity and enhanced performance. This thesis focuses on designing and optimizing beam-steering microstrip patch antennas for 5G communication, with specific emphasis on the sub-6 GHz frequency band and millimeter-wave applications. A comprehensive methodology is presented, integrating traditional antenna design principles with machine learning-based predictive modeling and optimization techniques. The initial phases of the research involve designing a 2×2 microstrip array antenna, simulated for beam-steering applications at 3.5 GHz. A dataset is curated through parametric studies, and eight machine learning models, including Random Forest, Decision Tree Regression, XGBoost, and Gaussian Process Regression, have been trained to predict antenna performance metrics such as return loss (S_{11}) and bandwidth. Among these, Decision Tree Regression emerged as the best overall performer, offering the most accurate predictions, while Random Forest also demonstrated close alignment with the actual values. Optimization strategies refined the antenna design by combining machine learning predictions with advanced algorithms like L-BFGS-B, Genetic Algorithms, and Simulated Annealing. The optimized S_{11} parameter improved significantly, reaching at -51.41 dB compared to the initial -45.21 dB, indicating the superior impedance matching at 3.5 GHz. Similarly, the optimized S_{22} value reduced to -53.09 dB from -49.57 dB, further enhancing performance. The gain of the antenna increased from 12.82 dBi to 13.58 dBi, and the directivity improved from 12.89 dBi to 13.69 dBi, demonstrating substantial performance enhancements. Port isolation has been maintained with S_{12} and S_{21} values below -10 dB. Additionally, the array antenna achieved a beam switching capacity ranging from $-17°$ to $+17°$, making it highly effective for beam-steering applications. This research contributes to the field by showcasing the potential of machine learning-assisted antenna design and optimization, addressing challenges such as computational complexity and design accuracy. The findings hold promise for 5G networks and satellite communications applications, paving the way for more efficient and reliable antenna systems.

Keywords: Array antenna, Beam switching, Beam-steering antenna, Both-sided MIC, Machine learning, Antenna Optimization, Decision Tree Regression (DTR), Random Forest Regression (RF).

Contents

List of Figures

List of Tables

List of Abbreviations

BW	Bandwidth
DTR	Decision Tree Regression
EMF	Electromagnetic Field
EMW	Electromagnetic Wave
FDTD	Finite Difference Time Domain
GA	Genetic Algorithm
GD	Gradient Descent
GPR	Gaussian Process Regression
L-BFGS-B	Limited-memory Broyden-Fletcher-Goldfarb-Shanno with Box constraints
MIC	Microwave Integrated Circuit
MIMO	Multiple Input Multiple Output
ML	Machine Learning
RF	Random Forest Regression
S_{11}	Return Loss
S_{12}	Port Isolation
S_{21}	Port Isolation (Reverse)
S_{22}	Input Reflection Coefficient
SA	Simulated Annealing
SLL	Side Lobe Level
SLSQP	Sequential Least Squares Quadratic Programming
UAV	Unmanned Aerial Vehicle
Wi-Fi	Wireless Fidelity

WLAN	Wireless Local Area Network
X-POL	Cross Polarization
XGBoost	Extreme Gradient Boosting

Chapter 1

Introduction

1.1 Introduction

In the modern technological world, beam steering antennas are highly sought-after antennas when a communication link must be formed between end users who are not aligned. Also, a beam steering antenna technology is needed for five-generation (5G) mobile connectivity, as well as other communication systems, including satellite and radar systems [1, 2]. Because moving traffic is increasing exponentially, the fixed-direction radiation beam must be modified.

Figure 1.1: Illustration of a beam-steering antenna dynamically directing its radiation towards users, enabling efficient connectivity in modern communication systems.

As a result of the microstrip array's ability to shape the radiation pattern into a desirable shape, array antennas can modify the fixed-direction radiation beam. Also, beam-steering microstrip patch antennas have gained attention due to their compact size, cost-effectiveness, and ability to dynamically direct signals, making them indispensable for 5G applications [3, 4].

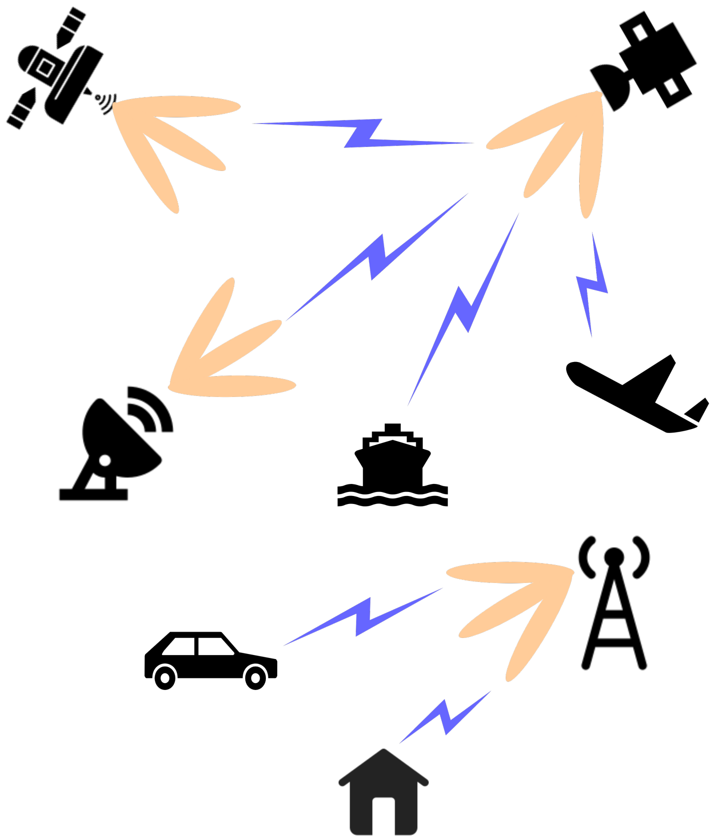

Figure 1.2: Visualization of beam-steering technology directing signals toward target locations, demonstrating dynamic adaptability for efficient communication systems.

This work simulates a 2×2 microstrip array antenna for beam-steering applications at 3.5 GHz. The design parameters are varied to create a dataset. Then, different machine learning algorithms try to predict the performance of the designed beam steering microstrip patch antenna, specifically the return loss. These trained models, along with different optimization methods, are used to predict the design parameter. This process results in an optimized, best-designed beam steering antenna that outperforms the initial design.

1.2 Motivation for the Research

In this era of artificial intelligence, data-driven technology has enabled an enormous need for faster internet and connectivity, which paved the way for adopting 5G from existing 4G, not only for speedier access but also for the remote connectivity communication system evolving to connect every dot in the surface. So, a smart antenna that can give faster access and be used in different communication systems is essential. Also, the ability to rotate radiation beams without changing the orientation and shape is highly sought.

Though the beam steering antenna has various applications, its performance is limited by the lack of proper design [5]. Since the EM simulation-based trial and error approach is time-consuming, the relevant theory to design a perfect antenna is not always present. So, if this trial and error can be replaced, the complex relation between the design and performance parameters is found. Machine learning can achieve this with the data-driven approach to accurately predict the performance and suggest design parameter change.

1.3 Importance of Machine Learning in Antenna Design

Machine learning has become a revolutionary tool in various research fields to predict the outcome and make reasoning from the data. It can play a pivotal role in antenna design and optimization. Traditional optimization is based on the theoretical analysis of the design and then a trial and error approach to get to the desired output. But algorithms like Random Forest, Decision Tree, Extreme Gradient Bost, and similar algorithms can find the theoretical relationship among design parameters, effectively predicting the antenna performance based on the design. At the same time predicted model can be further utilized to create an optimization process that can lead to the best possible output at the quickest of times, the fastest time. Traditionally, EM simulation software takes much time to give performance parameters for the design. So, incorporating different ML models leads to adaptable and high-performance antenna designs [6].

1.4 Challenges in Antenna Design and Optimization

Designing a beam steering microstrip antenna that automatically changes its beam direction is highly challenging work. Maintaining all the performance parameters at their best level, i.e., perfect impedance matching, high gain, directivity, and beam switching capability, depends on various design parameters [7, 8]. The simple antenna has lower design space, which can be explored, but in the context of a beam-s prediction, it is highly time-consuming, both in theory and simulation.

Also, challenge. Thence of the designed antenna, the data size needed is a challengerous work as ML model doNumeroussed on the given data. Also, the quality of the dataset is essential. Also, numerous methods can be explored to predict the performance, and the optimization method will optimize the design parameter to improve performance.

1.5 Objectives

The primary objective of this research is to develop and optimize a beam-steering microstrip patch antenna for 5G applications within the sub-6 GHz frequency band. The specific goals of this study are as follows:

1. To create an array antenna capable of dynamically steering its beam across specified angles within the sub-6 GHz band.
2. To apply machine learning models, such as Random Forest Regression, Decision Tree Regression, and XGB Regression, to accurately predict critical performance metrics of the antenna.
3. To refine key design parameters, including patch dimensions and feed line positions, ensuring improved overall performance.
4. To validate the proposed antenna design through simulations and compare its performance against existing designs.

1.6 Organization of the Thesis

The structure of this thesis is as follows:

- **Chapter 2** discusses theoretical concepts, performance metrics, machine learning models, and optimization methods relevant to this research.
- **Chapter 3** presents the design and simulation results of the beam-steering microstrip patch antenna.
- **Chapter 4** explores the application of machine learning models in predicting antenna performance and optimizing design parameters.
- **Chapter 5** highlights the optimization results and discusses the performance improvements achieved through ML-based techniques.
- **Chapter 6** concludes the thesis, summarizing the findings and offering recommendations for future research directions.

Chapter 2

Literature Review & Theoretical Background

This chapter explores the key parameters that were used to evaluate both the performance of the designed antenna and the efficiency of the machine learning models. Understanding these parameters is crucial as they directly influence the effectiveness of the antenna for its intended beam-steering application and how well the machine learning models can predict and optimize these characteristics. Additionally, we will introduce some fundamental terminologies that will be referred to later, ensuring a comprehensive understanding of the following discussion.

Total work can be divided into three parts: designing the beam steering antenna, predicting its performance using machine learning techniques, and optimizing the antenna design parameter to improve performance further.

2.1 Beam Steering Antenna Design

The first stage of this work is to design the beam steering microstrip patch array antenna. The following sections will present various important terminologies and theories with related work.

2.1.1 Antenna Parameter

This section offers an in-depth explanation of key antenna parameters that are crucial for the remainder of this thesis. These concepts will form the foundation for much discussion later in this work.

2.1.1.1 Return Loss

Return loss is a critical parameter used to evaluate how effectively an antenna is matched to its transmission line. It quantifies the proportion of power reflected back to the source due to impedance mismatches, providing insights into the antenna's ability to radiate energy effectively. In simpler terms, return loss measures how much energy is radiated versus how much is reflected [9].

The return loss (RL) is expressed in decibels (dB) and is derived using the reflection coefficient (Γ), which represents the ratio of the reflected voltage (V_r) to the incident voltage (V_i). Mathematically, the reflection coefficient is defined as:

$$\Gamma = \frac{V_r}{V_i} \tag{2.1}$$

Alternatively, Γ can also be expressed in terms of the load impedance (Z_L) and the characteristic impedance of the transmission line (Z_0) as follows:

$$\Gamma = \frac{Z_L - Z_0}{Z_L + Z_0} \tag{2.2}$$

In an ideal scenario, where the antenna is perfectly matched to the transmission line ($Z_L = Z_0$), the reflection coefficient becomes $\Gamma = 0$, meaning there is no reflected power. However, in practical applications, impedance mismatches cause some power to be reflected, quantified by the magnitude of Γ.

The return loss is calculated using a logarithmic expression:

$$RL = -20 \log |\Gamma| \tag{2.3}$$

For the beam-steering microstrip patch antenna designed in this work, a return loss of -10 dB or lower is considered acceptable, indicating that at least 90% of the input power. A return loss of -15 dB or better is targeted to ensure higher efficiency and better impedance matching. This minimizes reflection and provides stable performance, particularly in dynamic beam-steering applications [9, 10].

2.1.1.2 Role of S-Parameters in Multi-Port Antennas

In multi-port configurations, such as beam-steering antennas, S-parameters (S_{11}, S_{12}, S_{21}, S_{22}) provide a more comprehensive assessment of antenna performance. These parameters are critical for understanding impedance matching and isolation in multi-port systems [7, 11]:

- S_{11} **- Input Reflection Coefficient at Port 1:** This parameter indicates the proportion of power reflected when power is applied to port 1. For a well-matched antenna, S_{11} should be less than -10 dB and ideally less than -15 dB, indicating minimal reflection at the input port.

- S_{22} **- Input Reflection Coefficient at Port 2:** Similar to S_{11}, this parameter evaluates the reflection at port 2. For good matching across all input ports, S_{22} should also be below -10 dB.

- S_{12} **and** S_{21} **- Transmission Coefficients:** These parameters describe the power transmitted between port 1 and port 2. S_{12} measures the power from port 2 reaching port 1, while S_{21} measures the power from port 1 reaching port 2. Achieving good port isolation is critical in beam-steering antennas to minimize interference between ports. Ideally, both S_{12} and S_{21} should be below -10 dB [9].

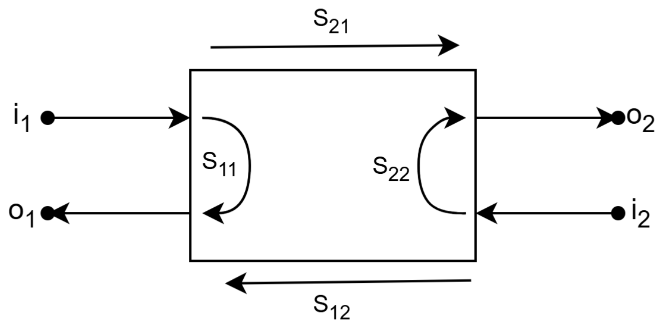

Figure 2.1: Representation of S-parameters (S_{11} and S_{22}) in a two-port network. This figure illustrates how the input reflection coefficients are analyzed at different ports for impedance matching and return loss calculations.

By analyzing return loss and S-parameters, the design and performance of beam-steering antennas can be optimized to achieve better impedance matching, higher efficiency, and effective port isolation. These parameters form the foundation for evaluating high-frequency antennas and ensuring their performance in modern applications, such as 5G and satellite communication systems [10, 12].

2.1.1.3 Gain and Directivity

Gain and directivity are two critical parameters used to evaluate an antenna's performance, particularly how effectively it radiates energy in a specific direction. While both relate to the antenna's radiation pattern, they differ in their scope and implications.

Directivity describes how focused the radiation is in a particular direction compared to an isotropic antenna, which radiates uniformly in all directions. Mathematically, it is defined as the ratio of the maximum radiation intensity of the antenna to the average radiation intensity over a sphere surrounding it. An antenna with high directivity concentrates its energy into a narrower beam, making it suitable for applications that require directional communication, such as satellite or point-to-point links [9, 10].

Gain, on the other hand, takes directivity one step further by factoring in the antenna's efficiency. It represents the actual amount of input power that the antenna converts into radiated power in a specific direction. Thus, gain accounts for any losses due to the antenna's internal inefficiencies, such as dielectric losses or mismatches. The relationship between gain (G), directivity (D), and efficiency (η) can be expressed as:

$$G = \eta \times D \tag{2.4}$$

Here: - G: Gain of the antenna. - D: Directivity of the antenna. - η: Efficiency of the antenna, ranging from 0 to 1, where 1 represents 100% efficiency.

In an ideal scenario, where $\eta = 1$, the gain is equal to the directivity. However, some power is inevitably lost in practical antennas due to internal resistance, material losses, or imperfect impedance matching, making 100% efficiency unattainable [9].

Understanding both gain and directivity is essential for designing and evaluating antennas. High gain ensures efficient power delivery in a desired direction, critical for applications like beam-steering antennas in 5G communication or satellite systems. Meanwhile, directivity helps determine how effectively the antenna can focus its energy, which is a key requirement for long-range communication systems or high-precision applications [12].

2.1.1.4 Radiation Pattern

The radiation pattern of an antenna describes the spatial distribution of the power radiated by the antenna as a function of direction. It provides a graphical or mathematical representation of how the antenna radiates or receives energy in space. Typically measured in the far-field region, the radiation pattern is a critical tool for understanding the directional characteristics of the antenna and evaluating its performance in specific applications [13].

A radiation pattern reveals key features of an antenna, including the direction of the main lobe (the region of maximum radiation), side lobes (unwanted radiation in other directions), and nulls (areas with minimal or no radiation). By analyzing these patterns, one can assess the antenna's ability to focus energy in a desired direction and minimize interference in undesired directions.

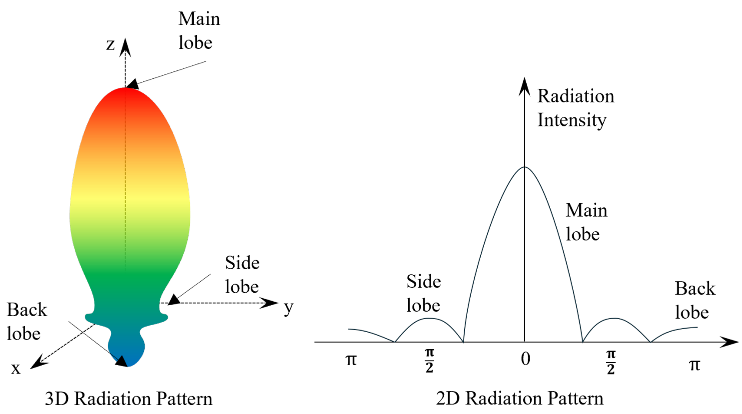

Figure 2.2: 3D and 2D radiation patterns of a directive antenna. The main beam focuses in the forward direction, demonstrating the antenna's directional properties [13].

Figure 2.2 illustrates both three-dimensional (3D) and two-dimensional (2D) radiation patterns. The 3D pattern provides a comprehensive view of the radiated energy in all directions, while the 2D pattern focuses on specific planes, such as the azimuth or elevation plane. These patterns help identify the primary direction of radiation and the extent of side lobe levels.

In the context of this thesis, which focuses on machine learning (ML)-assisted beam-steering microstrip patch antennas, radiation patterns play a central role in evaluating beam steering performance. By analyzing the patterns, the effectiveness of steering the beam in different directions can be quantified.

2.1.2 Theoretical Analysis

This section provides an in-depth overview of the fundamental concepts of beam steering, laying the groundwork for the proposed methodology in this thesis. It begins with a theoretical discussion of beam-steering principles and their relevance to modern communication systems. Additionally, the section includes a concise description of microstrip antenna feed types and the role of both-sided microwave integrated circuit (MIC) technology in antenna design.

2.1.2.1 Beam Steering

Beam steering antennas are highly valued in modern wireless communication systems due to their ability to dynamically direct radiation beams toward desired directions. This capability is essential for forming communication links between users in motion or located at different positions, particularly in 5G mobile networks and other advanced systems like satellite and radar communication. As the volume of moving traffic continues to rise exponentially, fixed radiation beams need to adapt dynamically. Microstrip array antennas, known for their ability to shape radiation patterns, are ideal for achieving this functionality. By electronically steering the beam, these antennas can effectively track and target moving devices, ensuring seamless connectivity [14].

Beam steering can be implemented in two primary ways: physically reorienting antenna elements or electrically adjusting the feeding network to tilt the radiated beam [15]. Among these methods, electronic beam steering, achieved by varying the phase of input signals, is preferred for its speed and flexibility.

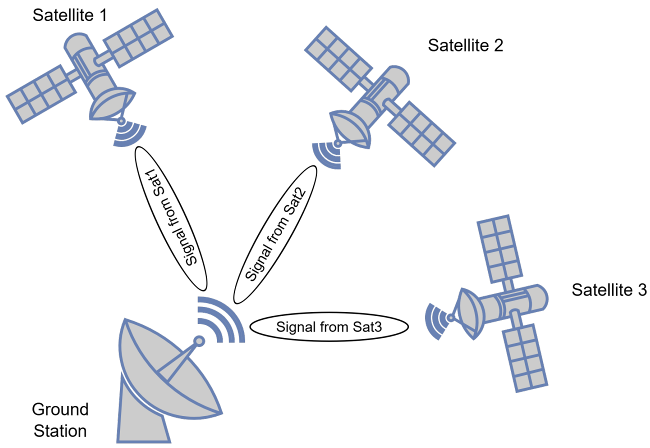

Figure 2.3: Conceptual representation of beam steering in a communication system, where an antenna dynamically directs its radiation beam to connect with multiple satellites. Each beam is steered toward a specific target using phase adjustments.

Figure 2.3 illustrates a conceptual diagram of beam steering in a satellite communication system. The antenna dynamically adjusts the direction of its radiated beam to maintain communication links with multiple satellites. By regulating the phase difference of input signals at the feed ports, the radiated beam can be steered toward different satellites or users. This adaptability is essential in scenarios where the source or target position changes frequently, such as in satellite, radar, or mobile communication systems.

2.1.2.2 Microstrip Antenna Feeding Techniques

Microstrip patch antennas can be fed using various techniques, broadly categorized into **contacting** and **non-contacting** methods. These techniques play a vital role in determining the antenna's performance characteristics, such as bandwidth, gain, return loss, and impedance matching [16]. Figure 2.4 illustrates the commonly used feeding strategies.

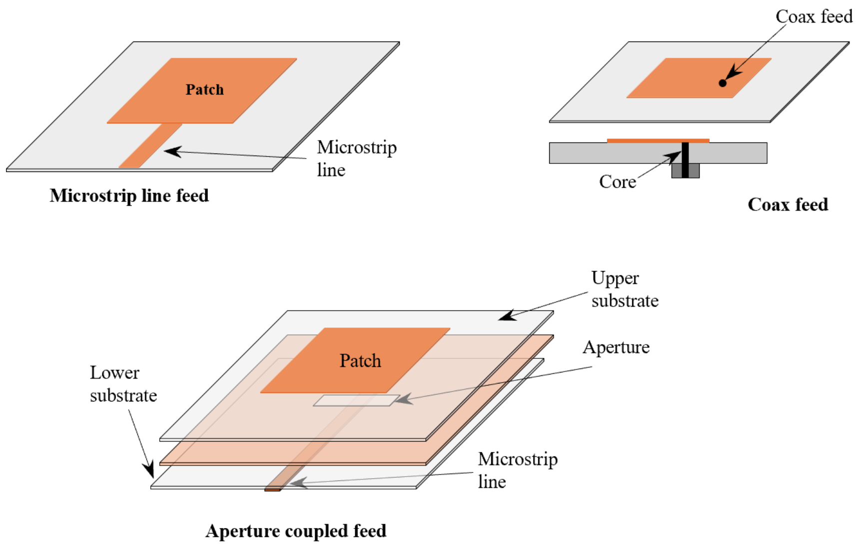

Figure 2.4: Microstrip patch antenna feeding techniques.

In **microstrip line feed**, a conducting strip is directly connected to the edge of the microstrip patch. This method enables the feeding line to be etched on the same substrate as the patch, resulting in a simple and planar design. It is a commonly used technique due to its ease of fabrication and integration.

The **coaxial feed** uses a coaxial cable to connect the patch. The inner conductor of the cable is soldered to the patch, while the outer conductor is attached to the ground plane. This approach provides good impedance matching and flexibility in feed point placement but can introduce complexity during fabrication.

The **aperture-coupled feed** involves two dielectric substrates separated by a ground plane with a slot acting as a coupling aperture. This method offers improved polarization purity and enhanced bandwidth, making it ideal for high-performance applications. However, it increases the complexity of the antenna design.

Each feeding method has its strengths and limitations. For instance, microstrip line feeds are easy to fabricate but may have limited bandwidth, while aperture-coupled feeds offer higher bandwidth at the cost of increased complexity [17]. Therefore, selecting the appropriate feeding technique is critical to optimizing the antenna's performance based on the design requirements.

2.1.2.3 Both-Sided MIC Technology

Microwave Integrated Circuit (MIC) technology, commonly referred to as both-sided or double-sided MIC technology, is an advanced approach in antenna design where both sides of the substrate are utilized to integrate microwave circuits. This innovative technique offers significant design flexibility, enabling the development of compact, efficient, and high-performance antennas [18]. By using both sides of the substrate, complex microwave structures can be incorporated without increasing the antenna's footprint, making it ideal for modern communication systems.

One of the key applications of both-sided MIC technology is the implementation of hybrid dividers, also known as Magic-T. These devices combine in-phase (**H**-port) and out-of-phase (**E**-port) signals to create a versatile signal distribution network. Magic-T dividers are critical components in many RF and microwave systems, as they facilitate precise signal division and phase control, which are essential for beam steering and impedance matching. Figure 2.5 demonstrates some examples of hybrid dividers designed using both-sided MIC technology.

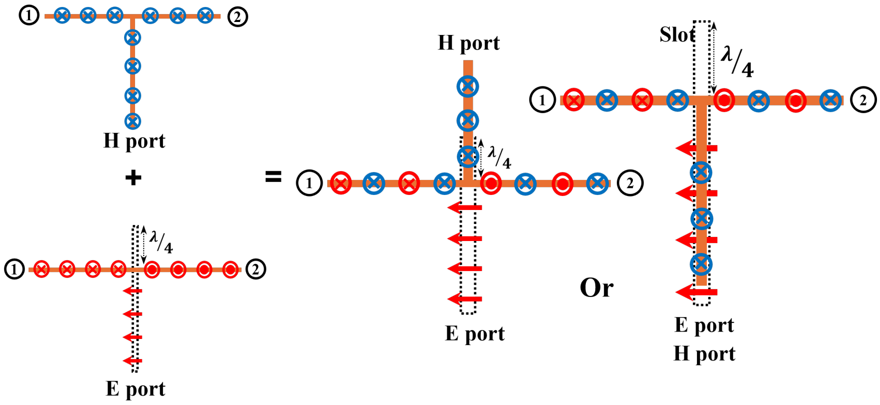

Figure 2.5: Examples of hybrid dividers (Magic-T) using both-sided MIC technology. The blue-colored ⊗ represents in-phase signals, while the red-colored ⊗ denotes out-of-phase signals.

This technology not only enables the seamless integration of in-phase and out-of-phase dividers but also improves the antenna's overall performance by optimizing signal distribution. By leveraging both-sided MIC technology, the proposed antenna design achieves enhanced efficiency, compactness, and better beam steering capabilities, making it suitable for advanced applications like 5G communication and satellite systems [19].

2.1.3 Related Work

This section provides an overview of recent advancements in beam-steering antenna technologies and highlights how machine learning (ML) models are being employed to predict and optimize antenna parameters for enhanced performance.

2.1.3.1 Beam Steering Antenna

The radiation beam can be directed in the direction of moving traffic using beam steering antennas [14], [20]. There are two ways to make these types of antennas: manually directing antenna elements in the desired direction or electrically configuring circuits or antenna elements so that the radiated beam tilts [15], [21].

Several previous studies have been conducted on how a radiated beam of microstrip array antennas can be steered. It can be easily achieved by varying the phase of the array's antenna elements. In addition to phase control, radio frequency (RF) signal amplitude control may also provide beam steering [22]. A defected ground structure that can increase capacitance or inductance and thus influence the antenna's current follow, causing phase variation and beam steering [23]. However, coupled oscillator arrays using a varactor diode with microstrip line are used to realize beam steering function without a phase shifter [24]. Altering the distance between the dielectric image line (DIL) and the moving reflector plate underneath it, is another method to realize beam steering [25], [26]. Though beam steering may be accomplished by assigning a separate phase to each antenna element in an array, they can only direct the radiated beam at specified angles. Additionally, although internal or external circuit configurations might result in beam steering, they can also increase circuit complexity or antenna size [27], [28]. Incorporating a double-sided microwave integrated circuit (MIC) into a microstrip array can minimize circuit complexity while also shrinking antenna size, resulting in improved circuit function and design flexibility. It may also be used with planar array antennas in a variety of ways to achieve several antenna design functions which makes the design easier [18]–[29].

Moreover, when compared to an antenna array, a single element antenna has limited directivity and gain. Because it offers superior gain and directivity than single element antennas, as well as being easier to build, operate, and install, the microstrip array antenna is the most useful in the communication field. They can also be used to create precise radiation patterns that a single element antenna would be unable to achieve. [30]–[31].

In this work, a microstrip array antenna for beam steering functions exploiting MIC applications is presented. The array antenna is intended to be simulated at resonance frequency 3.5 GHz in sub-6 GHz 5G frequency band due to the enormous expanding number of smartphone users, increasing streaming demand. And in the 4G saturated age, it is required to switch generation while making the implementation effective. For efficient implementation of 5G frequency band, immediate frequency band for this is the sub-6 GHz frequency band [32], [33]. The operational concept of the designed beam-steering array antenna is shown in Figure 3.1. $\Delta\Phi$ denoted in the figure is the difference in phase between two input signals. The microstrip line-slot stub junction works as a hybrid coupler in this design and provides signals to the right and left side elements with a phase difference.

2.2 Machine Learning Based Prediction and Optimization

This section will focus on the theoratrical background of different machine learning model, performance metrics which will be used to evaluate the trained model performance, optimization techiniques to improve the antenna performacne by modifying the design parameters.

2.2.1 Machine Learning Model Selection

Machine learning model selection plays a crucial role in accurately predicting the return loss (S11) values of microstrip patch antennas. Due to the non-linear and complex relationships between the antenna design parameters and performance metrics, various models were explored to find the best fit for this prediction task. The models selected for this study were Linear Regression, Ridge Regression, Lasso Regression, Random Forest Regression, Decision Tree Regression, XGBoost Regression, Bayesian Linear Regression, and Gaussian Process Regression, each with distinct advantages for capturing different aspects of the problem.

2.2.1.1 Models Used

The following machine learning models were used in this study to predict the S11 values ($Y \in \mathbb{R}^{n\times 101}$) of the antenna design across multiple frequencies, given the input features ($X \in \mathbb{R}^{n\times 11}$) representing the design parameters:

- **Linear Regression**: Linear Regression aims to establish a linear relationship between the features and the target, represented by:

$$Y = X\beta + \epsilon \tag{2.5}$$

where $Y \in \mathbb{R}^{n\times 101}$ represents the S11 values at different frequencies, $X \in \mathbb{R}^{n\times 11}$ is the feature matrix of antenna design parameters, $\beta \in \mathbb{R}^{11\times 101}$ is the coefficient matrix, and $\epsilon \in \mathbb{R}^{n\times 101}$ is the error term [34].

- **Ridge Regression**: Ridge Regression adds an L2 regularization term to prevent overfitting, with the cost function given by:

$$J(\beta) = \sum_{i=1}^{n} \|Y_i - X_i\beta\|^2 + \lambda \sum_{j=1}^{11} \|\beta_j\|^2 \tag{2.6}$$

where λ is the regularization parameter that controls the magnitude of the penalty [35].

- **Lasso Regression**: Lasso Regression incorporates an L1 regularization term to encourage sparsity in the coefficients, with the cost function:

$$J(\beta) = \sum_{i=1}^{n} \|Y_i - X_i\beta\|^2 + \lambda \sum_{j=1}^{11} |\beta_j| \tag{2.7}$$

where λ is the regularization parameter [36].

- **Random Forest Regression**: Random Forest Regression constructs an ensemble of decision trees, and the final output is obtained by averaging their predictions:

$$\hat{Y} = \frac{1}{T}\sum_{t=1}^{T} f_t(X) \tag{2.8}$$

where T is the number of trees, and $f_t(X)$ is the prediction of the t-th tree [37].

- **Decision Tree Regression**: Decision Tree Regression splits the dataset into regions based on feature values, and predicts using the average value of the observations in each leaf node [38].

- **XGBoost Regression**: XGBoost uses gradient boosting to iteratively refine predictions:

$$\hat{Y}^{(t)} = \hat{Y}^{(t-1)} + \eta \cdot g_t(X) \tag{2.9}$$

where η is the learning rate, and $g_t(X)$ is the output of the t-th weak learner [39].

- **Bayesian Linear Regression**: Bayesian Linear Regression estimates the posterior distribution over model parameters:

$$Y = X\beta + \epsilon, \quad \epsilon \sim \mathcal{N}(0, \sigma^2 I) \tag{2.10}$$

  where the priors on β follow a Gaussian distribution [40].

- **Gaussian Process Regression**: Gaussian Process Regression is a non-parametric method that models the distribution over functions:

$$Y \sim \mathcal{GP}(m(X), k(X, X')) \tag{2.11}$$

  where $m(X)$ is the mean function, and $k(X, X')$ is the covariance function defining relationships between data points [41].

2.2.1.2 Multi-output Regression Approach

The antenna design problem involves predicting return loss (S11) across 101 frequency points, making it a multi-output regression problem. To handle this scenario, models like Decision Tree, Random Forest, and XGBoost were wrapped using the `MultiOutputRegressor` from scikit-learn. This wrapper enables these models to predict multiple outputs simultaneously by training separate estimators for each output dimension.

Gaussian Process Regression inherently supports multi-output predictions through the use of covariance functions that model the relationships between outputs. The goal of the multi-output regression approach is to maintain the correlations between S11 values across different frequencies, ensuring that the predictions are consistent and realistic.

$$\hat{Y} = f(X), \quad \hat{Y} \in \mathbb{R}^{n\times 101} \tag{2.12}$$

where $f(X)$ represents the multi-output mapping from the input feature space to the target output space.

2.2.2 Model Evaluation Metrics

2.2.2.1 Metrics Overview

To evaluate the performance of the machine learning models used for predicting the return loss ($Y \in \mathbb{R}^{n\times 101}$), several regression metrics were calculated. Each metric provides a unique perspective on the model's performance, helping to assess accuracy, error, and variance. Below are the metrics used, along with their respective mathematical formulations [42, 43, 44]:

- **Mean Absolute Error (MAE)**: The MAE measures the average magnitude of errors between predicted ($\hat{Y}$) and true values (Y) without considering their direction. It is given by:

$$\text{MAE} = \frac{1}{n\times m}\sum_{i=1}^{n}\sum_{j=1}^{m}\left|Y_{ij} - \hat{Y}_{ij}\right| \tag{2.13}$$

  where n is the number of samples and m is the number of outputs (101 frequency points).

- **Mean Squared Error (MSE)**: The MSE represents the average squared difference between predicted and true values, penalizing larger errors more heavily:

$$\text{MSE} = \frac{1}{n\times m}\sum_{i=1}^{n}\sum_{j=1}^{m}\left(Y_{ij} - \hat{Y}_{ij}\right)^2 \tag{2.14}$$

- **Mean Squared Logarithmic Error (MSLE)**: MSLE measures the squared logarithmic differences between predicted and true values, making it suitable for capturing relative errors:

$$\text{MSLE} = \frac{1}{n\times m}\sum_{i=1}^{n}\sum_{j=1}^{m}\left(\log(1+|Y_{ij}|) - \log(1+|\hat{Y}_{ij}|)\right)^2 \tag{2.15}$$

- **Root Mean Squared Logarithmic Error (RMSLE)**: RMSLE is the square root of MSLE, providing a more interpretable measure of logarithmic error:

$$\text{RMSLE} = \sqrt{\text{MSLE}} \tag{2.16}$$

- **Mean Absolute Percentage Error (MAPE)**: MAPE expresses the prediction error as a percentage of the true values:

$$\text{MAPE} = \frac{1}{n\times m}\sum_{i=1}^{n}\sum_{j=1}^{m}\left|\frac{Y_{ij} - \hat{Y}_{ij}}{Y_{ij}}\right| \times 100 \tag{2.17}$$

- **R-squared (R^2)**: R^2 measures the proportion of variance in the true values that is captured by the model:

$$R^2 = 1 - \frac{\sum_{i=1}^{n} \sum_{j=1}^{m} \left(Y_{ij} - \hat{Y}_{ij}\right)^2}{\sum_{i=1}^{n} \sum_{j=1}^{m} \left(Y_{ij} - \bar{Y}_j\right)^2} \tag{2.18}$$

  where $\bar{Y}_j$ represents the mean of the j-th output across all samples.

- **Variance Score**: The variance score measures the degree to which the predicted output captures the variability in the true output. It can be expressed as:

$$\text{Variance Score} = \frac{1}{m} \sum_{j=1}^{m} \left(1 - \frac{\text{Var}(Y_{\cdot j} - \hat{Y}_{\cdot j})}{\text{Var}(Y_{\cdot j})}\right) \times 100 \tag{2.19}$$

  where $\text{Var}(Y_{\cdot j})$ is the variance of the true values for the j-th output.

2.2.2.2 Comparison of Model Performance

Each model was evaluated using the abovementioned metrics to assess their predictive performance for antenna return loss (S11) across 101 frequencies. The performance comparison enabled the identification of the model that provided the most accurate and generalizable predictions. A detailed analysis of the model results and their strengths or weaknesses based on these metrics is presented in the later chapter.

2.2.3 Optimization Techniques Implemented

2.2.3.1 L-BFGS-B Optimization Method

The Limited-memory Broyden–Fletcher–Goldfarb–Shanno with Box constraints (L-BFGS-B) [45] is a gradient-based optimization algorithm that was applied to refine the antenna design parameters predicted by machine learning models. The objective function used the training dataset to minimize the return loss ($S11$) at the target frequency of 3.5 GHz. The optimization process was initialized with the parameters predicted by the models.

- **Input:**
  - Initial parameter set from ML model predictions: $\mathbf{x}_{\text{initial}} = [x_1, x_2, \ldots, x_{11}]$.

- Objective function: Return loss $S11$ at 3.5 GHz, defined as:

$$f(\mathbf{x}) = S11_{\text{pred}}(f = 3.5 \text{ GHz}) \tag{2.20}$$

- Bound constraints for each parameter based on the training dataset, represented as $\mathbf{l} \leq \mathbf{x} \leq \mathbf{u}$, where $\mathbf{l}$ and $\mathbf{u}$ are the lower and upper bounds, respectively.

- **Initialization:**
  - Set initial parameters: $\mathbf{x}_0 = \mathbf{x}_{\text{initial}}$.
  - Define stopping criteria: maximum iterations N_{max} and tolerance ϵ for convergence.

- **Iteration** (for $k = 0, 1, 2, \ldots, N_{\text{max}}$):
  - **Gradient Calculation:** Compute the gradient $\nabla f(\mathbf{x}_k)$, which represents the rate of change of return loss with respect to each design parameter:

$$\nabla f(\mathbf{x}_k) = \left[\frac{\partial f}{\partial x_1}, \frac{\partial f}{\partial x_2}, \ldots, \frac{\partial f}{\partial x_{11}} \right]_{\mathbf{x}=\mathbf{x}_k} \tag{2.21}$$

  - **Update Parameters:** Use the L-BFGS-B algorithm to update the parameter vector, using a limited-memory approximation of the Hessian matrix:

$$\mathbf{x}_{k+1} = \mathbf{x}_k - \alpha_k H_k^{-1} \nabla f(\mathbf{x}_k) \tag{2.22}$$

    Here, H_k^{-1} is an approximation of the inverse Hessian, and α_k is the step size.
  - **Check Convergence:** If $\|\nabla f(\mathbf{x}_{k+1})\| < \epsilon$, stop the iteration.

- **Output:** Optimized parameter set $\mathbf{x}_{\text{opt}}$ that minimizes $S11$ at 3.5 GHz.

The L-BFGS-B method effectively fine-tuned the parameters predicted by the machine learning models, resulting in improved antenna performance.

2.2.3.2 TNC Optimization Method

The Truncated Newton Conjugate-Gradient (TNC) method [46] was employed for its capability to handle high-dimensional problems with bound constraints. This method used the predicted design parameters as a starting point and aimed to minimize $S11$ at 3.5 GHz.

- **Input:**
  - Initial parameter set from ML predictions: $\mathbf{x}_{\text{initial}}$.
  - Bound constraints for each parameter.
- **Initialization:**
  - Set initial parameters: $\mathbf{x}_0 = \mathbf{x}_{\text{initial}}$.
  - Define stopping criteria: tolerance ϵ and maximum iterations N_{max}.
- **Iteration** (for $k = 0, 1, 2, \ldots, N_{\text{max}}$):
  - **Gradient Calculation:** Compute the gradient $\nabla f(\mathbf{x}_k)$.
  - **Hessian Approximation:** Approximate the Hessian matrix H_k for the objective function.
  - **Newton Step:** Calculate the search direction $\mathbf{p}_k$ by solving:

$$H_k \mathbf{p}_k = -\nabla f(\mathbf{x}_k) \tag{2.23}$$

  - **Line Search:** Determine the step size α_k.
  - **Update Parameters:** Update the parameter vector:

$$\mathbf{x}_{k+1} = \mathbf{x}_k + \alpha_k \mathbf{p}_k \tag{2.24}$$

  - **Check Convergence:** If $\|\nabla f(\mathbf{x}_{k+1})\| < \epsilon$, stop the iteration.
- **Output:** Optimized parameters $\mathbf{x}_{\text{opt}}$ that reduce $S11$ at 3.5 GHz.

TNC effectively handled high-dimensional parameter adjustments, refining the antenna design for better performance.

2.2.3.3 SLSQP Optimization Method

Sequential Least Squares Programming (SLSQP) [47] was used to optimize return loss while maintaining certain design constraints. This method handled both bound constraints and relationships between design parameters.

- **Input:**
  - Initial parameter set from ML model predictions: $\mathbf{x}_{\text{initial}}$.
  - Bound constraints $\mathbf{l} \leq \mathbf{x} \leq \mathbf{u}$.

  - Additional inequality constraints $g_i(\mathbf{x}) \leq 0$.

- **Initialization:**

  - Set initial parameters: $\mathbf{x}_0 = \mathbf{x}_{\text{initial}}$.
  - Define stopping criteria: maximum iterations and tolerance.

- **Iteration** (for $k = 0, 1, 2, \ldots, N_{\max}$):

  - **Quadratic Approximation:** Construct a quadratic approximation of the objective function.
  - **Solve Subproblem:** Solve the quadratic subproblem with linearized constraints:
$$\min_{\mathbf{p}} \quad \frac{1}{2}\mathbf{p}^T H_k \mathbf{p} + \nabla f(\mathbf{x}_k)^T \mathbf{p} \tag{2.25}$$
    subject to $g_i(\mathbf{x}_k + \mathbf{p}) \leq 0$.
  - **Update Parameters:** Update the parameter vector:
$$\mathbf{x}_{k+1} = \mathbf{x}_k + \mathbf{p}_k \tag{2.26}$$
  - **Check Convergence:** If constraints are satisfied and $\|\nabla f(\mathbf{x}_{k+1})\| < \epsilon$, stop the iteration.

- **Output:** Optimized parameter set $\mathbf{x}_{\text{opt}}$ that satisfies both the objective and constraints.

SLSQP was particularly useful for refining the design while respecting physical and practical constraints.

2.2.3.4 Genetic Algorithm (GA) Optimization Method

The Genetic Algorithm (GA) [48] was used as a global optimization technique to explore a more expansive design space. GA simulates natural selection, evolving a population of potential solutions to optimize the antenna parameters.

- **Initialization:**

  - **Population:** Generate an initial population of N individuals, each representing a parameter set $\mathbf{x}_i$.
  - **Fitness Function:** Evaluate the fitness of each individual using:
$$f(\mathbf{x}_i) = S11_{\text{pred}}(f = 3.5 \text{ GHz}) \tag{2.27}$$

- **Evolution:**
  - **Selection:** Select the top-performing individuals based on their fitness scores.
  - **Crossover:** Pair individuals and create offspring by combining their parameters.
  - **Mutation:** Introduce random mutations to some individuals to maintain diversity.
  - **Evaluate:** Recalculate fitness for the new population.
- **Convergence:**
  - Repeat the selection, crossover, and mutation process for a set number of generations or until improvement is minimal.
- **Output:** Best individual representing the optimal parameter set $\mathbf{x}_{\text{opt}}$.

GA allowed broad exploration, avoiding local minima and identifying potentially optimal antenna configurations.

2.2.3.5 Simulated Annealing (SA) Optimization Method

Simulated Annealing (SA) [49] was applied to explore the design space probabilistically. Starting with an initial solution $\mathbf{x}_0$ from the machine learning predictions, SA allowed for both downhill and occasional uphill moves to escape local minima, making it effective for navigating complex optimization landscapes.

- **Initialization:**
  - Set initial solution $\mathbf{x}_0 = \mathbf{x}_{\text{initial}}$.
  - Set initial temperature T_0 and cooling rate α.
- **Iteration:**
  - For each iteration k:
    * **Generate New Solution:** Propose a new solution $\mathbf{x}_{k+1} = \mathbf{x}_k + \Delta\mathbf{x}$, where $\Delta\mathbf{x}$ is a small random change.
    * **Evaluate:** Compute $f(\mathbf{x}_{k+1})$.
    * **Acceptance Probability:** Calculate:

    $$P(\text{accept}) = \exp\left(\frac{-\Delta f}{T_k}\right) \tag{2.28}$$

    where $\Delta f = f(\mathbf{x}_{k+1}) - f(\mathbf{x}_k)$.

    * **Accept or Reject:** Accept $\mathbf{x}_{k+1}$ with probability $P(\text{accept})$.
    * **Cooling:** Update temperature $T_{k+1} = \alpha T_k$.

- **Convergence:**
  - Stop when T_k is sufficiently low or when improvements are minimal.
- **Output:** Optimized parameter set $\mathbf{x}_{\text{opt}}$.

SA was particularly useful in escaping local minima early in the optimization process.

2.2.3.6 Summary of Optimization Techniques

Combining these optimization techniques ensured a comprehensive exploration of the design space. Gradient-based methods (L-BFGS-B, TNC, SLSQP) provided efficient local refinement, while global methods (GA and SA) enabled broader exploration to identify the best possible design configurations. Together, these approaches significantly improved key performance metrics, including reduced return loss, enhanced gain, and better directivity.

2.2.4 Related Work on Machine Learning Based Prediction

ML has become an indispensable tool for simplifying complex tasks, particularly in the AI era. Its ability to automate iterative and computationally intensive processes has proven invaluable in domains like antenna design, which traditionally require extensive manual parameter tuning using electromagnetic modeling solutions. ML can significantly streamline this process by training models to predict performance outcomes based on design parameters, thereby reducing the time and effort needed for manual adjustments [50].

In the field of antenna design, ML techniques are primarily employed for two key purposes: performance prediction and design parameter optimization. This subsection focuses on related works that leverage ML for performance prediction, particularly in the context of 5G band microstrip patch antennas. Several studies have demonstrated the efficacy of ML algorithms in forecasting key antenna performance metrics, including resonance frequency, gain, bandwidth, and return loss.

For instance, Haque et al. [51] utilized seven ML techniques, including ridge regression and linear regression, to predict the frequency and directivity of a quasi-Yagi antenna designed for UMTS 2100 MHz LTE applications. Ridge regression excelled in directivity prediction, while linear regression demonstrated superior accuracy in frequency prediction. In a related study, the gain and directivity of a quasi-Yagi antenna were predicted using eight models, with Gaussian process regression achieving a remarkable 98% accuracy in gain predictions [52].

Further advancements in ML-based performance prediction include the use of artificial neural networks (ANN), decision tree regression, random forest regression, and XGB to forecast bandwidth and resonant frequency for Yagi-Uda antennas [53]. Random forest regression, in particular, exhibited over 95% accuracy in gain prediction, as highlighted in a study by Al et al. [54]. Similarly, the gain of a 5G 28 GHz MIMO antenna was accurately predicted using six different ML models [55].

In another notable study, Jain et al. [56] applied four ML models—decision tree, random forest, XGB, and KNN—to predict the S11 parameter for four distinct antenna designs. The performance of these models was evaluated using metrics such as Mean Absolute Error (MAE), Mean Squared Error (MSE), and R^2, with predictions compared against actual S11 data points. Meanwhile, Joshiba et al. [57] explored the use of random forest, XGB, decision tree regression, and linear regression models to predict the return loss of an eye bolt-shaped antenna. XGB outperformed the other models, as measured by variance score, MAE, Root Mean Square Error (RMSE), and MSE, although the study lacked visualization of the predictions.

For THz antennas designed for 6G communication, Jain et al. [58] employed KNN, XGBoost, decision tree, and random forest models to predict return loss, with random forest achieving the highest accuracy (82%) and the lowest MSE (3.816). Additionally, Sudha et al. [50] found that XGB regression surpassed random forest, decision tree, and linear regression in forecasting the return loss of an eye bolt-shaped antenna, based on comprehensive evaluation metrics such as variance score, MAE, RMSE, and MSE.

Finally, Babale et al. [59] designed a tri-band antenna to generate datasets for training various ML models, including linear regression, decision tree regression, support vector machines (SVM), Gaussian process regression, efficient linear regression, and kernel regression. The comparative analysis across these models highlighted their potential in accurately predicting return loss and optimizing antenna performance.

These studies collectively underscore the transformative potential of ML in antenna design, particularly in performance prediction, where ML-driven approaches offer enhanced accuracy and efficiency compared to traditional methods.

2.2.5 Related Work on Machine Learning based Optimization

Machine learning (ML) has emerged as a transformative tool in antenna design, addressing traditional challenges such as time-intensive simulations and complex parameter tuning. Early work by Sharma et al. [60] applied ML techniques, including LASSO regression, artificial neural networks (ANNs), and K-Nearest Neighbors (KNN), to optimize the design of a double T-shaped monopole antenna. Their study demonstrated how ML models could effectively predict performance parameters, reducing the dependency on iterative trial-and-error processes.

Further advancements were made by Ji et al. [61], who introduced a hybrid framework combining Support Vector Machines (SVM) with Gaussian Process Regression (GPR). This dual-stage approach improved the efficiency of antenna optimization, as SVM filtered parameter spaces before regression. Around the same time, Shakya et al. [62] conducted a comparative analysis of ML algorithms for predicting S11 values across different antenna types. Their findings highlighted the advantages of ensemble models in enhancing prediction accuracy and computational efficiency.

In subsequent years, the focus expanded to applying ML to specialized antenna designs. Huang et al. [63] utilized Random Forest, Decision Trees, and Extreme Gradient Boosting (XGB) models to optimize rectangular microstrip patch antennas. By integrating Grid Search CV for hyperparameter tuning, their approach achieved remarkable precision, demonstrating ML's potential to streamline complex design processes. Similarly, Devnath et al. [64] employed Random Forest Regression and KNN to design a dual-band cylindrical dielectric resonator antenna, achieving high impedance bandwidths in the Ku and Ka frequency bands.

Notably, Kaushik et al. [65] explored ML-driven approaches to optimize circularly polarized antennas for 5G applications. Their use of KNN and ANN models enabled highly accurate predictions of design parameters, achieving an impressive accuracy of 98.7%. Complementing this work, Kaushal and Chandel [66] implemented inverse artificial neural networks for multiband antenna design. Their framework rapidly generated optimized parameters for user-specific requirements, showcasing the efficiency of ML in handling diverse frequency bands and operational constraints.

These studies collectively highlight how ML has revolutionized antenna design by reducing computational costs, improving accuracy, and enabling rapid prototyping. As the integration of ML techniques in engineering continues to evolve, future developments are likely to bring even greater innovations in antenna performance and customization.

Chapter 3

Beam Steering Microstrip Array Antenna

The development of beam-steering technologies is crucial to enhancing the capabilities of next-generation wireless communication systems, particularly in the 5G sub-6 GHz frequency band. This chapter explores the design, simulation, and performance analysis of a 2×2 microstrip array antenna, engineered explicitly for beam steering applications in the 5G frequency range centered at 3.5 GHz. The analysis presented in this chapter provides a comprehensive understanding of the beam steering mechanism, the design Complexities, and the performance outcomes of the microstrip array antenna.

3.1 Beam Steering Concept

This work presents a microstrip array antenna for beam steering functions exploiting MIC applications. The array antenna is intended to be simulated at resonance frequency 3.5 GHz in sub-6 GHz 5G frequency band due to the enormous expanding number of smartphone users, increasing streaming demand. And in the 4G saturated age, it is required to switch generation while making the implementation effective. For efficient implementation of the 5G frequency band, the immediate frequency band for this is the sub-6 GHz frequency band [32], [33]. The operational concept of the designed beam-steering array antenna is shown in Figure 3.1. $\Delta\Phi$ denoted in the figure is the difference in phase between two input signals. In this design, the microstrip line-slot stub junction works as a hybrid coupler, providing signals to the right and left side elements with a phase difference.

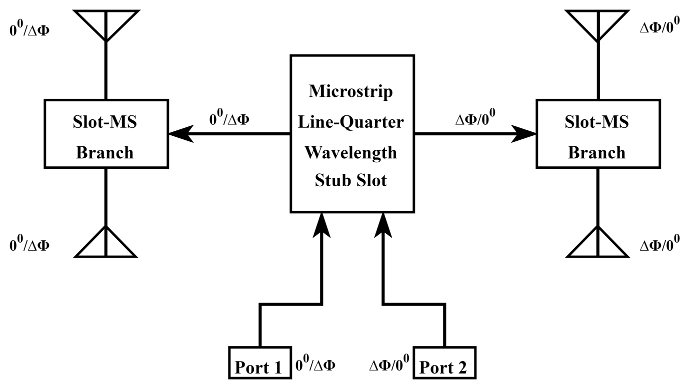

Figure 3.1: Basic concept of the proposed beam-steering array antenna

The entire simulation is done using keysight technologies advanced design system (ADS) software.

3.2 Design Method

This section discusses the proposed antenna architecture, including its feed network and operating principle. The subsection antenna structure describes the antenna's construction. The antenna configuration establishes the feed network with its impedance-matching results, and the array functioning concept is described in the array operating principle.

3.2.1 Antenna Architecture

The array antenna presented is composed of four square microstrip patches organized in a 2×2 arrangement. Each patch is designed with a resonance frequency of 3.5 GHz. Two quarter wavelength transformers connect the patches on the left and right sides, which are then linked to the source via Magic-T through a slot line by two coupled microstrip lines. Figure 3.2 shows the geometry of the proposed array antenna with a top view in Figure 3.2(a) and the cross-sectional view along AA' in Figure 3.2(b). In the ground plane underneath the substrate layer, a T-type slot line is formed. The patches and microstrip lines are attached to the top layer of a 0.8 mm thick substrate. The relative dielectric constant of the Teflon glass fiber substrate employed in this design is 2.15.

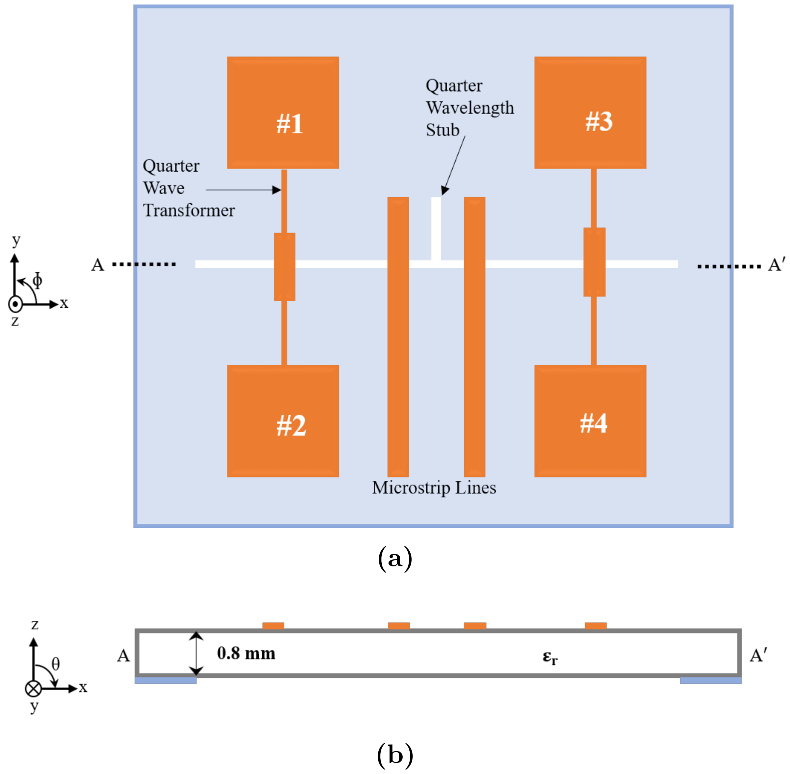

Figure 3.2: Structure of the proposed beam steering microstrip array antenna (a) top view and (b) cross-section of the antenna along AA'

3.2.2 Antenna Configuration

The impedance of the microstrip line is 50 Ω. The slot impedance must be 100 Ω in the microstrip-slot branch circuit because it is a parallel power divider. This divider divides the signal into two equal amplitudes in phase signals. The strip impedance must also be 50 Ω in the slot-microstrip branch circuit as it is a series power divider [67].

This divider divides the signal into two equal amplitudes out of phase signals. For better impedance matching, quarter wave transformers are used which have an impedance of 92.95 Ω calculated using (3.1).

$$Z = \sqrt{Z_1 \times Z_2} \tag{3.1}$$

The slot line at the slot-microstrip branch is extended by a quarter-wavelength for enhanced antenna characteristics, and the quarter-wavelength microstrip line is likewise extended at the microstrip-slot branch. Figure 3.3 shows the configuration of the proposed array antenna where it can be seen that two slot-microstrip branches are used to link the four antenna elements. Slot-line impedance is twice the microstrip line impedance. Two input port with 50 Ω impedance is set to two microstrip lines of width 2.6 mm. Another four ports with each of impedance 172 Ω are inserted into four quarter wave transformer terminals as shown in Figure 3.3. Figure 3.4 shows the frequency response of the array configuration for different values of F_d where F_d is the distance between two input microstrip lines. The feed network shows the best impedance matching when the distance between two microstrip lines is 15.2 mm. For F_d=15.2 mm, quarter wave transformer terminal impedances with respect to input impedance are also shown in Figure 3.4 and the design parameters are shown in Table 3.1.

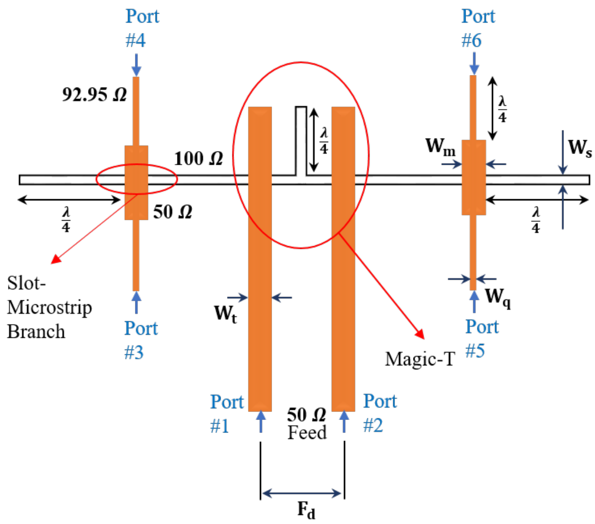

Figure 3.3: Configurations of the proposed array antenna which contains four radiating square patches, microstrip lines, quarter wave transformers, slot line. Where, W_t=W_m=2.6 mm, W_q=0.8 mm, W_s=0.2 mm, F_d =15.2 mm

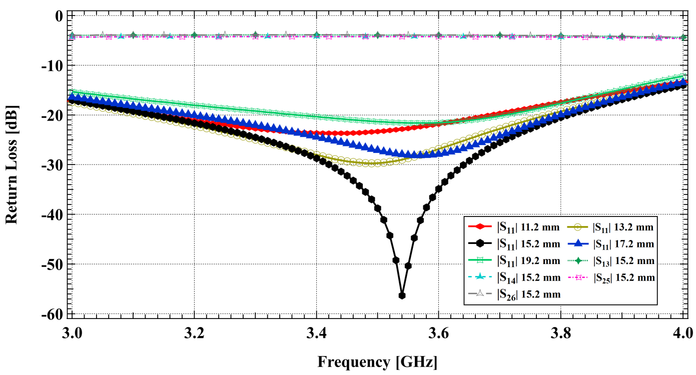

Figure 3.4: Frequency response of the feed network of the array antenna

Table 3.1: Antenna design parameters

Parameter	Value	Parameter	Value
Single patch dimension	30×30 mm^2	Substrate thickness	0.8 mm
Microstrip line width, w_t=w_m	2.6 mm	Patch thickness	0.035 mm
Slot-line width, w_s	0.2 mm	Relative dielectric constant, ϵ_r	2.15
Substrate material	Teflon glass fiber	Quarter wave transformer width, w_q	0.8 mm

3.2.3 Array operating principle

Before moving on to the explanation of the array operating concept, Figure **??** shows how a quarter wavelength stub works when input is only at port #1 in Figure 3.5(a) when input is only at port #2 in Figure 3.5(b), and when both ports have simultaneous input signal in Figure 3.5(c). The quarter wavelength slot of the T-type slot line in the ground plane allows the design to function in a Magic-T fashion. The figures gives an schematic explanation with field lines behaviour on the slot line and microstrip line to have a clear idea of the proposed antennas Magic-T operation.

Magic-T, also known as MIC 180-degree hybrid, is a signal division technique that uses both-sided MIC technology to split a signal into two equal amplitude signals that are in phase or out of phase. The quarter wavelength slot and two microstrip lines in the design of the proposed array in this paper are built in such a way that if two input signals with a phase difference are fed simultaneously with two microstrip lines and divided in such a way that in phase and out of phase signals propagate through the slot lines, as shown in Figure 3.5. The schematic electric field distribution is shown in Figures 3.5(a) and 3.5(b) when the input signal is fed to ports 1 and 2 separately.

When only port 1 receives an input signal, it propagates through the microstrip line and is divided into two equal amplitudes in-phase signals at the microstrip-slot branch, as it is a parallel power divider. The quarter wavelength stub allows the signal to be blocked from propagating to the right side of the slot lines. As a result, port 1 serves as the divider's H port. The signal propagates only to the left side along the slot line. When excited individually, port 2 also acts as an H port of the divider, as shown in Figure 3.5(b).

The microstrip lines, on the other hand, act as both H and E ports when two ports are excited simultaneously with a phase difference between them. They generate both even and odd component signals as the signal propagates between them and as they are coupled microstrip lines. This orthogonal mode signal is then fed to slot lines, which propagate a sum signal on one side and a difference signal on the other as shown in Figure 3.5(c).

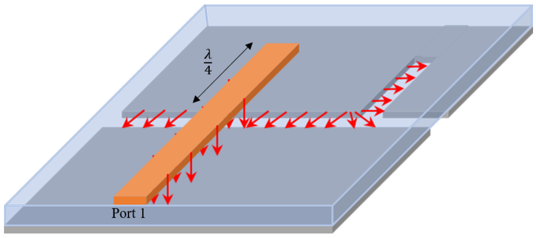

(a)

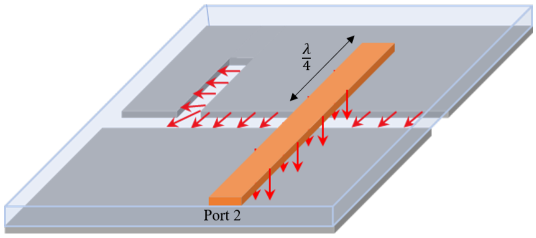

(b)

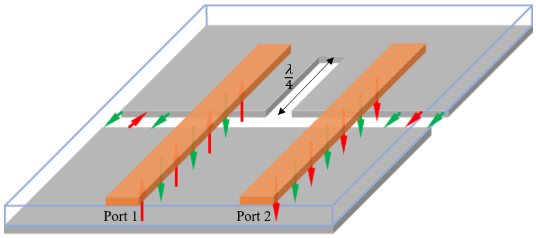

(c)

Figure 3.5: Hybrid coupler structure with schematic electric fields (a) when only port 1 is excited with an RF signal, (b) when only port 2 is excited with an RF signal, and (c) when both ports is excited with RF signals having a phase difference between them

At the microstrip-slot junction of the array, a hybrid coupler is formed by the microstrip feed lines and the T-type slot. The signal propagates on the microstrip coupling line in the orthogonal mode of the common phase component (even mode) and the reverse phase component (odd mode) when two radio frequency (RF) signals are fed to microstrip lines with a phase difference as shown in Figure 3.6. After that, the hybrid coupler is used to convert the mode to a slot line. Through a slot-microstrip branch, the signal is then fed to the antenna element. The upper and lower antenna elements are fed with equal amplitude out-of-phase signals because the slot-microstrip branch is a series power divider. So, the antenna elements on the left side and the right side are fed by twice the phase difference of that signal fed at the input point. Thus, the beam steering function is realized.

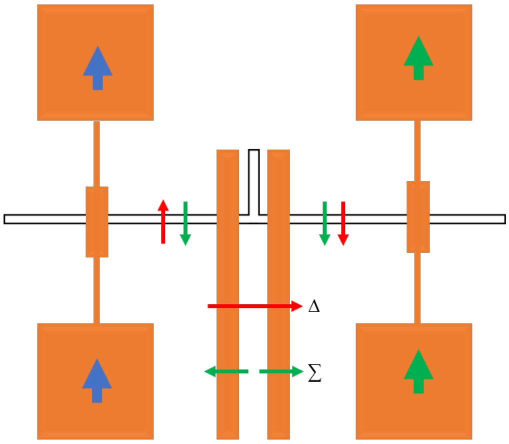

Figure 3.6: Operation principle of the proposed beam-steering array antenna

3.3 Simulated Result Analysis

The simulated outcomes and analysis of the results are presented in this section. The following paragraph examines whether the antenna design is impedance matched. The beam steering capability of the antenna is visualized by radiation patterns of the antenna in subsection 3.3.2. The next subsection describes the design's gain and directivity, followed by a comparison with other existing works.

3.3.1 Impedance matching and isolation

Figure 3.7 depicts the reflection coefficient of a beam steering array antenna. It shows the antenna has a return loss of less than -40 dB at a resonant frequency of 3.5 GHz for port 1 and port 2, indicating that impedance matching is good. It is clear from the figure that, 10 dB impedance bandwidth range is from 3.47 GHz to 3.53 GHz. Though it's a narrow bandwidth antenna but operates at the center frequency of the 5G sub-6 GHz frequency band.

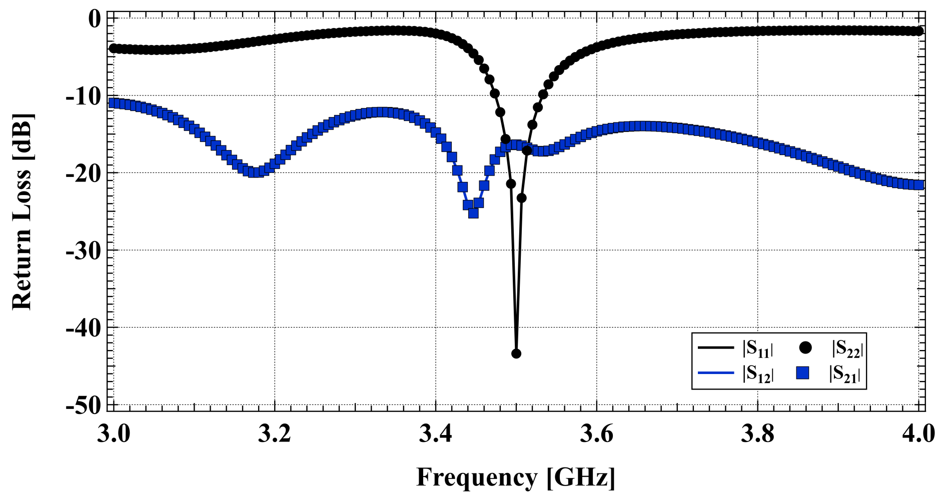

Figure 3.7: Return loss of the proposed beam-steering array antenna

The antenna also shows a good isolation between two input ports. From the Figure 3.7, it is evident that return losses of less than -10 dB are achieved by S12 and S22, ensuring good port isolation. Hence it can be said that both ports show good impedance matching and better isolation between them.

3.3.2 Radiation pattern

The 3D radiation pattern of the antenna in two cases while feeding the ports are shown in Figure 3.8 and Figure 3.9. The pattern for port 2 phase variation is shown in Figure 3.8. The phase of port 1 has been maintained, while the phase of port 2 has been increased by 15°.

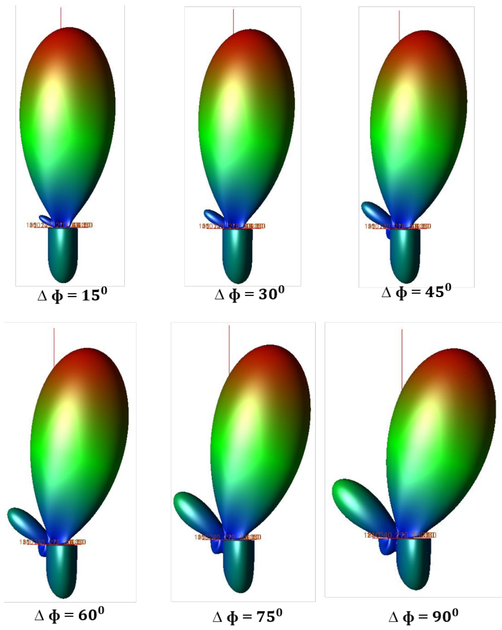

Figure 3.8: Simulated 3D radiation pattern of the proposed microstrip array antenna, when the phase of the port 2 signal is varied

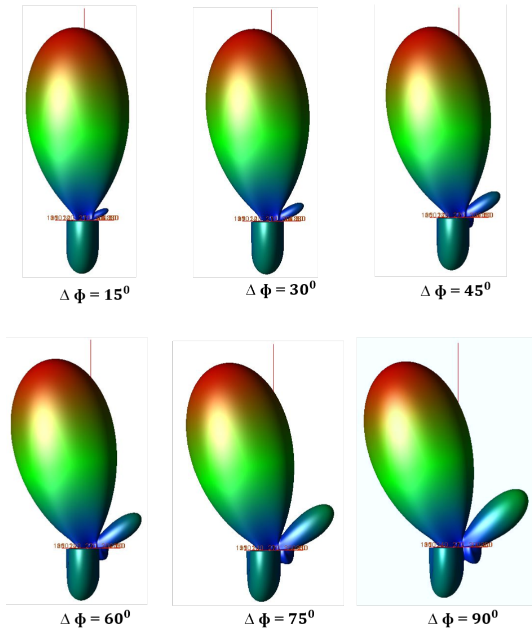

Figure 3.9: Simulated 3D radiation pattern of the proposed microstrip array antenna, when the phase of port 1 signal is varied

In the second case, the phase of port 1 has been increased by 15° while the phase of port 2 has remained unchanged shown in Figure 3.9. In both cases, the radiated beam appears to be tilted at a certain angle. The radiated beam tilts in the first case to the opposite direction in the second case, ensuring radiation along the elevation angle, as shown in the figures.

Figure 3.10 and Figure 3.11 depict the 2D radiation pattern for an antenna cut at phi=0°. Figure 3.10 depicts the radiation pattern when port 1 is fed a signal with zero-degree phase variation and port 2 is fed a signal with a certain degree of phase shift. An increment of 15° is used to change the phase of the port 2 signal. The beam tilts -17° when the phase difference between two ports is 90°. Figure 3.11 shows the pattern for a 15-degree phase shift in port 1, while the port 2 signal has no phase variation. The maximum beam tilt angle in this case is +17°. In both figures, the blue color pattern represents the pattern for a zero-phase difference between two input signals. The phase difference between two input signals is denoted in the diagram by $\Delta\Phi$.

The 2D radiation pattern for a 90-degree phi cut is shown in Figure 3.12. Because beam steering for this proposed design occurred along an elevation angle, it clearly shows that there is no tilting in the pattern. As a result, when the main beam is tilted, the pattern intensity decreases along the zero degree of the plot for phi=90-degree cut.

3.3.3 Directivity and gain analysis

The proposed antenna's directivity in the phi=0-degree plane and phi=90-degree plane are shown in Figure 3.13 and Figure 3.14 respectively. The curve has a shift in the theta axis for the phase difference between two equal amplitude signals fed to ports 1 and 2, but the main lobe directivity remains nearly 25 dB. The curves for the phase difference between ports are shown in Figure 3.13, where the maximum directivity is at -17° for a 90-degree phase difference between two signals when the port 1 signal has a zero-degree phase shift. And has a maximum directivity at +17° for a 90-degree phase difference between two input signals when the port 2 signal has a zero-degree phase shift while the port 1 signal's phase is increased at a step of 15°. From Figure 3.14, it is visisble that the amplitude only decreases along phi = 90°, indicating steering of beam only hapens along phi = 0°.

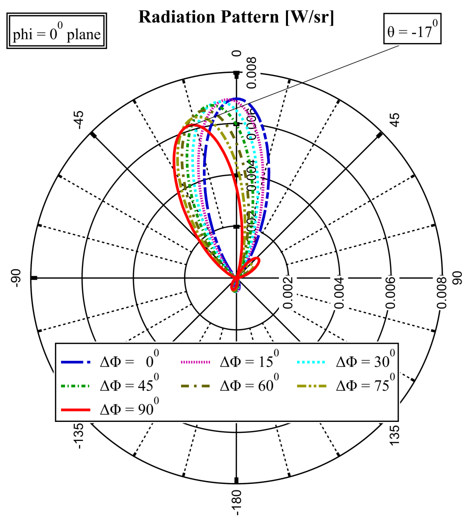

Figure 3.10: Simulated 2D radiation pattern of the array antenna for phi=0° plane, when the phase of port 2 signal is varied

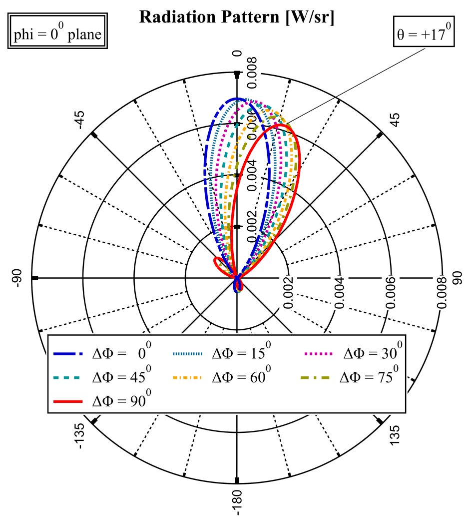

Figure 3.11: Simulated 2D radiation pattern of the array antenna for phi=0° plane, when the phase of port 1 signal is varied

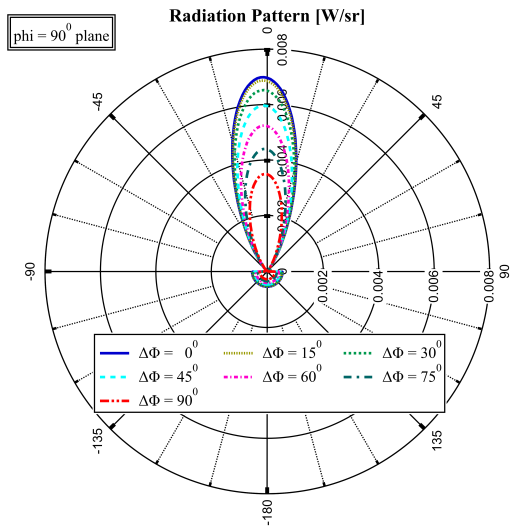

Figure 3.12: 2D Radiation pattern of the array antenna for phi=90° plane

The gain of the proposed antenna array is shown in Figure 3.15 and Figure 3.16 for phi=0 degree and phi=90° plane respectively. The main beam can be steered from -17° to +17° for a maximum phase difference of 90° between two input signals while keeping the side lobe (SL) gain below 10 dB, as shown in Figure 3.15.

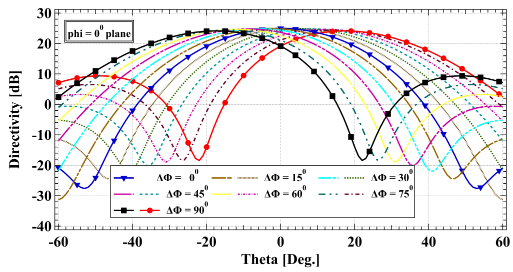

Figure 3.13: Directivity of the proposed array antenna for phi=0° plane

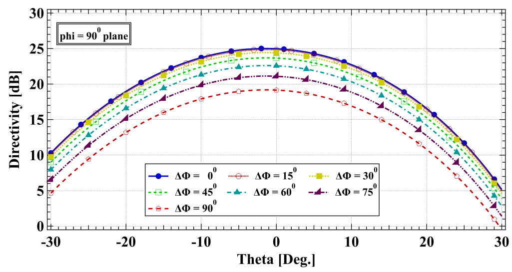

Figure 3.14: Directivity of the proposed array antenna for phi=90° plane

From Figure 3.16, it can be seen that all the gain curve has a maximum for several phase difference between two input signals. It confirms that beam steering occurs only in the phi=0-degree plane. Figure 3.17 shows the gain curve in dBi versus frequency. At the resonant frequency of the antenna array, the gain is 12.5786 dBi, as shown in the figure. This means the array antenna has a high gain in the operating frequency.

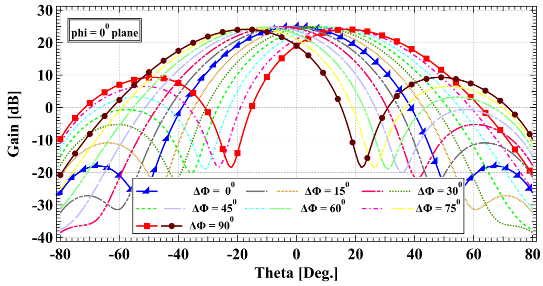

Figure 3.15: Gain of the proposed array antenna for phi=0° plane

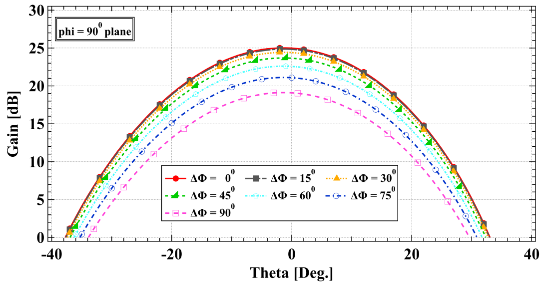

Figure 3.16: Gain of the proposed array antenna for phi=90° plane

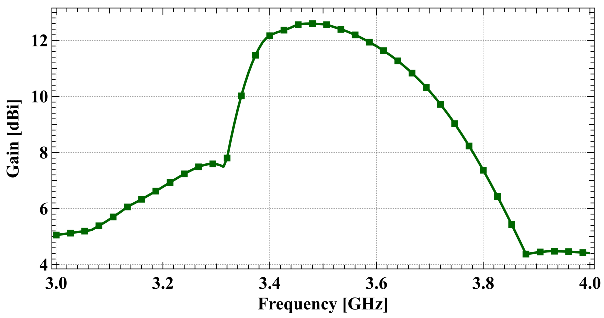

Figure 3.17: Gain of the array antenna versus frequency

Table 3.2 shows the overall radiation pattern, which includes gain, directivity, and the maximum angle of beam steering, as determined by the phase difference between two input signals. The proposed array antenna has a gain of about 13 dBi at a resonant frequency of 3.5 GHz, as shown in the table. It is possible to achieve maximum beam steering of $-17°$ to $+17°$.

Table 3.2: Radiation pattern data analysis of the array antenna.

Φ_1	Φ_2	Gain (dBi)	Directivity (dBi)	Gain (dB)	SL Gain (dB)	Directivity (dB)	Θ_{Max}
0°	0°	12.5786	12.5786	25.111	-16.729	25.111	0°
0°	15°	12.5688	12.5688	25.089	-10.025	25.089	-3°
0°	30°	12.5381	12.5381	25.023	-4.677	25.023	-6°
0°	45°	12.4809	12.4831	24.903	-0.274	24.903	-9°
0°	60°	12.3827	12.4011	24.704	+2.966	24.741	-11°
0°	75°	12.2526	12.29	24.436	+6.537	24.551	-14°
0°	90°	12.0844	12.1424	24.090	+9.48	24.206	-17°
15°	0°	12.5688	12.5688	25.089	-10.025	25.089	+3°
30°	0°	12.5381	12.5381	25.023	-4.677	25.023	+6°
45°	0°	12.4809	12.4831	24.903	-0.274	24.903	+9°
60°	0°	12.3827	12.4011	24.704	+2.966	24.741	+11°
75°	0°	12.2526	12.29	24.436	+6.537	24.551	+14°
90°	0°	12.0844	12.1424	24.090	+9.48	24.206	+17°

3.3.4 Comparison with other works

Table 3.3 presents a comparison of various previous works that use microstrip patches for beam steering. The table clearly shows that this work has the best steering angle among the others. Some of them, among others, use diodes, which require switching operations to operate beam steering and using diodes in an antenna circuit requires biasing, which can compromise antenna performance in terms of impedance matching. Some of them necessitate an external feed circuit, which complicates the design. Despite the fact that one of the compared works has a greater steer angle than this work, this proposed work outperforms the other antenna parameter by having a high gain and excellent impedance matching performance.

Table 3.3: Performance comparison of the proposed microstrip array antenna with other works

Reference	Array element no	Gain (dBi)	Return loss	Use of diodes	Max steered angle
[8]	1×2	-	-23 dB	No	27°
[9]	1×2	-	-19 dB	No	15°
[11]	1×8	-	<-10 dB	No	17°
[13]	1×4	6.39	-33 dB	Yes	14°
[14]	1×4	10.98	-27 dB	No	10°
[This work]	2×2	> 12	-43 dB	No	17°

3.4 Summary

This chapter presents the design and analysis of a beam-switching microstrip array antenna employing double-sided MIC technology. The suggested array antenna provides a significant increase in gain and directivity, measuring around 13 dBi. This array antenna achieves a beam switching capacity ranging from $-17°$ to $+17°$. The antenna exhibits a favorable input impedance at the central frequency of 3.5 GHz inside the sub-6 GHz frequency range.

Chapter 4

Machine Learning Based Prediction

This chapter provides an in-depth exploration of how machine-learning techniques are utilized to predict the performance of microstrip patch array antennas. It describes preparing the dataset, selecting appropriate machine learning models, tuning hyperparameters, evaluating model performance, analyzing feature importance, and predicting performance.

4.1 Introduction to Machine Learning-Based Antenna Prediction

Machine learning has emerged as a powerful tool for addressing the complexities associated with antenna design, particularly in reducing the computational costs and time required for iterative simulations [50, 51, 54]. Traditional methods often rely on manual parameter tuning and exhaustive simulations, which are both time-consuming and resource-intensive. Machine learning models provide a significant advantage by predicting key performance metrics such as return loss, gain, bandwidth, and directivity, effectively bridging the gap between initial design and performance evaluation without solely depending on electromagnetic simulation software [56, 57]. These models are adept at capturing the non-linear relationships between design parameters and performance, making them highly suitable for optimizing antenna characteristics [53, 54].

4.2 Dataset Preparation and Preprocessing

4.2.1 Dataset Generation

The dataset for this study was generated by varying the design parameters of an initial microstrip patch antenna designed in ADS (Advanced Design System). Figure 4.1 shows the geometry of the antenna used, which provides a visual reference for the design parameters being varied. Table 4.1 lists the initial antenna design parameters, including dimensions such as patch size, transmission line length, and slot-line dimensions. To create a dataset suitable for machine learning, multiple parameters were varied systematically over specific ranges, as shown in Table 4.2. The dataset captures the effect of different combinations of these parameters on the antenna's return loss (S11) between 3 GHz and 4 GHz, providing a comprehensive dataset for model training and evaluation. The generated dataset contains 944 samples, each with 11 design features and 101 corresponding output values representing the S11 response at different frequencies.

Table 4.1: Antenna design parameters

Parameter	**Value**	**Parameter**	**Value**
Single patch dimension, WL_sp	30×30 mm^2	Substrate thickness	0.8 mm
Microstrip line width, W_t=W_m	2.6 mm	Patch thickness	0.035 mm
Slot-line width, W_s	0.2 mm	Relative dielectric constant, ϵ_r	2.15
Substrate material	Teflon glass fiber	Quarter wave transformer width, W_q	0.8 mm
Length of transmission line, L_t	19.5 mm	Length of the stub, L_{stub}	16.1 mm
Feed distance, F_d	15.2 mm	Feed to patch distance, P_d	18.9 mm
Slot-line length, L_s	18 mm	Quarter wave transformer length, L_q	16.5 mm

4.2.2 Feature and Target Splitting

The dataset was divided into features (input parameters) and targets (output values) for training the machine learning models. The input feature matrix for this study can be represented as $X = [x_1, x_2, \ldots, x_{11}] \in \mathbb{R}^{n\times 11}$, where each feature x_i corresponds to one of the antenna design parameters listed in Table 4.2.

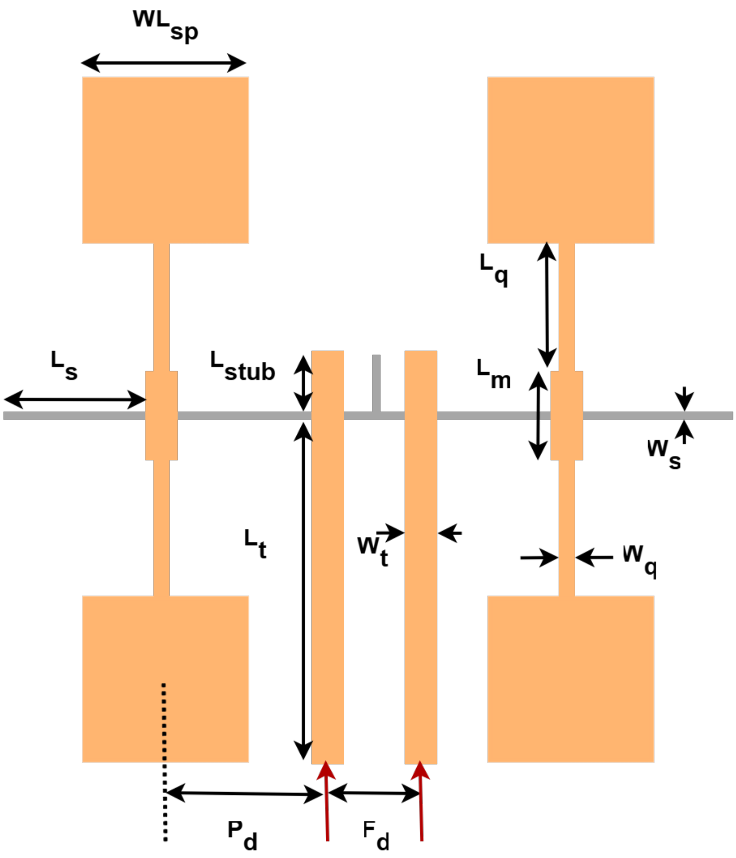

Figure 4.1: Antenna geometry illustrating the key design parameters used in dataset generation.

Table 4.2: Antenna design parameter variation

Variable Name (mm)	**Variation Range**	**Variation Step (mm)**	**No. of Data Points**
L_t	15.0 - 60.0	0.30	151
L_{stub}	15.0 - 30.0	0.10	151
W_t	2.0 - 4.0	0.10	21
F_d	15.0 - 25.0	0.10	101
P_d	18.0 - 30.0	0.10	121
L_m	12.0 - 20.0	0.10	81
W_q	0.2 - 1.0	0.10	9
L_q	15.0 - 20.0	0.10	51
W_s	0.1 - 0.3	0.05	4
L_s	15.0 - 20.0	0.10	51
WL_sp	20.0 - 40.0	0.10	201

The target variable matrix is denoted by $Y = [y_1, y_2, \ldots, y_{101}] \in \mathbb{R}^{n\times101}$, where each target y_i represents the return loss (S11) value at a specific frequency point

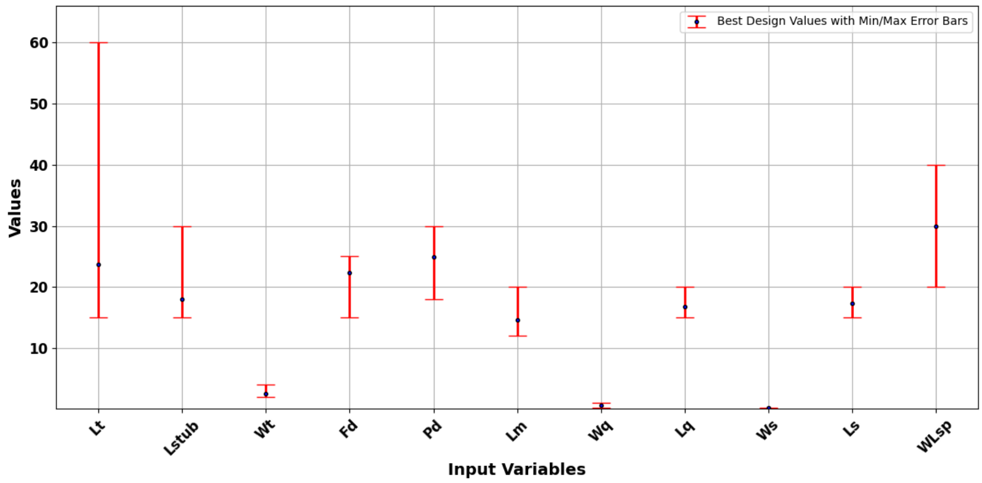

Figure 4.2: Best design values of input variables with min/max error bars, showing the variability and range of parameters used in the dataset generation.

between 3 GHz and 4 GHz. The goal is to establish a mapping $f : X \rightarrow Y$, which predicts the S11 response given the antenna design parameters.

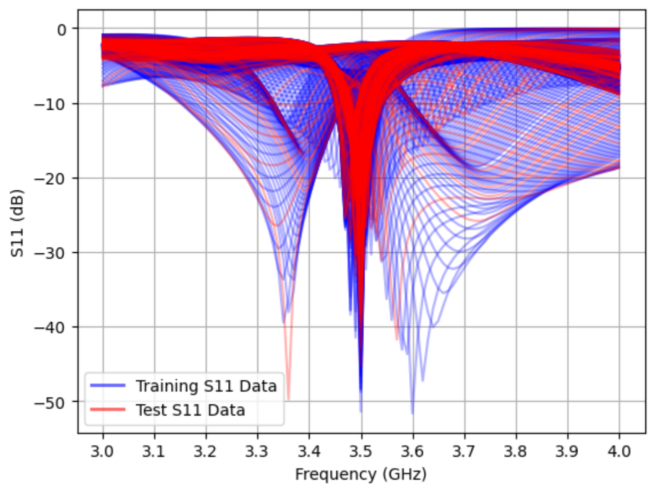

Figure 4.3: Visualization of S11 data for training and testing sets across frequencies from 3 GHz to 4 GHz, highlighting the range of responses captured in the dataset.

4.2.3 Train-Test Split

The dataset was split into training and testing sets to evaluate model performance effectively. Specifically, the feature matrix X and target matrix Y were divided into training sets $X_{\text{train}}, Y_{\text{train}}$ and testing sets $X_{\text{test}}, Y_{\text{test}}$ with an 80:20 ratio. Mathematically, this can be represented as follows:

$$X_{\text{train}}, Y_{\text{train}}, X_{\text{test}}, Y_{\text{test}} = \text{train\_test\_split}(X, Y, \text{test\_size} = 0.2, \text{random\_state} = 42)$$

Stratified sampling was employed to ensure that the distribution of the stratification labels representing different parameter ranges was maintained in both sets. The training and testing distributions are summarized in Table 4.3. This stratified approach helps maintain consistency across the train and test datasets, providing a balanced representation of different parameter combinations.

Table 4.3: Train-Test split summary

Dataset	**Number of Samples**
Training Set	755
Testing Set	189

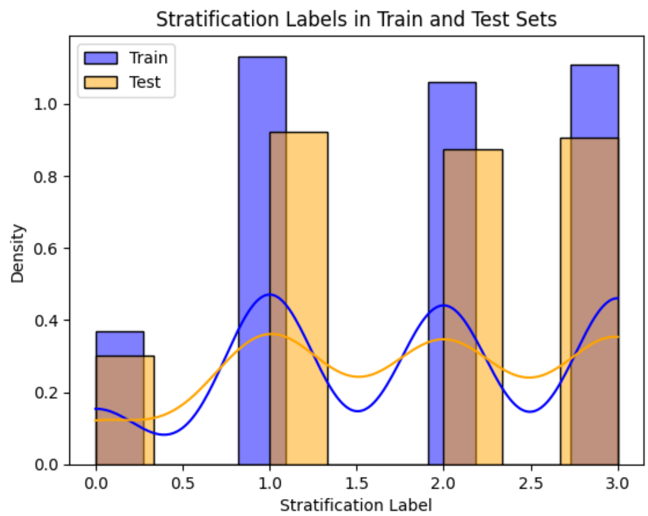

Figure 4.4: Visualization of stratification labels in training and testing sets to ensure balanced representation of parameter distributions.

4.3 Model Results

4.3.1 Model Performance Summary

This section presents the performance results of various machine learning models for predicting the microstrip patch antenna's return loss (S11). The models were evaluated using different metrics, including MAE, MSE, MSLE,RMSLE, MAPE, R^2, and Variance Score. Table 4.4 provides a summary of the numerical performance of each model.

Table 4.4: Performance of machine learning models

Algorithm	**MAE**	**MSE**	**MSLE**	**RM-SLE**	**MAPE**	**R-Square**	**Var Score**
Random Forest Regression	**6.52**	**10.32**	**0.044**	**2.09**	**0.96**	**99.44**	98.44
Decision Tree Regression	9.65	15.91	0.072	2.68	1.43	99.01	98.55
XGB Regression	10.95	20.66	0.103	3.21	1.70	98.71	97.66
Gaussian Process Regression	7.84	21.49	0.148	3.85	1.24	99.18	**99.85**
Ridge Regression	126.41	776.19	11.16	33.41	46.14	32.79	27.40
Bayesian Linear Regression	126.67	778.64	11.15	33.39	45.89	32.58	26.14
Linear Regression	126.74	778.92	11.19	33.45	46.21	32.75	27.46
Lasso Regression	143.07	836.87	12.63	35.55	50.29	20.86	11.54

Figures 4.5, 4.6, and 4.7 provide visual comparisons of the models based on key metrics such as MAE, Variance Score, and R-Square.

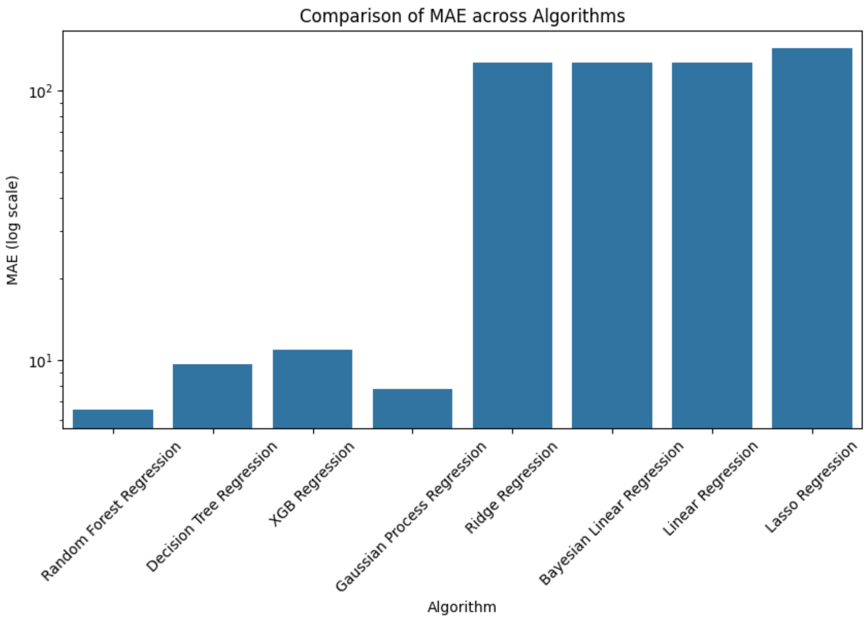

Figure 4.5: Comparison of MAE across different algorithms. Random Forest Regression achieved the lowest MAE, indicating the best performance in minimizing absolute errors.

The performance results show distinct differences between the models:

- **Random Forest Regression**: This model demonstrated the best overall

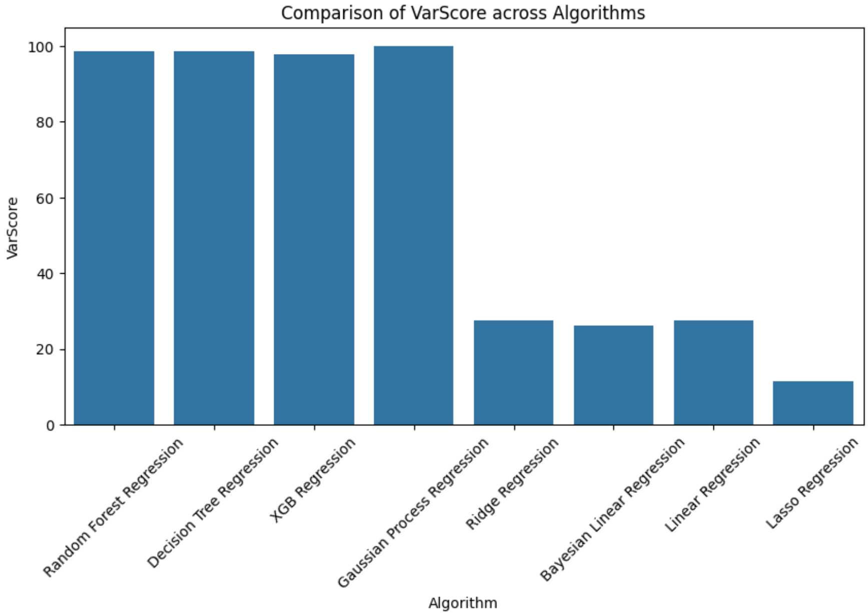

Figure 4.6: Comparison of Variance Score across algorithms. Gaussian Process Regression had the highest variance score, effectively capturing the variability in the data.

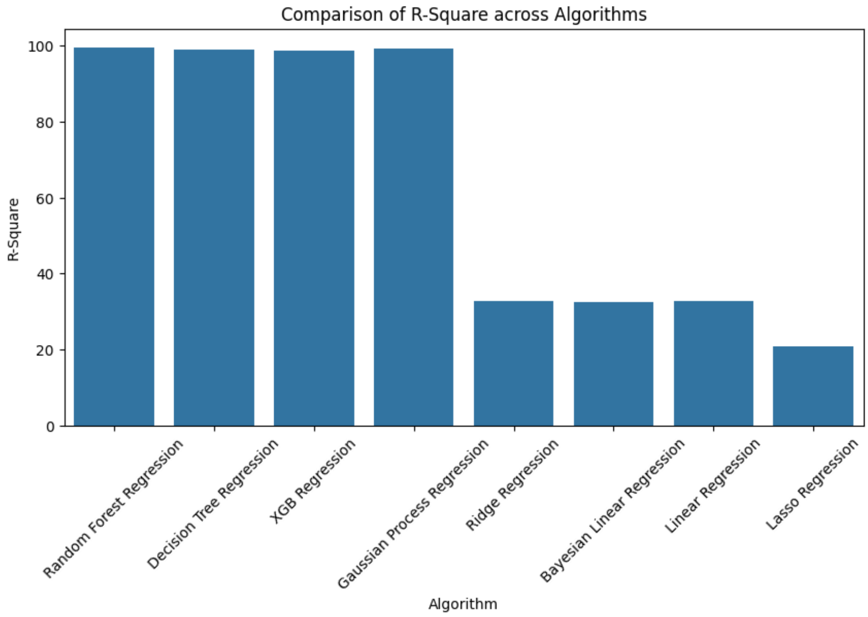

Figure 4.7: Comparison of R-Square values across algorithms. Random Forest and Gaussian Process Regression exhibited high R^2 values, suggesting a strong correlation between predicted and true values.

performance, achieving the lowest MAE of 6.52 and a high R^2 value of 99.44. The ensemble nature of Random Forest allows it to handle non-linear relationships effectively, which contributes to its superior predictive accuracy.

- **Decision Tree and XGB Regression**: Decision Tree Regression showed a reasonable performance with a slightly higher MAE compared to Random Forest. XGB Regression, although more computationally intensive, had similar performance but was less accurate in minimizing error metrics such as RMSLE and MAPE.

- **Gaussian Process Regression**: This model provided good results, with a high Variance Score of 99.85 and high R^2 of 99.18, indicating its strong ability to capture data variability. However, its MAE was higher than Random Forest's, suggesting it might have had more difficulties with smaller errors.

- **Ridge, Linear, and Bayesian Linear Regressions**: These models struggled significantly compared to ensemble methods, with high MAE, MSE, and MAPE values. The poor performance of these models suggests that the linearity assumption does not adequately represent the complex relationships between the input parameters and the S11 response.

- **Lasso Regression**: Lasso Regression performed the worst among all models, with the highest MAE (143.07) and the lowest R^2 (20.86). The model's L1 regularization might have been too restrictive, leading to underfitting.

The visual comparisons in Figures 4.5, 4.6, and 4.7 support these findings, with Random Forest Regression consistently outperforming the other models across key metrics. Gaussian Process Regression also performed well but was slightly less consistent in minimizing absolute errors compared to Random Forest. On the other hand, linear models failed to capture the complexities in the dataset, leading to significantly worse performance.

The results highlight the advantage of using ensemble methods like Random Forest and boosting methods like XGB for complex non-linear problems such as predicting antenna return loss, where the relationships between parameters are intricate and highly non-linear.

4.4 Hyperparameter Tuning Approaches

4.4.1 Grid Search

Grid search is a traditional and exhaustive hyperparameter tuning approach, where a predefined range of hyperparameters is provided, and all possible combinations are evaluated. This method systematically searches through the parameter grid and identifies the combination that yields the best performance based on a chosen evaluation metric. Although computationally intensive, grid search is effective in finding the optimal hyperparameter settings for the machine learning models.

Mathematically, given a parameter grid $\mathcal{P}$ with hyperparameters, $p_1, p_2, \ldots, p_k$, the goal of grid search is to find:

$$\hat{p} = \arg\min_{p \in \mathcal{P}} L(\theta_p)$$

where, $L(\theta_p)$ represents the loss function for model parameters θ_p under hyperparameter setting p.

In this study, the best parameters obtained using grid search are shown in Table 4.5. The corresponding model performance results using these parameters are presented in Table 4.6.

Table 4.5: Best parameters from grid search for each model

Algorithm	**Parameter**	**Value**
Random Forest Regression	n_estimators	300
	bootstrap	True
	min_samples_split	2
	min_samples_leaf	1
Decision Tree Regression	max_depth	50
	min_samples_split	2
	min_samples_leaf	1
XGB Regression	max_depth	10
	n_estimators	100
	learning_rate	0.05
	colsample_bytree	1.0

Table 4.6: Model performance using grid search

Algorithm	**MAE**	**MSE**	**MSLE**	**RMSLE**	**MAPE**	**R-Square**
Random Forest Regression	6.53	10.27	0.042	2.06	0.95	99.45
Decision Tree Regression	9.65	15.20	0.072	2.68	1.45	99.02
XGB Regression	12.67	24.77	0.110	3.32	2.32	98.79

4.4.2 Randomized Search

Randomized search offers a more efficient alternative to grid search by sampling a fixed number of hyperparameter combinations from the parameter grid. Instead of exhaustively exploring every possible combination, randomized search selects random combinations, which can be advantageous when the parameter space is large. This reduces computational time significantly while still allowing the exploration of a diverse set of hyperparameters.

Mathematically, randomized search can be described as selecting n random combinations from the parameter grid $\mathcal{P}$, instead of evaluating every possible combination:

$$\hat{p} = \arg \min_{p \in \{p_1, p_2, \ldots, p_n\}} L(\theta_p)$$

The best parameters found using randomized search are shown in Table 4.7, and their performance is presented in Table 4.8.

Table 4.7: Best parameters from randomized search for each model

Algorithm	Parameter	Value
Random Forest Regression	n_estimators	300
	max_depth	30
	bootstrap	True
Decision Tree Regression	max_depth	50
	min_samples_split	2
	min_samples_leaf	1
XGB Regression	max_depth	7
	n_estimators	100
	learning_rate	0.1

Table 4.8: Model performance using randomized search

Algorithm	MAE	MSE	MSLE	RMSLE	MAPE	R-Square
Random Forest Regression	7.63	16.06	0.052	2.29	1.15	99.37
Decision Tree Regression	9.65	15.26	0.072	2.68	1.45	99.02
XGB Regression	12.18	23.86	0.112	3.35	2.18	98.82

4.4.3 Final Parameter Selection and Analysis

After analyzing both grid search and randomized search results, the best parameter combinations were selected by evaluating their performance across all metrics. The final parameter settings for each model are summarized in Table 4.9, and the corresponding performance results are provided in Table 4.10.

Table 4.9: Final best parameters for each model

Algorithm	**Parameter**	**Value**
Random Forest Regression	n_estimators	300
	max_depth	None
	min_samples_split	2
	min_samples_leaf	1
	bootstrap	True
Decision Tree Regression	max_depth	50
	min_samples_split	2
	min_samples_leaf	1

Table 4.10: Final model performance results

Algorithm	**MAE**	**MSE**	**MSLE**	**RMSLE**	**MAPE**	**R-Square**
Random Forest Regression	**6.53**	**10.27**	**0.042**	**2.06**	**0.95**	**99.45**
Decision Tree Regression	9.65	15.20	0.072	2.68	1.45	99.02

The hyperparameter tuning process highlighted the impact of various hyperparameters on model performance. For instance, the depth of the tree-based models (e.g., max_depth) directly influenced the complexity of the model and its ability to capture intricate patterns in the data. A higher value of max_depth allowed the model to better capture non-linear relationships, but it also increased the risk of overfitting. Parameters like min_samples_split and min_samples_leaf played a critical role in controlling the growth of the trees, thereby preventing overfitting and improving generalizability.

For Random Forest and XGB models, the number of estimators (n_estimators) was an important hyperparameter, determining the number of decision trees used in the ensemble. A larger number of estimators generally led to better performance due to improved averaging, but at the cost of increased computation time. Similarly, the learning rate in XGB Regression (learning_rate) had a significant impact on convergence, where a lower learning rate ensured a more stable training process but required more iterations.

Overall, the hyperparameter tuning process using both grid and randomized search yielded significant improvements in model performance compared to default settings. Random Forest Regression emerged as the best model across various metrics, demonstrating the importance of ensemble methods in handling complex, non-linear datasets.

4.5 Feature Importance Analysis

4.5.1 Importance of Design Parameters

The feature importance analysis was conducted using various machine learning models, including Random Forest, Decision Tree, XGB Regression, Ridge Regression, Lasso Regression, and Linear Regression. Each model's respective method for feature importance calculation was employed. For tree-based models like Random Forest and Decision Tree, the importance is derived from the reduction in impurity (e.g., Gini impurity) across splits involving that feature (using `feature_importances_` attribute). For linear models such as Ridge and Lasso Regression, the feature importance was estimated based on the magnitude of the coefficients (using `coef_` attribute).

Figure 4.8 shows the importance of each feature across different models. The feature importance values were extracted using a custom function, which handled both tree-based models (using `feature_importances_`) and linear models (using `coef_`). This analysis allows us to understand which design parameters significantly impact the antenna's performance.

$$\text{Feature Importance (Tree Models)} = \sum_{t=1}^{T} \Delta I_t(f), \quad f \in \text{features} \tag{4.1}$$

$$\text{Feature Importance (Linear Models)} = \beta_j, \quad j \in \{1, \ldots, p\} \tag{4.2}$$

The parameter variations in the dataset were systematically designed to cover a wide range of possible antenna configurations. Each feature's range and step size were carefully selected to ensure a comprehensive exploration of the design space. The following equation represents the variation of each feature [68]:

$$x_{i,j} = x_{i,\min} + j\Delta x_i, \quad j = 0, 1, \ldots, N_i - 1, \quad i \in \{1, \ldots, m\} \tag{4.3}$$

where $x_{i,j}$ represents the value of feature i at step j, $x_{i,\min}$ is the minimum value of feature i, Δx_i is the step size, and N_i is the number of steps for feature i. This equation helps in systematically varying the input parameters during the dataset generation process.

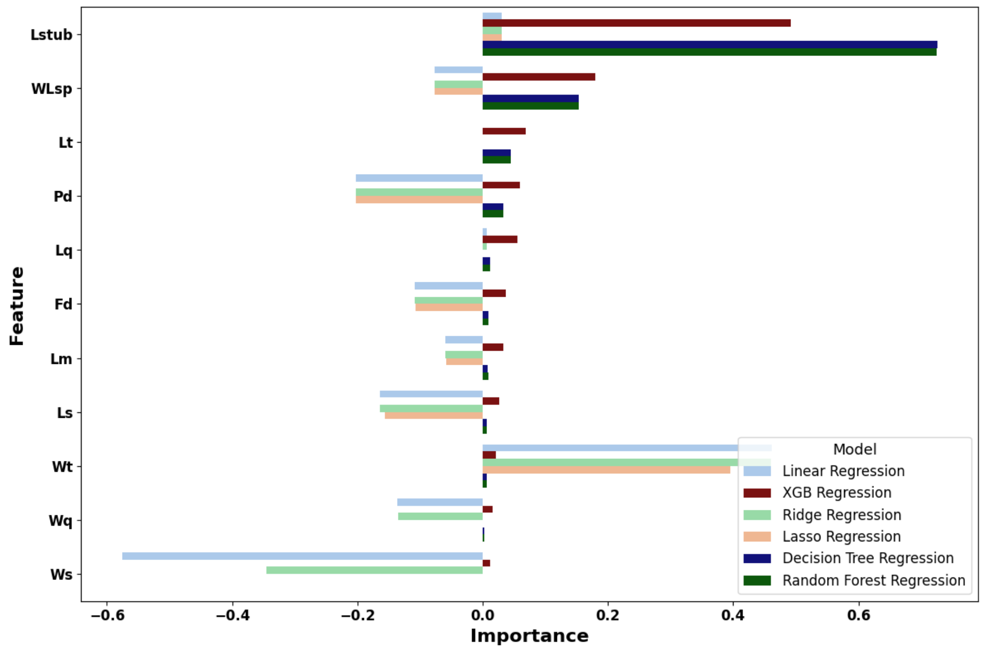

Figure 4.8: Feature importance values across different machine learning models. The bar chart shows the impact of each feature (design parameter) on the model predictions, providing insight into which features are most influential.

4.5.2 Impact of Features on Antenna Performance

The feature importance analysis offers valuable insights into how different design parameters influence antenna performance, particularly the return loss (S11) at 3.5 GHz. Below, we elaborate on the impact of the most influential features based on the analysis, supported by visualizations.

- **Stub Length (L_{stub})**: The feature importance study indicates that stub length is one of the most influential parameters. Variations in L_{stub} lead to significant changes in the return loss (S11) values. A properly tuned L_{stub} helps achieve optimal impedance matching, minimizing the return loss at 3.5 GHz. The data reveals that specific values of L_{stub} result in sharper dips in S11, indicating resonance and better matching. The impedance at the input of the stub can be represented as [69]:

$$Z_{in} = jZ_0 \tan\left(\frac{2\pi L_{stub}}{\lambda}\right) \tag{4.4}$$

where Z_0 is the characteristic impedance and λ is the wavelength. Figure 4.9 illustrates the impact of different L_{stub} values on the S11 response.

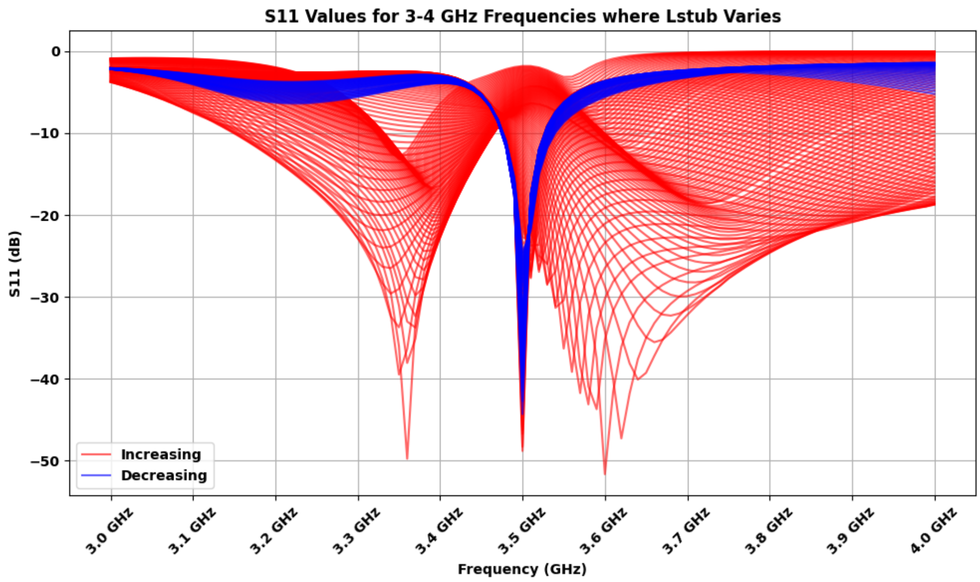

Figure 4.9: S11 values for 3-4 GHz frequencies with varying L_{stub}.

- **Patch Width (WL_{sp}):** Patch width (WL_{sp}) is another key parameter highlighted in the feature importance analysis. Increasing WL_{sp} generally leads to a shift in the resonant frequency and a broader bandwidth. This is evident in the S11 response, where wider patches tend to decrease the return loss across a broader frequency range, thus improving bandwidth performance. The resonant frequency is given by [9]:

$$f_r = \frac{c}{2WL_{sp}\sqrt{\epsilon_r}} \tag{4.5}$$

where c is the speed of light and ϵ_r is the relative dielectric constant of the substrate. Figure 4.10 shows the S11 response for varying WL_{sp}, indicating a shift in resonance as the width changes.

- **Transmission Line Length (L_t):** The length of the transmission line (L_t) plays a crucial role in impedance matching. Changes in L_t have a direct impact on the reflection coefficient and, consequently, on S11. A properly tuned L_t minimizes reflections and improves energy transfer, which is reflected in the reduced S11 values for certain lengths. The reflection coefficient is given by [69]:

$$\Gamma = \frac{Z_{in} - Z_0}{Z_{in} + Z_0} \tag{4.6}$$

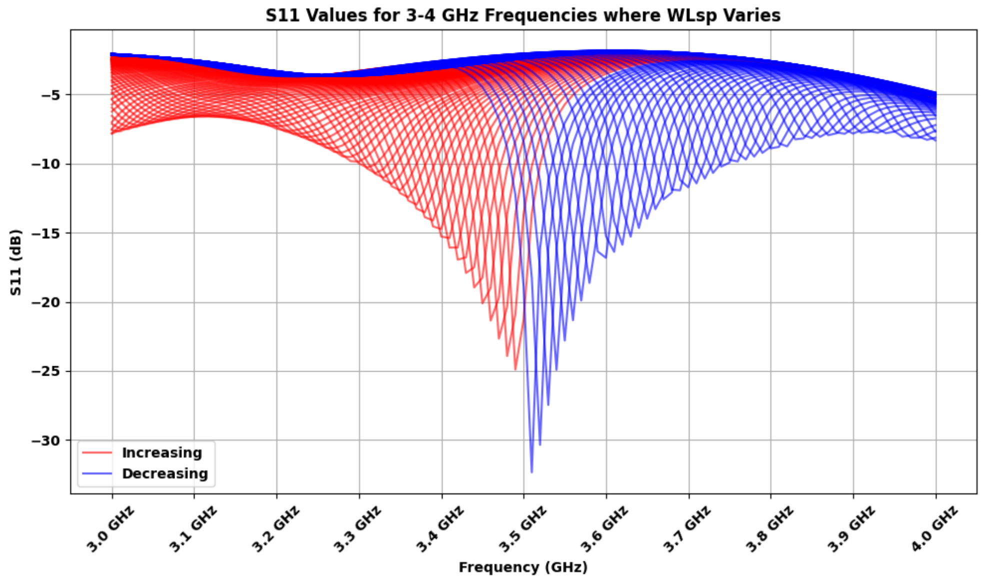

Figure 4.10: S11 values for 3-4 GHz frequencies with varying WL_{sp}.

where Z_{in} is the input impedance and Z_0 is the characteristic impedance of the transmission line. Figure 4.11 presents the effect of different L_t values on the S11 response.

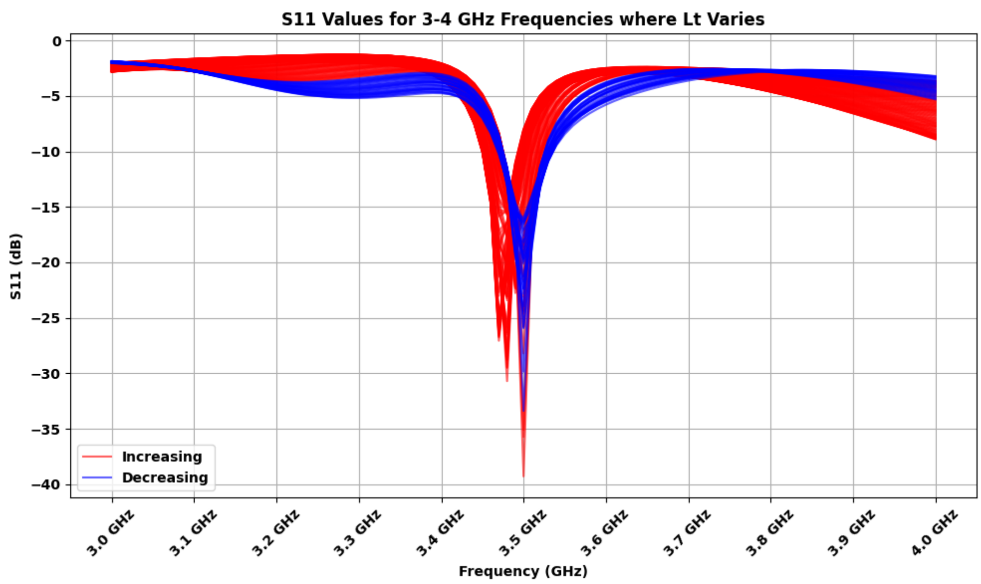

Figure 4.11: S11 values for 3-4 GHz frequencies with varying L_t.

- **Slot Width (W_s)**: The slot width (W_s) has been identified as an important feature, particularly for its effect on current distribution and impedance bandwidth. Narrower slot widths tend to increase the return loss, whereas wider slots improve impedance matching and reduce S11, resulting in a broader bandwidth. The input impedance of the slot can be approximated as [68]:

$$Z_{slot} \propto \frac{1}{W_s} \tag{4.7}$$

Figure 4.12 shows how the S11 response changes for different values of W_s.

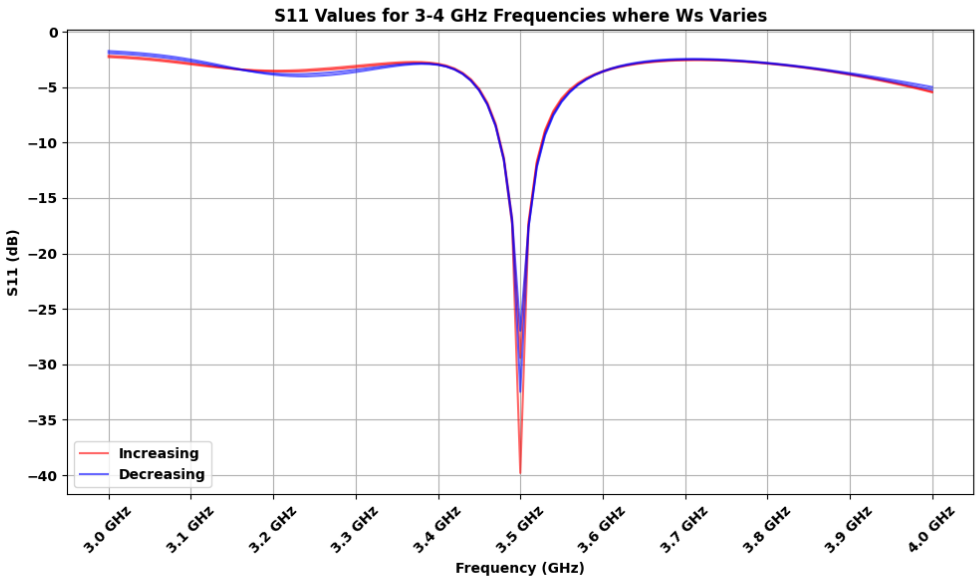

Figure 4.12: S11 values for 3-4 GHz frequencies with varying W_s.

- **Feed Distance (F_d)**: The feed distance (F_d) directly impacts the excitation of the patch and hence the impedance matching. Adjusting F_d influences the S11 values significantly. Optimal feed positions result in better impedance matching, reducing the return loss at the target frequency. The relationship between Z_{in} and F_d can be represented as [69]:

$$Z_{in} = Z_0 \left(1 + \frac{j\omega L}{1 - \omega^2 LC}\right) \tag{4.8}$$

  where L and C are the inductance and capacitance associated with the feed point. Figure 4.13 illustrates the effect of different F_d values on S11.

The feature importance study highlights these parameters' critical role in determining antenna performance. Careful tuning of these features can substantially improve return loss and overall efficiency.

4.5.3 Summary of Top Influential Features

The trend analysis reveals that features with higher importance scores generally have a greater impact on the return loss, thus validating the feature importance

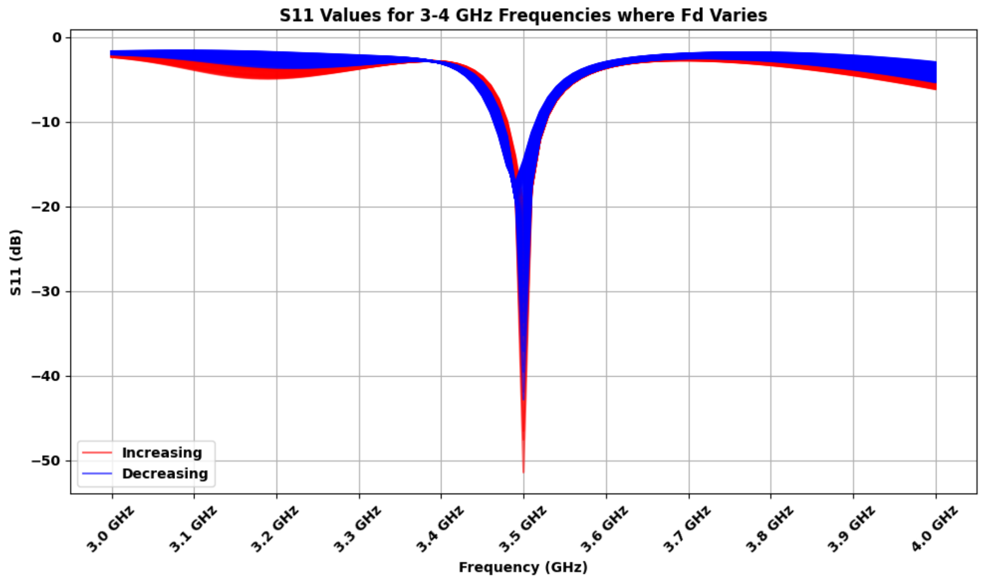

Figure 4.13: S11 values for 3-4 GHz frequencies with varying F_d.

findings. The top influential features identified include:

- **Stub Length** (L_{stub}): Critical for impedance tuning, directly impacting return loss minimization.
- **Patch Width** (WL_{sp}): Influences resonant frequency and bandwidth, impacting both return loss and antenna efficiency.
- **Transmission Line Length** (L_t): Affects impedance matching, ensuring minimal reflections and better energy transfer.
- **Slot Width** (W_s): Impacts current distribution, resonant frequency, and impedance bandwidth.
- **Feed Distance** (F_d): Crucial for optimal excitation and impedance matching, reducing return loss.

These features are key in optimizing antenna performance, especially in reducing return loss and enhancing efficiency.

4.6 Residual Analysis

4.6.1 Residual Plots

Residual plots are a key diagnostic tool used to assess the fit of a regression model by plotting the residuals (the differences between observed and predicted values) against the predicted values. Ideally, the residuals should be randomly scattered around zero, indicating that the model captures the underlying data pattern well and that there are no systematic errors.

The residuals can be mathematically calculated as follows:

$$r_{i,\text{train}} = y_{i,\text{train}} - \hat{y}_{i,\text{train}}, \quad i = 1, \dots, n \tag{4.9}$$

where r_i represents the residual for the i-th data point, y_i is the observed value, and $\hat{y}_i$ is the predicted value.

Figures 4.14 to 4.19 show the residual plots for different regression models used in this study, including XGB Regression, Ridge Regression, Lasso Regression, Decision Tree Regression, Random Forest Regression, and Linear Regression.

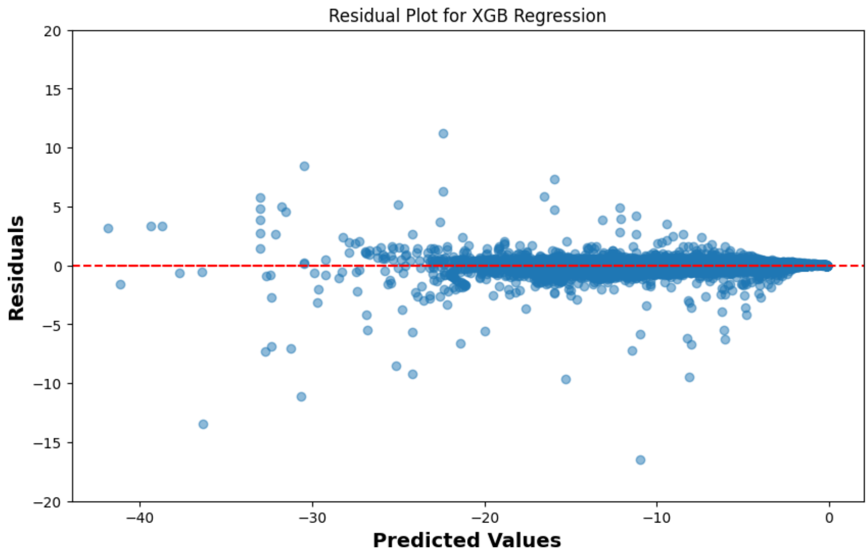

Figure 4.14: Residual Plot for XGB Regression. The residuals are mostly scattered around zero, indicating a good model fit with minimal bias. The XGB model shows low variance in the residuals, suggesting it captures the data pattern well.

4.6.2 Residual Histogram

The residual histogram is used to assess whether the residuals are approximately normally distributed, which is an assumption of many regression models. Ideally, the histogram should resemble a normal distribution centered around zero.

The residuals can be represented in a histogram to visualize their distribution:

$$f(r_{\text{train}}) = \frac{1}{n} \sum_{i=1}^{n} I(r_{i,\text{train}} \in \text{bin range}) \tag{4.10}$$

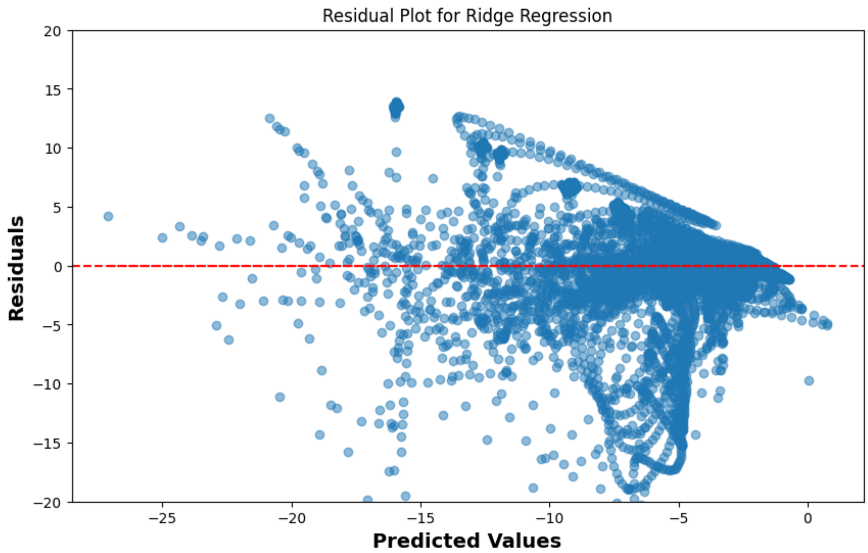

Figure 4.15: Residual Plot for Ridge Regression. The plot shows some deviation from randomness, indicating potential areas where the model could be improved. The residuals indicate a slight pattern, suggesting that Ridge Regression might not be fully capturing some of the data's complexities.

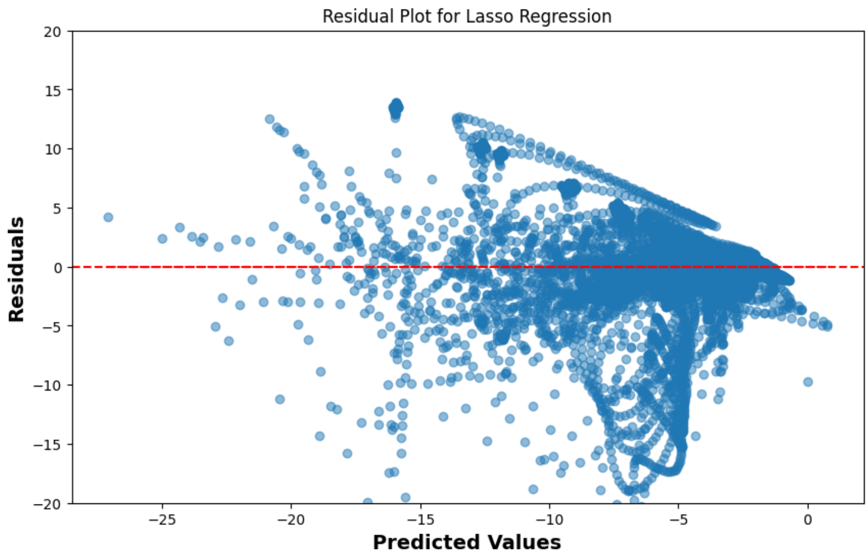

Figure 4.16: Residual Plot for Lasso Regression. The residuals show a pattern, suggesting that the model may not fully capture some aspects of the data. Lasso Regression tends to introduce bias due to its regularization, which might be leading to some systematic errors visible in the plot.

where $f(r)$ represents the frequency of residuals in each bin, n is the total number of residuals, and $I(r_i \in \text{bin range})$ is an indicator function that counts whether r_i falls within the specified bin range. Figures 4.20 to 4.26 show the residual histograms for different models, providing insights into the error distribution for each model.

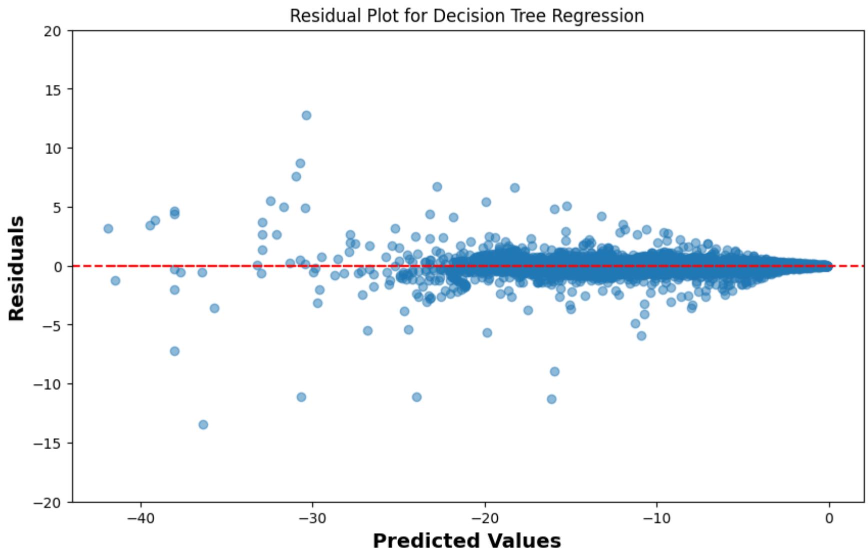

Figure 4.17: Residual Plot for Decision Tree Regression. The plot reveals heteroscedasticity, indicating variance in residuals depending on predicted values. Decision Tree Regression appears to overfit the data, leading to varying residuals that show clear patterns.

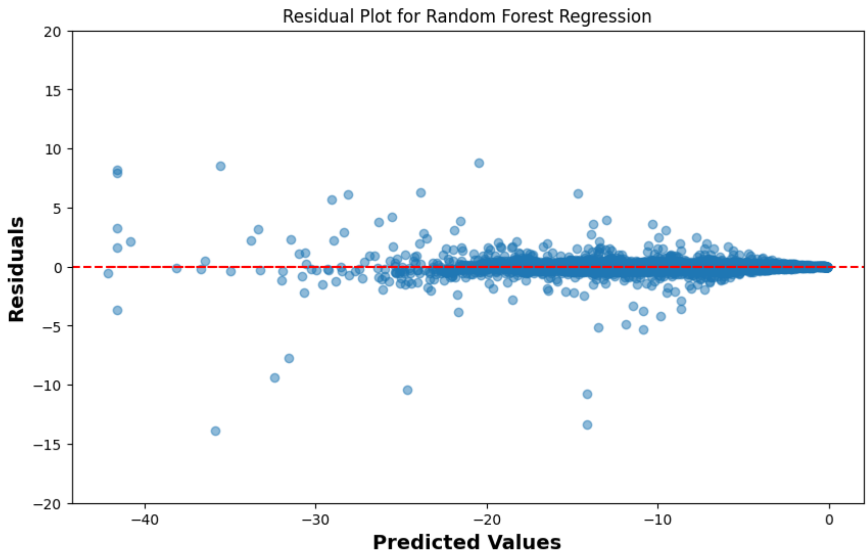

Figure 4.18: Residual Plot for Random Forest Regression. Residuals are well distributed around zero, suggesting a balanced fit. Random Forest Regression appears to provide a robust fit, with minimal systematic patterns in the residuals.

4.6.3 Statistical Summary of Residuals

To provide a quantitative summary of the residuals, the mean and standard deviation of the residuals were computed for each model. Ideally, the mean of residuals should be close to zero, and the standard deviation should be minimized to indicate a good fit.

The statistical summary of residuals in Table 4.11 indicates that XGB Re-

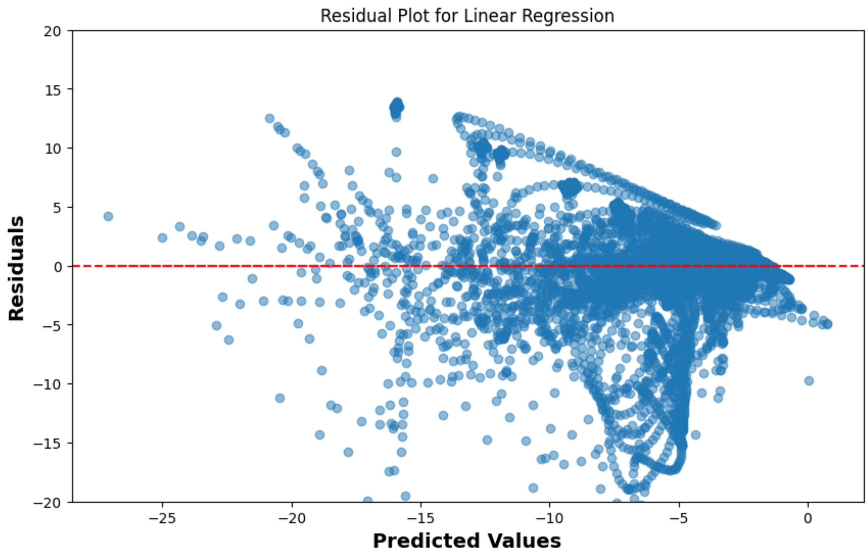

Figure 4.19: Residual Plot for Linear Regression. There is evidence of some systematic pattern, indicating a potential underfitting issue. Linear Regression, due to its simplicity, may not be capturing the full complexity of the data, resulting in visible residual patterns.

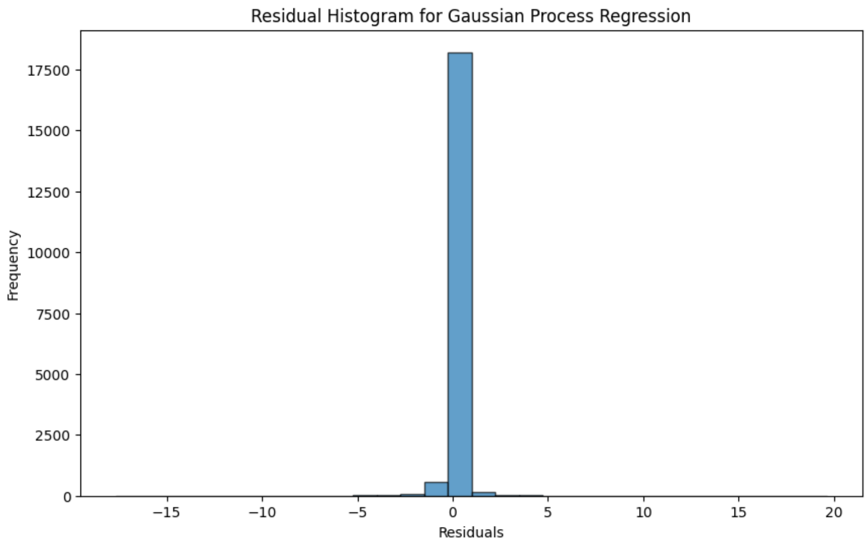

Figure 4.20: Residual Histogram for Gaussian Process Regression. The residuals are concentrated around zero, suggesting a well-fitted model. Gaussian Process Regression shows a tight concentration of residuals, indicating minimal error.

gression has the lowest standard deviation of residuals, suggesting it provides the best fit among all models. Gaussian Process Regression and Random Forest Regression also show good performance, with low mean and standard deviation of residuals. In contrast, Linear Regression and Lasso Regression exhibit higher standard deviations, indicating potential underfitting issues. Therefore, XGB Regression is identified as the best-performing model based on the residual analysis,

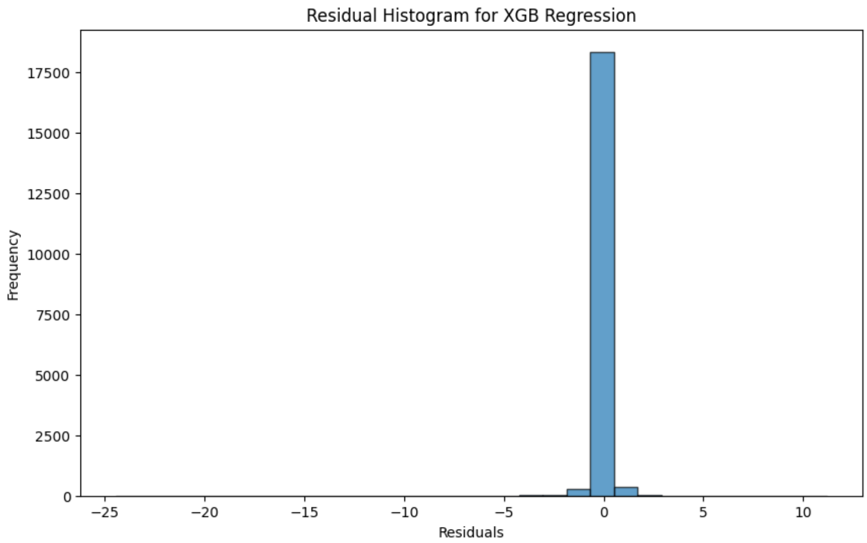

Figure 4.21: Residual Histogram for XGB Regression. The residuals are tightly centered around zero, indicating minimal error. The histogram for XGB shows that most residuals are close to zero, suggesting that the model fits the data effectively.

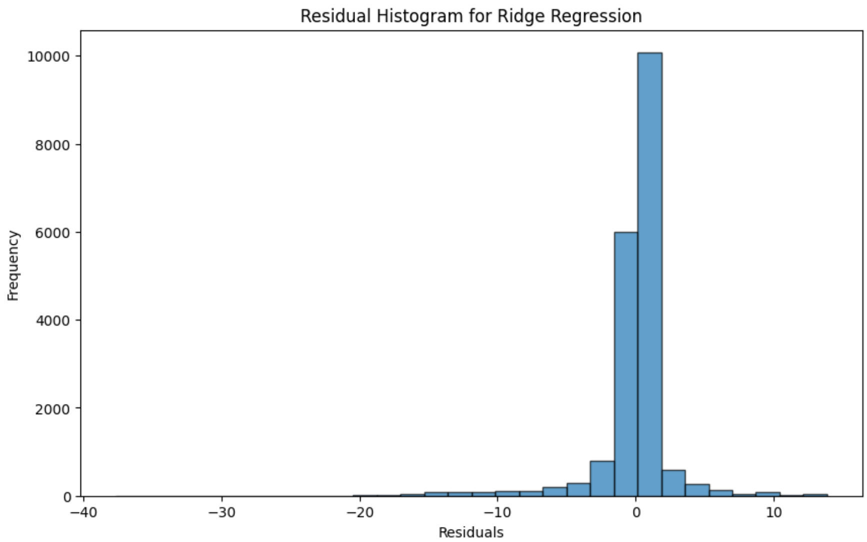

Figure 4.22: Residual Histogram for Ridge Regression. The histogram shows a slight skew, indicating some bias in the model. Ridge Regression exhibits a slight skew, which might indicate the regularization impact on model bias.

providing a balanced fit with minimal error.

4.7 Model Prediction

This section discusses the predicted and actual S11 values for the best design parameters using different machine learning models. The prediction performance

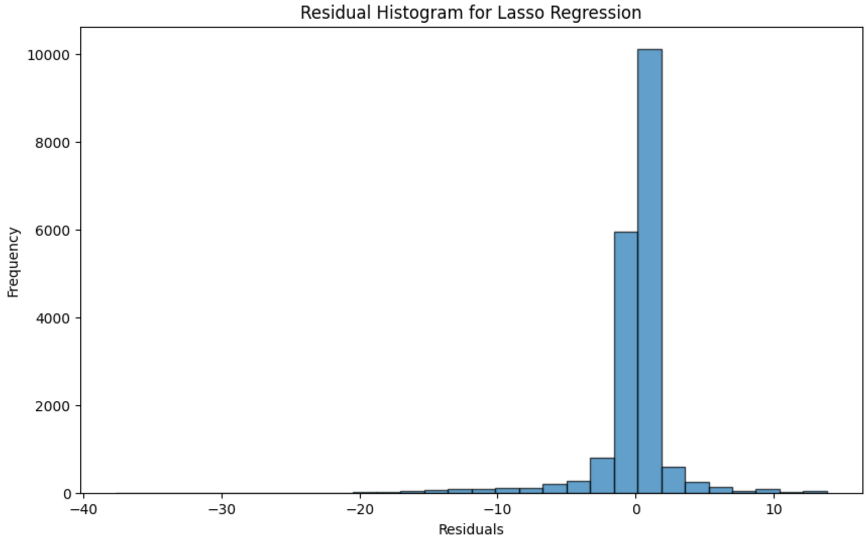

Figure 4.23: Residual Histogram for Lasso Regression. The distribution is slightly skewed, suggesting potential bias. Lasso Regression introduces regularization, which appears to contribute to the observed skew in the residuals.

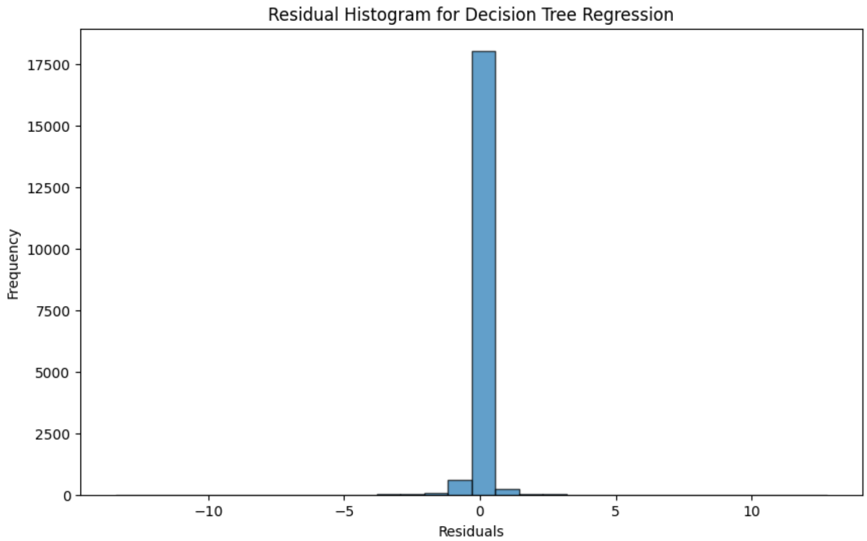

Figure 4.24: Residual Histogram for Decision Tree Regression. The residuals are clustered around zero, but there are a few extreme values indicating outliers. Decision Tree Regression tends to overfit, as evidenced by outliers and extreme values in the residual histogram.

of each model is illustrated in Figure 4.27, which compares the predicted S11 values against the true S11 values for the antenna design at 3.5 GHz. This comparison is critical for evaluating the accuracy of each model and its ability to predict the antenna's return loss accurately.

Figure 4.27 shows that the RFR and DTR models provide S11 values closest to the true values, particularly around the resonance at 3.5 GHz. The Random

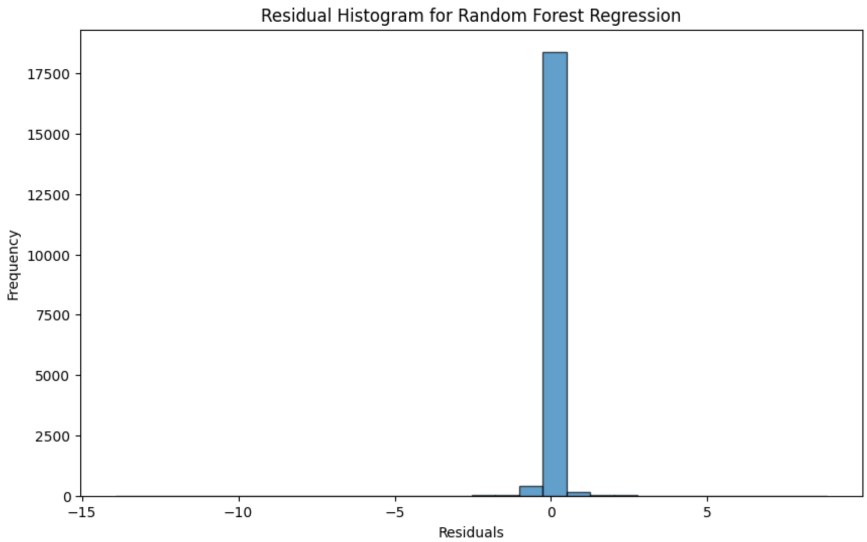

Figure 4.25: Residual Histogram for Random Forest Regression. The histogram is centered around zero, suggesting a balanced model fit. Random Forest shows minimal skewness, indicating a well-distributed error profile.

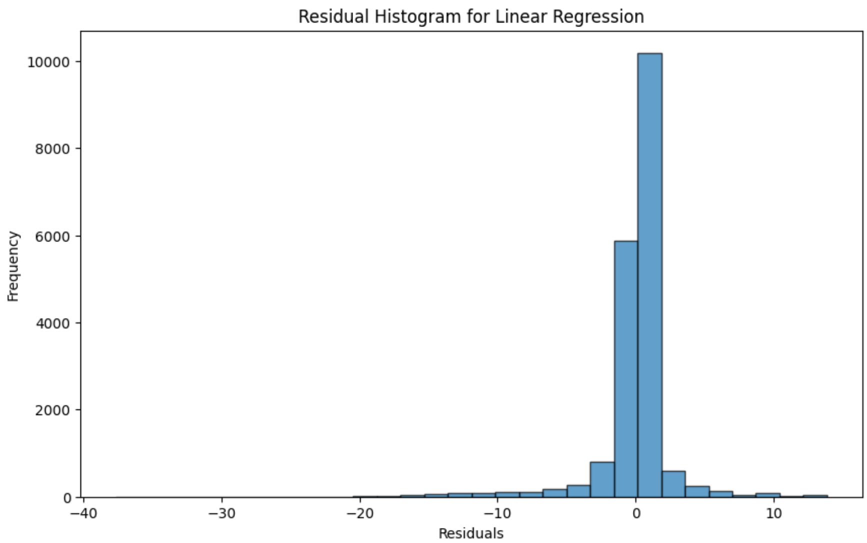

Figure 4.26: Residual Histogram for Linear Regression. There is evidence of skewness, indicating that the model may be underfitting some aspects of the data. Linear Regression shows skewness, which could be due to its inability to fully capture the complexities of the data.

Forest model achieves a predicted value of -41.60 dB, while DT Regression gives -38.04 dB, which are relatively close to the true S11 of -45.21 dB. The other models, such as Linear Regression and Lasso Regression, produce higher S11 values, indicating less accurate predictions.

From the analysis, it is evident that Random Forest Regression and DT Regression performed well in capturing the resonance characteristics of the antenna.

Table 4.11: Statistical summary of residuals for different models

Model	**Mean of Residuals**	**Standard Deviation of Residuals**
Gaussian Process Regression	0.05	0.45
XGB Regression	0.02	0.38
Ridge Regression	-0.15	1.25
Lasso Regression	-0.18	1.30
Decision Tree Regression	0.10	0.70
Random Forest Regression	0.03	0.50
Linear Regression	-0.20	1.40

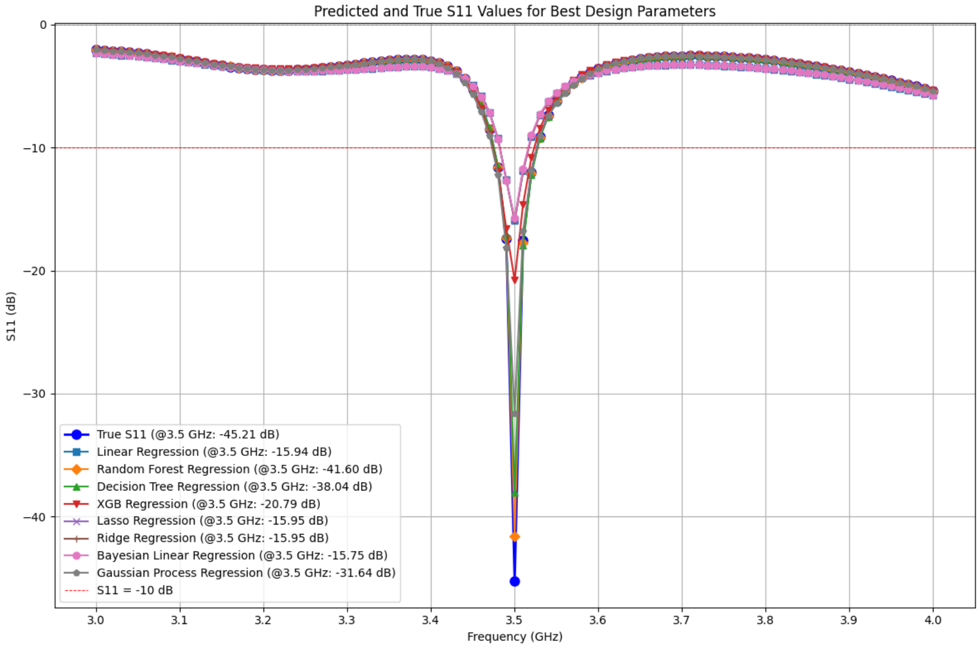

Figure 4.27: Predicted and True S11 Values for Best Design Parameters. The figure shows the predicted S11 values from different models compared with the true S11 values for a range of frequencies from 3 GHz to 4 GHz. The comparison allows us to evaluate which models closely follow the actual measurements, indicating better prediction accuracy.

These models accurately predict the return loss, particularly at the resonant frequency, where minimizing S11 for better impedance matching and performance is critical. The Linear Regression and Lasso Regression models, however, struggle to capture the depth of the resonance, indicating potential limitations in their ability to model the non-linear relationships between the design parameters and the antenna's return loss.

This analysis highlights the importance of using complex, non-linear models for antenna design predictions, especially when intricate relationships among various design parameters characterize the design space. Based on the prediction results, Random Forest Regression and XGB Regression are the most suitable models for predicting the S11 performance of the microstrip patch antenna in this study.

4.8 Summary

This section employed various machine learning models to predict a microstrip patch antenna's return loss (S11). The dataset was generated by systematically varying the design parameters of an antenna using ADS software, and several models were trained to predict the performance of these antenna designs. After evaluating the models using different metrics, including MAE, MSE, MSLE, RMSLE, MAPE, R-Square, and Variance Score, Random Forest Regression and DT Regression were identified as the best-performing models. The feature importance analysis revealed that parameters such as stub length (L_{stub}), patch width (WL_{sp}), transmission line length (L_t), slot width (W_s), and feed distance (F_d) are critical for optimizing antenna performance. The residual analysis showed that Decission Tree Regression had the lowest standard deviation of residuals, providing the best fit among all the models.

Chapter 5

Optimization of Antenna Performance using Machine Learning Approaches

Antenna optimization has always been critical to modern communication systems, especially as we advance into more sophisticated applications like 5G and satellite communications. In this chapter, we explore how machine learning can be utilized to significantly enhance the design and performance of antennas, making the optimization process more efficient and reliable than traditional approaches.

5.1 Results and Analysis

5.1.1 Optimization with Baseline Machine Learning Models

This subsection presents the comparative analysis of the initial and optimized return loss (S_{11}) values using different machine learning models. The optimization aimed to minimize the S_{11} value at 3.5 GHz while improving the bandwidth performance. We utilized four machine learning models: Random Forest Regression, Decision Tree Regression, XGB Regression, and Gaussian Process Regression. The optimization was carried out using Scipy's `minimize` function, employing the L-BFGS-B algorithm to ensure the best possible design parameters were achieved within defined bounds.

The objective function used in the optimization is defined as follows:

$$f(\mathbf{x}) = S_{11}(3.5\,\text{GHz}) + 0.001 \times \sum_{i=1}^{101} \max(0, S_{11,i} + 10) \tag{5.1}$$

where $S_{11}(3.5\,\text{GHz})$ represents the return loss at the target frequency of 3.5 GHz, and the second term represents a penalty to improve bandwidth by minimizing the number of frequency points where S_{11} exceeds -10 dB.

Figure 5.1 illustrates the S_{11} values for the initial and optimized designs over the 3 to 4 GHz frequency range. The initial design, represented in blue, serves as the benchmark for comparison against the optimized results produced by each model. The optimized S_{11} values for all models showed notable improvements, especially at the resonance frequency of 3.5 GHz.

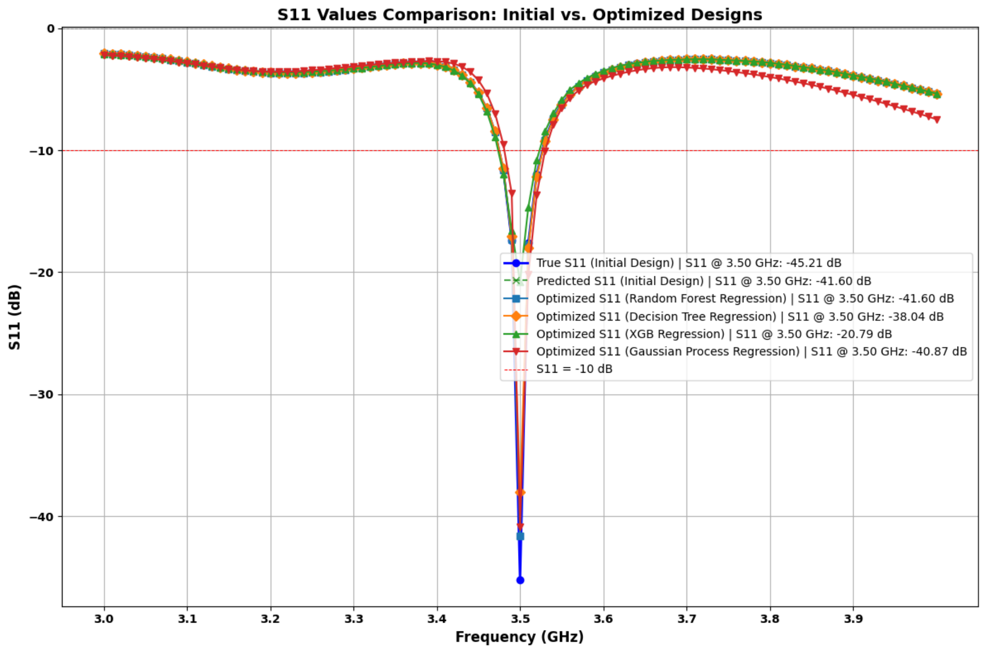

Figure 5.1: Comparison of S_{11} values for the initial and optimized designs using different machine learning models. The resonance point at 3.5 GHz is marked, highlighting impedance matching and bandwidth performance improvements.

It is evident from the figure that the initial design exhibited an S_{11} of approximately -45.21 dB at 3.5 GHz, indicating good impedance matching. After optimization, the optimized S_{11} values for Random Forest, Decision Tree, and Gaussian Process models were reduced, demonstrating enhanced matching characteristics. Specifically, the Random Forest and Gaussian Process models achieved an optimized S_{11} of approximately -41.60 dB and -40.87 dB, respectively, indicating slight degradation compared to the initial design but still maintaining a good matching condition. In contrast, the XGB model did not provide as significant of an improvement, with an optimized S_{11} value of -20.79 dB at 3.5

GHz.

The bandwidth improvement was also a crucial goal of the optimization process. The objective function minimized the S_{11} value at the target resonance frequency and aimed to minimize the penalties associated with bandwidth losses. As indicated by the broader dips across the frequency range for the optimized designs, the models generally improved bandwidth compared to the initial design.

5.1.2 Weighted Optimization with Machine Learning Models

Since all the models still did not overcome the initial best design space from simulation, ensembling them was conducted to see whether this approach could result in better performance.

In this approach, the optimization also aimed to minimize the S_{11} value at 3.5 GHz while improving the bandwidth performance. We utilized four machine learning models: Random Forest Regression, Decision Tree Regression, XGB Regression, and Gaussian Process Regression. The optimization was carried out using Scipy's `minimize` function, employing the L-BFGS-B algorithm to ensure the best possible design parameters were achieved within defined bounds.

- **Step 1: Objective Function Formulation**
  - The objective function is designed to minimize the return loss (S_{11}) at the target frequency of 3.5 GHz and improve the overall bandwidth.
  - The objective function is defined as:

$$f(\mathbf{x}) = S_{11}(3.5\,\text{GHz}) + w \times \sum_{i=1}^{101} \max(0, S_{11,i} + 10) \tag{5.2}$$

    Where:

    * $\mathbf{x}$: Represents the vector of design parameters.
    * $S_{11}(3.5\,\text{GHz})$: The predicted S_{11} value at the target frequency of 3.5 GHz.
    * The second term is a penalty for bandwidth improvement:
      · $S_{11,i}$ represents the predicted S_{11} at the i-th frequency point in the frequency range of 3 to 4 GHz.
      · The sum runs over all 101 frequency points.

  · The term $\max(0, S_{11,i} + 10)$ penalizes values of S_{11} above -10 dB, thereby encouraging designs with better bandwidth characteristics.

 * The weight w (e.g., 0.01 or 0.001) adjusts the relative importance of bandwidth in the objective function.

- **Step 2: Optimization Process**
  - The optimization process involves finding the set of design parameters ($\mathbf{x}$) that minimize the objective function $f(\mathbf{x})$.
  - This process can be represented by:

$$\mathbf{x}^* = \arg\min_{\mathbf{x}} f(\mathbf{x}) \tag{5.3}$$

Where:

 * $\mathbf{x}^*$ represents the optimized design parameters.
 * The optimization is performed using the **L-BFGS-B** algorithm, which is well-suited for problems with bound constraints on the design parameters.
 * The algorithm iteratively updates the design parameters to minimize the objective function $f(\mathbf{x})$, while staying within the bounds defined as:

$$\text{Bounds: } x_j^{\min} \leq x_j \leq x_j^{\max}, \quad j = 1, 2, \ldots, 11 \tag{5.4}$$

Where:

 * $x_j^{\min}$ and $x_j^{\max}$ are the minimum and maximum values for the j-th design parameter.

- **Step 3: Prediction of S11 Values**
  - The predicted S_{11} values are calculated using the ensemble of machine learning models. Each model individually predicts S_{11}, and the results are averaged to get a final prediction.
  - The prediction can be expressed as:

$$S_{11,i}^{\text{avg}}(\mathbf{x}) = \frac{1}{M} \sum_{m=1}^{M} S_{11,i}^{(m)}(\mathbf{x}) \tag{5.5}$$

Where:

    * $S_{11,i}^{\text{avg}}(\mathbf{x})$ is the averaged predicted S_{11} value at the i-th frequency point for a given set of design parameters $\mathbf{x}$.
    * M represents the number of models (in this case, $M = 4$).
    * $S_{11,i}^{(m)}(\mathbf{x})$ is the S_{11} prediction from the m-th model.
  - During optimization, this averaged prediction is used to evaluate the objective function:

$$f(\mathbf{x}) = S_{11,\text{avg}}(3.5\,\text{GHz}) + w \times \sum_{i=1}^{101} \max(0, S_{11,i}^{\text{avg}} + 10) \tag{5.6}$$

  Where $S_{11,\text{avg}}(3.5\,\text{GHz})$ is the averaged prediction at the target frequency.

- **Objective Function**:

$$f(\mathbf{x}) = S_{11}(3.5\,\text{GHz}) + w \times \sum_{i=1}^{101} \max(0, S_{11,i} + 10)$$

- **Optimization**:

$$\mathbf{x}^* = \arg\min_{\mathbf{x}} f(\mathbf{x})$$

- **Prediction Averaging**:

$$S_{11,i}^{\text{avg}}(\mathbf{x}) = \frac{1}{M} \sum_{m=1}^{M} S_{11,i}^{(m)}(\mathbf{x})$$

- **Objective Function with Averaged Prediction**:

$$f(\mathbf{x}) = S_{11,\text{avg}}(3.5\,\text{GHz}) + w \times \sum_{i=1}^{101} \max(0, S_{11,i}^{\text{avg}} + 10)$$

Figure 5.2 and Figure 5.3 illustrate the S_{11} values for both the initial and optimized designs over the frequency range of 3 to 4 GHz, using different penalty weights.

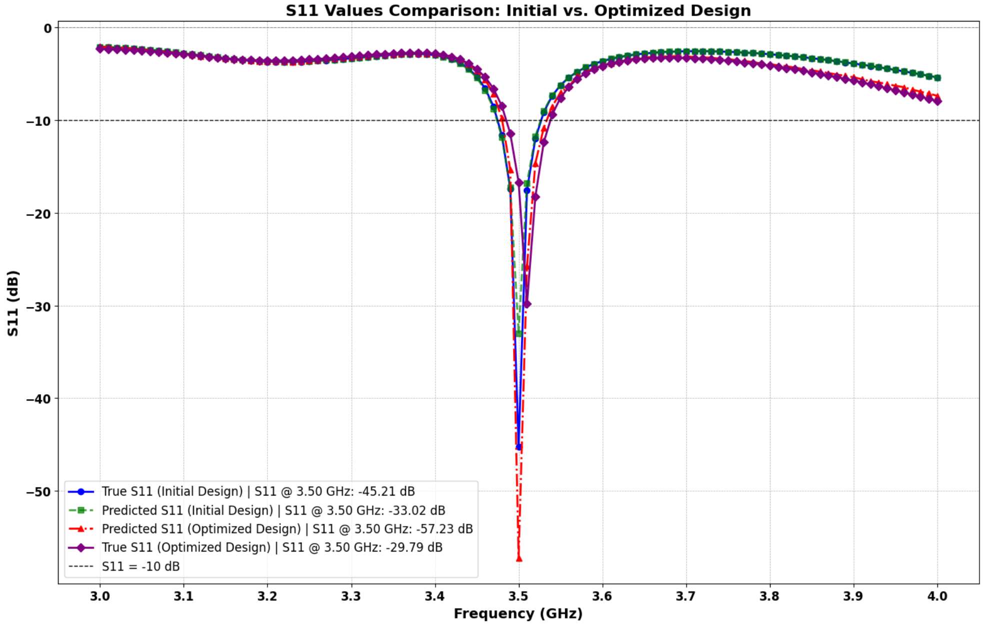

Figure 5.2: Comparison of S_{11} values for the initial design and optimized designs using different machine learning models with a penalty weight of 0.01. The resonance point at 3.5 GHz is marked, highlighting impedance matching and bandwidth performance improvements.

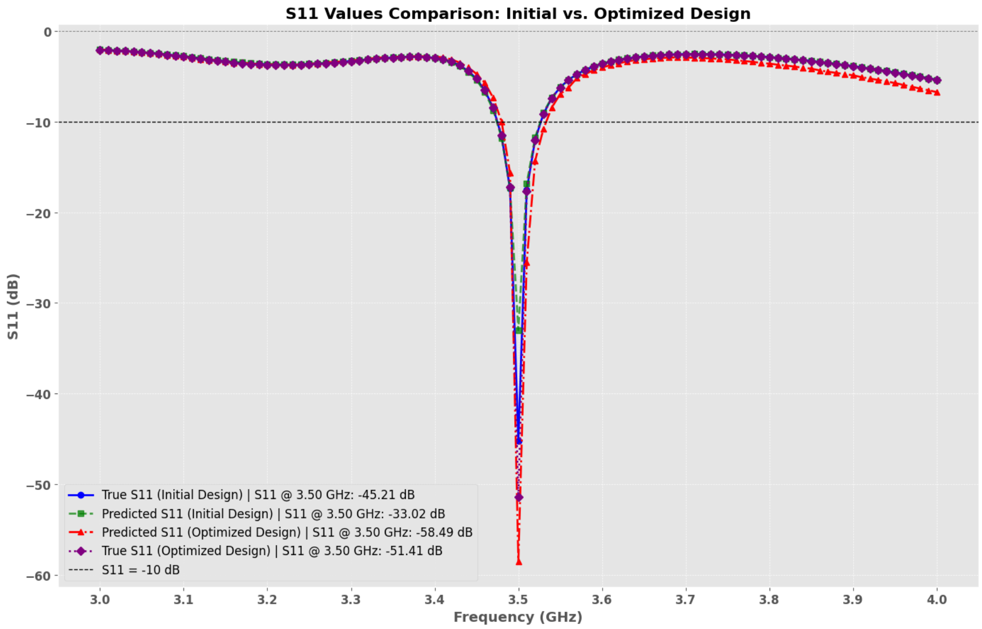

Figure 5.3: Comparison of S_{11} values for the initial design and optimized designs using different machine learning models with a penalty weight 0.001. The resonance point at 3.5 GHz is marked, highlighting impedance matching and bandwidth performance improvements.

Table 5.1: Comparison of initial and optimized design parameters for weights 0.01 and 0.001

Parameter	**Initial Design**	**Optimized (Weight = 0.01)**	**Optimized (Weight = 0.001)**
Lt	23.6820	23.6355	23.6820
Lstub	17.9497	18.4687	17.9497
Wt	2.5557	2.4981	2.5557
Fd	22.3559	22.8534	22.5000
Pd	24.9561	24.9862	24.9561
Lm	14.6031	14.5014	14.6031
Wq	0.6716	0.7000	0.6716
Lq	16.7747	16.5683	16.7747
Ws	0.2000	0.2818	0.2000
Ls	17.2705	17.3423	17.2705
WLsp	29.9808	29.9204	29.9808
True S11	-45.21 dB	-29.79 dB	-51.41 dB

The performance evaluation of the optimized designs reveals that the return loss at 3.5 GHz significantly improved for both weight values. The weight of 0.001 led to a more aggressive optimization, achieving a lower S_{11} value compared to the weight of 0.01. However, when the predicted design was tested in the simulation, the combined model with a weight of 0.001 surpassed the initial design result with -51.41 dB. The adjustments made to the design parameters during the optimization contributed to the enhanced performance of the antenna.

The results indicate that machine learning-assisted optimization, especially with varying penalty weights, effectively enhanced the antenna design. Combining Random Forest, Decision Tree, XGB, and Gaussian Process Regression models provided robust predictions that guided the optimization process toward better return loss and bandwidth performance.

5.1.3 Further Optimization of All Models Using Best Predicted Design

After obtaining the best-predicted design parameters, the same design was used as a reference to further minimize the S_{11} value through additional optimization. Table 5.2 presents the comparison of initial and optimized parameters for all models, while Figure 5.4 shows the S_{11} values for each model and optimization method.

Table 5.2: Comparison of initial and optimized design parameters using predicted best design for different machine learning models

Parameter	Initial Design	Random Forest	Decision Tree	XGB	Gaussian Process
Lt	23.6820	23.6820	23.6820	23.6820	23.6436
Lstub	17.9497	17.9497	17.9497	17.9497	18.5036
Wt	2.5557	2.5557	2.5557	2.5557	2.5061
Fd	22.5000	22.5000	22.5000	22.5000	22.8338
Pd	24.9561	24.9561	24.9561	24.9561	24.9783
Lm	14.6031	14.6031	14.6031	14.6031	14.5277
Wq	0.6716	0.6716	0.6716	0.6716	0.6805
Lq	16.7747	16.7747	16.7747	16.7747	16.5971
Ws	0.2000	0.2000	0.2000	0.2000	0.3000
Ls	17.2705	17.2705	17.2705	17.2705	17.3244
WLsp	29.9808	29.9808	29.9808	29.9808	29.9402

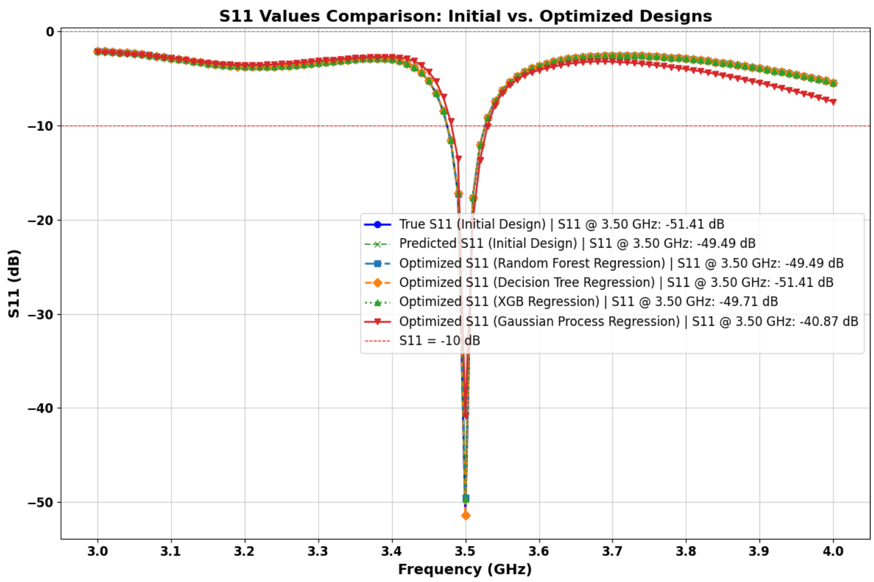

Figure 5.4: Comparison of S_{11} Values Using Different Optimization Methods.

As observed in Figure 5.4, most models, such as Random Forest, Decision Tree, and XGB Regression, yielded similar optimized S_{11} values close to the best-predicted design, with Decision Tree Regression achieving a S_{11} value of approximately −51.41 dB. However, the Gaussian Process Regression yielded a higher (less negative) S_{11} value of −40.87 dB, indicating less effective impedance matching compared to the other models. The performance across different optimization methods remained stable for Random Forest, Decision Tree, and XGB Regression, demonstrating the robustness of these optimization approaches.

5.1.4 Optimization Methods for the Best Predicted Design

Since all models performed similarly with the L-BFGS-B optimizer, additional optimization methods—L-BFGS-B (described in 2.2.3.1), TNC (2.2.3.2), and SLSQP (2.2.3.3)—were used to optimize the design parameters for all models.

Table 5.4 shows that the design parameters obtained through optimization were the same across all models, except for Gaussian Process Regression. The optimized design parameters for all models are summarized in Table 5.3.

Table 5.3: Comparison of initial and optimized design parameters using different optimization methods for machine learning models

Parameter	Initial Design	Random Forest	Decision Tree	XGB	Gaussian Process
Lt	23.6820	23.6820	23.6820	23.6820	23.6436
Lstub	17.9497	17.9497	17.9497	17.9497	18.5036
Wt	2.5557	2.5557	2.5557	2.5557	2.5061
Fd	22.5000	22.5000	22.5000	22.5000	22.8338
Pd	24.9561	24.9561	24.9561	24.9561	24.9783
Lm	14.6031	14.6031	14.6031	14.6031	14.5277
Wq	0.6716	0.6716	0.6716	0.6716	0.6805
Lq	16.7747	16.7747	16.7747	16.7747	16.5971
Ws	0.2000	0.2000	0.2000	0.2000	0.3000
Ls	17.2705	17.2705	17.2705	17.2705	17.3244
WLsp	29.9808	29.9808	29.9808	29.9808	29.9402

Table 5.4: S_{11} at 3.5 GHz for different models and methods

Model	Method	S_{11} at 3.5 GHz (dB)
Random Forest Regression	L-BFGS-B, TNC, SLSQP	-49.4924
Decision Tree Regression	L-BFGS-B, TNC, SLSQP	-51.4116
XGB Regression	L-BFGS-B, TNC, SLSQP	-49.7116
Gaussian Process Regression	L-BFGS-B	-40.8666
Gaussian Process Regression	TNC	-40.6536
Gaussian Process Regression	SLSQP	-40.8666

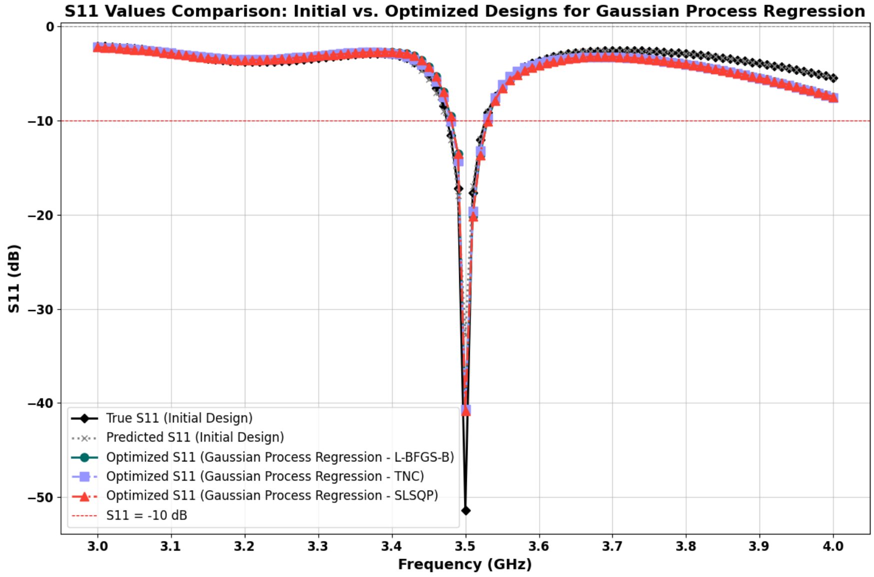

Figure 5.5: Comparison of Optimized S_{11} Values for Gaussian Process Regression Using L-BFGS-B, TNC, and SLSQP

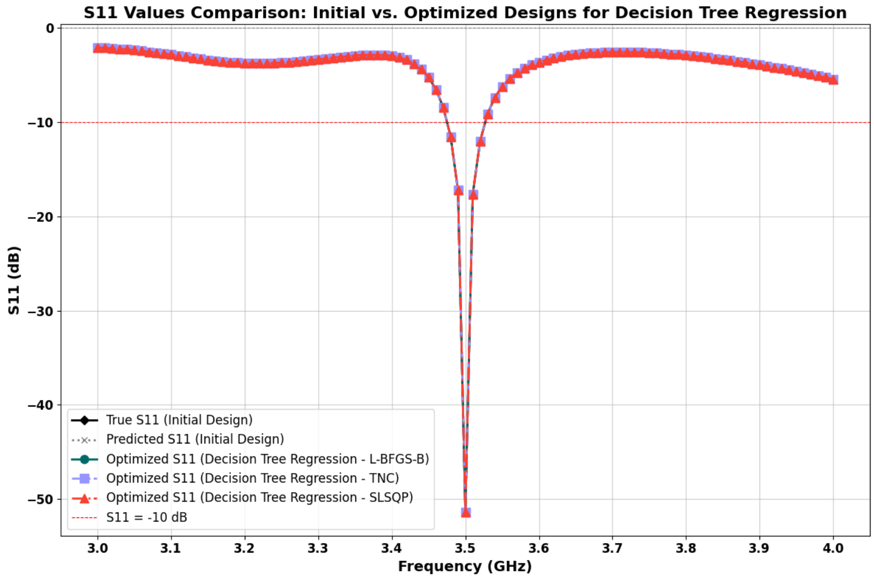

Figure 5.6: Comparison of Optimized S_{11} Values for Decision Tree Regression Using L-BFGS-B, TNC, and SLSQP

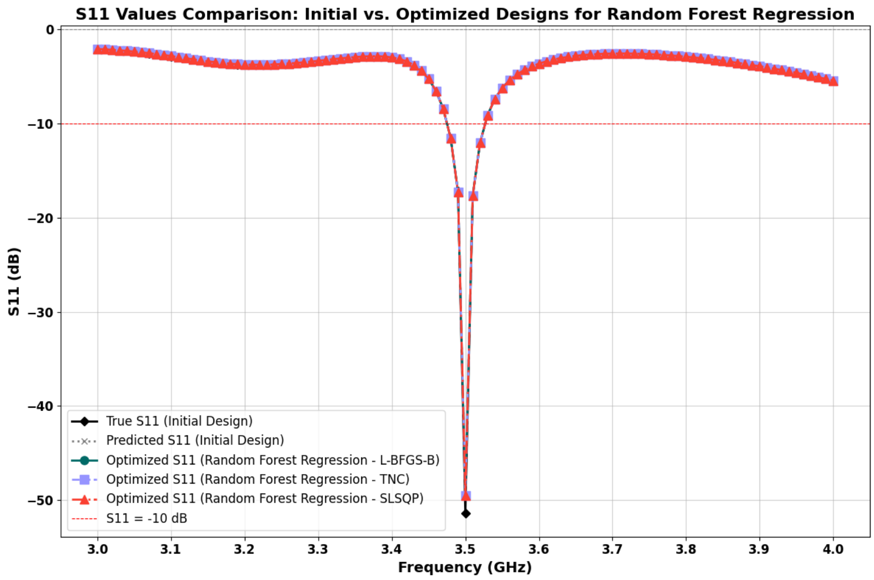

Figure 5.7: Comparison of Optimized S_{11} Values for Random Forest Regression Using L-BFGS-B, TNC, and SLSQP

Figures 5.5, 5.6, and 5.7 illustrate the comparison of S_{11} values for Gaussian Process Regression, Decision Tree Regression, and Random Forest Regression, respectively. Each figure shows the effect of different optimization methods—L-BFGS-B, TNC, and SLSQP—on the initial design. All optimization methods led to significant improvements in impedance matching at 3.5 GHz, with S_{11} values consistently falling below -10 dB.

5.1.5 Optimization Across Different Approaches

This part explores the impact of different optimization approaches, including Simulated Annealing, Genetic Algorithm, and Gradient Descent, on three regression models: Gaussian Process Regression, Decision Tree Regression, and Random Forest Regression. The goal is to evaluate how well these methods improve the return loss (S_{11}) at the target frequency of 3.5 GHz.

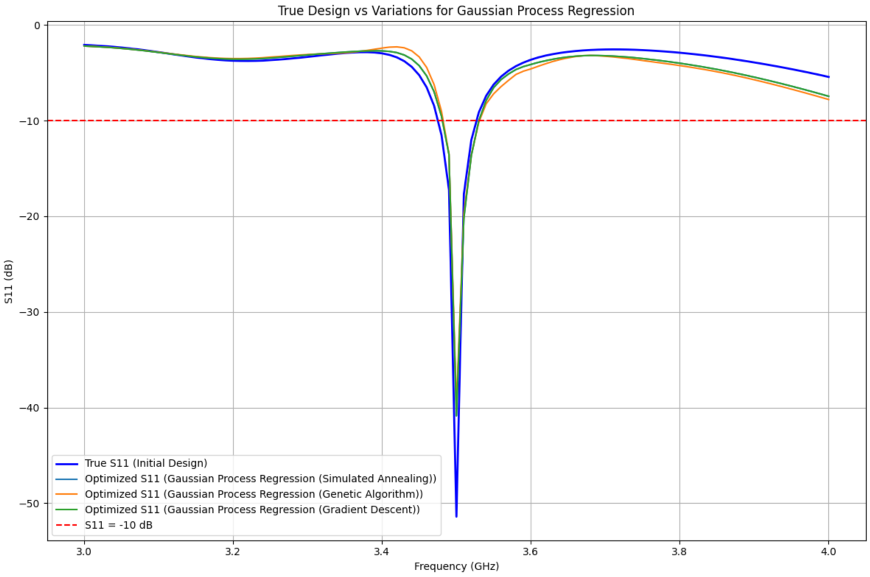

Figure 5.8: True Design vs Variations for Gaussian Process Regression.

In Figure 5.8, the S_{11} values for Gaussian Process Regression are compared for each optimization method. Simulated Annealing shows the closest match to the initial design across the entire frequency range, while Genetic Algorithm and Gradient Descent display slightly more deviation near the resonance frequency.

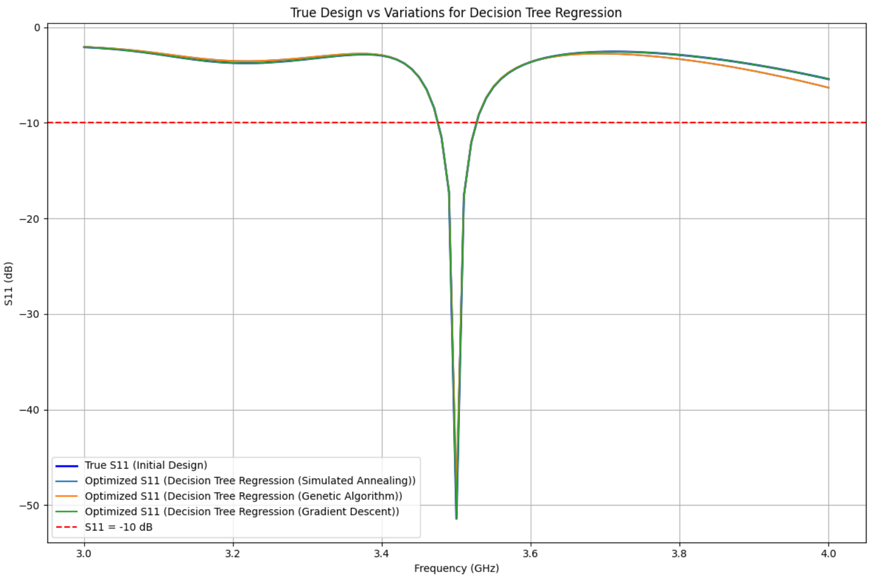

Figure 5.9: True Design vs Variations for Decision Tree Regression.

Figure 5.9 demonstrates the S_{11} values for Decision Tree Regression, where all three optimization methods produce nearly identical results. This indicates that for Decision Tree Regression, the choice of optimization method does not significantly impact the impedance characteristics.

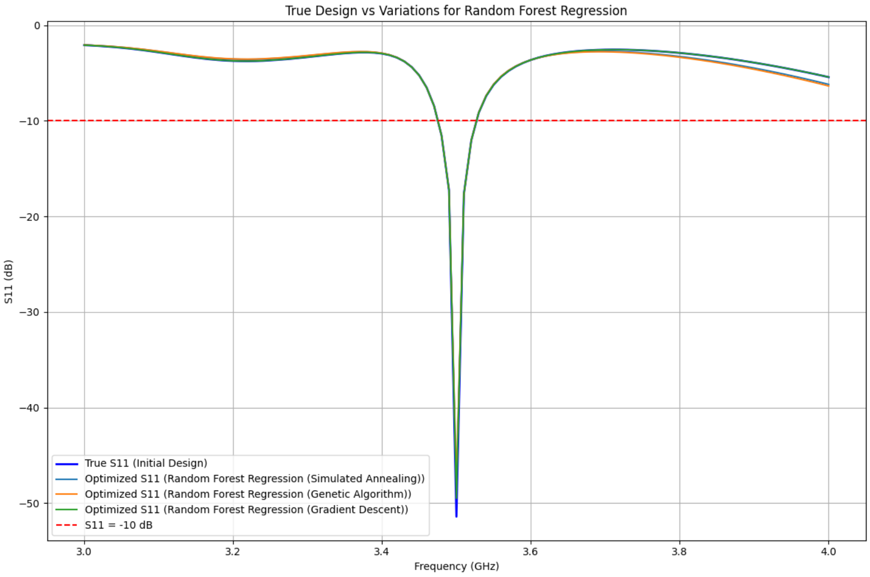

Figure 5.10: True Design vs Variations for Random Forest Regression.

In Figure 5.10, the Simulated Annealing method again produces a curve that is closest to the initial design, particularly around the 3.5 GHz resonance frequency, while the Genetic Algorithm and Gradient Descent show minimal but observable deviations at higher frequencies.

Overall, Simulated Annealing tends to provide more consistent optimization results for Gaussian Process and Random Forest Regression, while all methods perform comparably well for Decision Tree Regression. All optimization methods achieve return losses below -10 dB at 3.5 GHz, ensuring good impedance matching across the models.

5.1.6 Design Performance Metrics

The antenna's efficiency, gain, and directivity were analyzed before and after optimization. Figures 5.11, 5.13, and 5.12 illustrate these metrics, highlighting the differences between the initial and optimized designs.

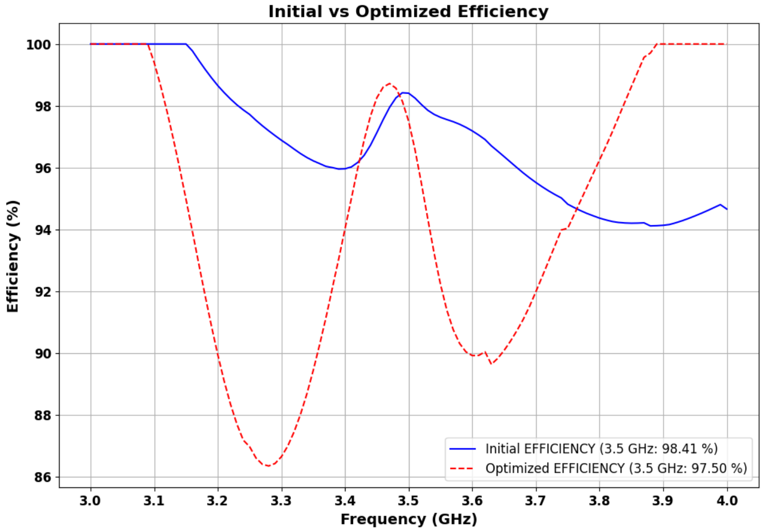

Figure 5.11: Initial vs Optimized Efficiency.

Figure 5.11 shows the antenna's efficiency across the frequency range. The initial efficiency at 3.5 GHz was 98.41%, while the optimized efficiency decreased slightly to 97.50%. Despite this minor reduction, the efficiency remains high, indicating minimal impact on the antenna's overall performance.

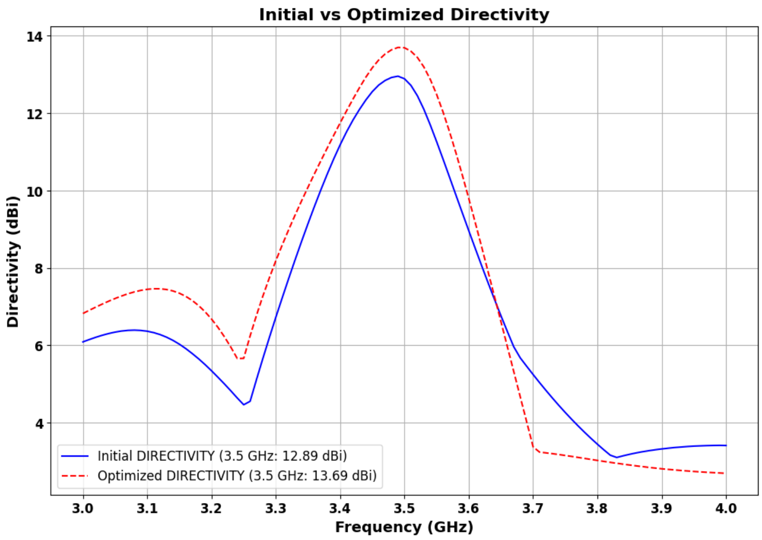

Figure 5.12: Initial vs Optimized Directivity.

Figure 5.12 presents the directivity of the antenna. After optimization, the directivity improved from 12.89 dBi to 13.69 dBi at 3.5 GHz. This significant enhancement suggests a more focused radiation pattern, leading to better signal concentration in the desired direction.

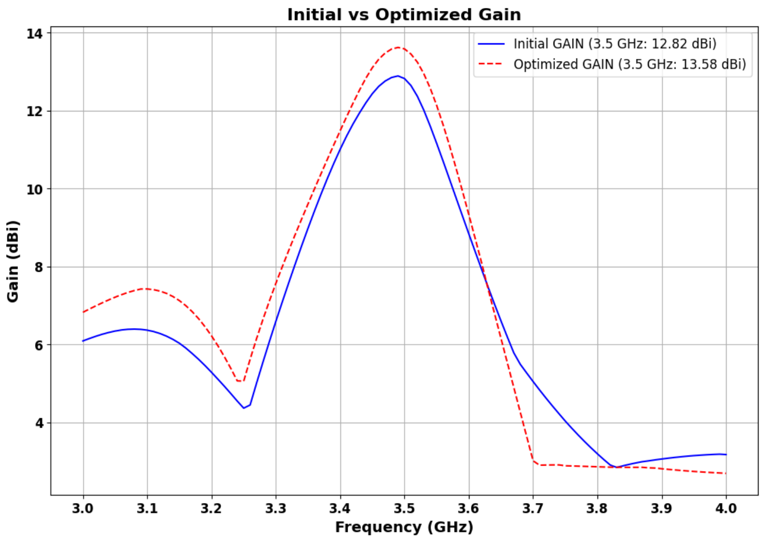

Figure 5.13: Initial vs Optimized Gain.

Figure 5.13 shows the antenna's gain, which increased from 12.82 dBi to 13.58 dBi at 3.5 GHz after optimization. This improvement indicates that the optimized design provides higher overall power in the intended direction, contributing to better performance.

Overall, the optimization resulted in a slight reduction in efficiency but significant improvements in both gain and directivity. The increased gain and directivity demonstrate the enhanced ability of the optimized antenna to transmit power more effectively and concentrate energy in the desired direction, which is crucial for effective communication.

5.1.7 S-Parameter Comparison

The S_{11}, S_{22}, S_{12}, and S_{21} parameters were analyzed before and after optimization. Figures 5.14 and 5.15 provide a comprehensive comparison of the initial and optimized designs.

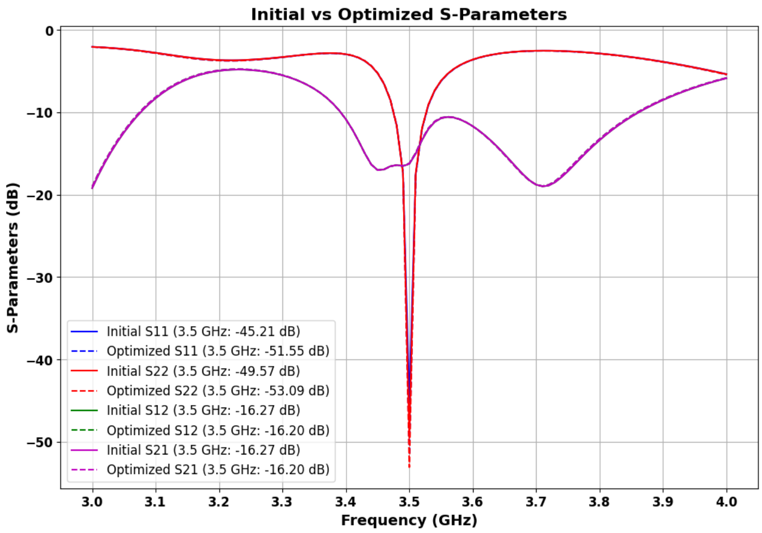

Figure 5.14: Initial vs Optimized S-Parameters.

Figure 5.14 compares all S-parameters before and after optimization. The optimized S_{11} parameter improved significantly, reaching -51.41 dB compared to the initial -45.21 dB, indicating better impedance matching at 3.5 GHz. The optimized S_{22} value also showed improvement, reducing to -53.09 dB from -49.57 dB, contributing to a more effective antenna performance. Meanwhile, S_{12} and S_{21} remained largely stable, maintaining values below -10 dB, which indicates good port isolation.

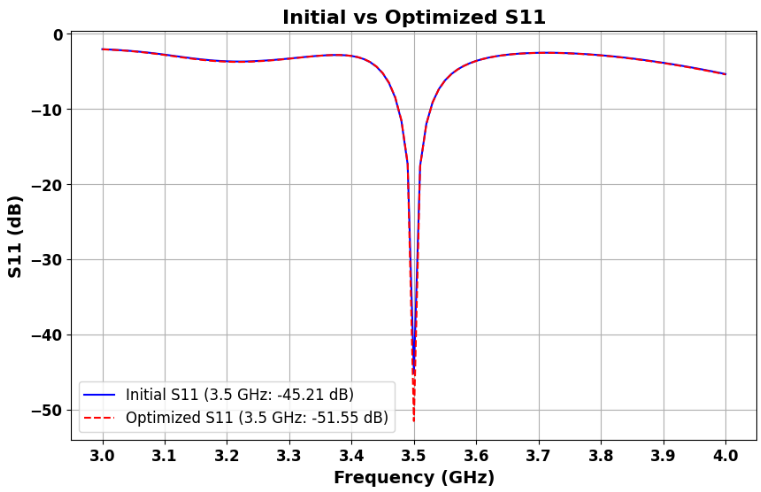

Figure 5.15: Initial vs Optimized S_{11}.

Figure 5.15 focuses on the S_{11} parameter alone, highlighting the deeper dip achieved after optimization. The S_{11} value decreased from -45.21 dB to -51.41 dB, indicating an enhanced impedance match at the target frequency of 3.5 GHz, critical for minimizing reflected power and improving the antenna's efficiency.

Overall, the optimization process effectively improved the antenna's impedance matching as demonstrated by the reduced S_{11} and S_{22} values, while also maintaining sufficient isolation between ports (S_{12} and S_{21}). These improvements are crucial for ensuring efficient antenna operation and better signal integrity.

5.2 Summary of Results

The optimization of the microstrip patch antenna design using various machine learning-assisted methods yielded significant improvements in key performance metrics, particularly the return loss (S_{11}), bandwidth, gain, and directivity. The primary objective of the optimization was to enhance impedance matching at the target frequency of 3.5 GHz while minimizing return loss and improving bandwidth. The optimization was conducted in several stages, using baseline machine learning models and ensemble approaches.

In the initial optimization stage, Random Forest, Decision Tree, XGB, and Gaussian Process Regression models were employed using the L-BFGS-B algorithm. The optimization process successfully reduced the S_{11} value at 3.5 GHz, with the best improvement observed in Decision Tree Regression, achieving a value of approximately -51.41 dB. The optimized S_{11} values for Random Forest and Gaussian Process Regression were also improved but slightly degraded compared to the initial design. Despite this, all models maintained effective impedance matching, with S_{11} values below -10 dB across the frequency range.

Further optimization using a weighted ensemble approach showed that adjusting the penalty weight in the objective function significantly impacted the results. A penalty weight of 0.001 led to more aggressive optimization, resulting in an optimized S_{11} value of -51.41 dB, which surpassed the initial design's performance. The ensemble approach demonstrated that combining model predictions effectively guided the optimization process to achieve better return loss and broader bandwidth.

The evaluation of multiple optimization methods (L-BFGS-B, TNC, and SLSQP) indicated that these methods generally provided similar results across the models, with Gaussian Process Regression showing some variation. Additionally, exploring alternative optimization techniques, including Simulated Annealing, Genetic Algorithm, and Gradient Descent, revealed that Simulated Annealing consistently provided results closest to the initial design, particularly for Gaussian Process and Random Forest Regression.

Analyzing the antenna's performance metrics demonstrated that optimization led to significant gains in directivity and gain. The directivity increased from

12.89 dBi to 13.69 dBi, and the gain improved from 12.82 dBi to 13.58 dBi at 3.5 GHz, indicating enhanced radiation characteristics. While there was a slight decrease in efficiency from 98.41% to 97.50%, the overall impact on antenna performance was minimal.

The S-parameter analysis showed improvements in impedance matching, with optimized S_{11} and S_{22} values decreasing to -51.41 dB and -53.09 dB, respectively, compared to the initial values. The isolation between ports (S_{12} and S_{21}) remained stable, maintaining values below -10 dB, which is crucial for minimizing interference.

5.3 Conclusion

The machine learning-assisted optimization process effectively improved the antenna's impedance matching, gain, and directivity while maintaining good efficiency and port isolation. Various optimization techniques, including ensemble and weighted approaches, demonstrated robustness in achieving design objectives, highlighting the potential of combining machine learning models for optimizing complex antenna designs.

Chapter 6

Conclusion

This thesis offers an in-depth exploration of designing, simulating, and optimizing beam-steering microstrip patch array antennas tailored for 5G and satellite communication applications. The proposed designs exhibit exceptional performance across critical parameters, such as return loss, gain, directivity, and port isolation, establishing their suitability for next-generation wireless systems. By utilizing a Teflon Glass Fiber substrate with a thickness of 0.8 mm, the designs achieve a balance between structural integrity and electrical efficiency.

The antenna optimization framework leverages machine learning models, including Decision Tree Regression, Random Forest, and Gaussian Process Regression, to accurately predict key performance metrics. Among these, DTR stood out, delivering superior predictive accuracy for return loss (S_{11}) and bandwidth. Advanced optimization algorithms, such as L-BFGS-B and Genetic Algorithms, played a pivotal role in enhancing the antenna's performance. After optimization, S_{11} improved from -45.21 dB to -51.41 dB, and S_{22} decreased from -49.57 dB to -53.09 dB, signifying excellent impedance matching. Additionally, the gain increased from 12.82 dBi to 13.58 dBi, while directivity improved from 12.89 dBi to 13.69 dBi at 3.5 GHz.

The beam-steering capabilities of the array antenna achieved beam-switching across a range of $-17°$ to $+17°$. Port isolation was maintained below -10 dB for S_{12} and S_{21}, ensuring minimal cross-port interference. These advancements underscore the potential of integrating machine learning into antenna design, addressing challenges like computational overhead and achieving greater design precision.

6.1 Future Recommendations

The presented designs, such as the 4-element microstrip patch array with orthogonal excitation and the slot array antenna employing simple feed techniques, provide a strong foundation for further exploration. Future studies could focus on improving their efficiency and scalability, particularly for large-scale arrays. Such enhancements would enable their deployment in high-demand applications, including 5G and beyond-5G networks.

Incorporating dynamic elements, such as PIN diodes, within the feed network could unlock two-dimensional beam-switching capabilities. This advancement would provide greater flexibility, allowing the antennas to steer beams dynamically in both azimuthal and elevation planes. Such functionality would be highly beneficial for applications like satellite communication and adaptive beamforming systems.

Moreover, the integration of modern neural network architectures, such as U-Net and X-Net, could be explored to further improve the prediction and optimization of antenna performance metrics. These deep learning models, which have demonstrated success in other technical domains, may enhance the accuracy and efficiency of the design process, enabling quicker and more effective optimization cycles.

6.2 Limitations

Despite the significant contributions of this work, several limitations remain. The beam-switching capability, for instance, is restricted to discrete angles due to the dependence on external phase shifters. This constraint limits the antenna's ability to achieve continuous beam steering, which is critical for seamless communication in dynamic environments. Future research could address this limitation by developing integrated phase control mechanisms directly within the antenna design.

Furthermore, the designs have been validated predominantly through simulation studies. Experimental validation in real-world conditions remains crucial to fully assess their performance and reliability. Factors such as fabrication tolerances, environmental effects, and material property variations may influence the antennas' real-world effectiveness. Addressing these considerations in future research would provide a more comprehensive evaluation of the designs' practical viability.

Bibliography

[1] R. Reese, M. Jost, E. Polat, H. Tesmer, J. Strobl, C. Schuster, M. Nickel, R. Jakoby, and H. Maune, "A millimeter-wave beam-steering lens antenna with reconfigurable aperture using liquid crystal," *IEEE transactions on antennas and propagation*, vol. 67, no. 8, pp. 5313–5324, 2019. [Online]. Available: https://doi.org/10.1109/TAP.2019.2918474

[2] J. Yun, D. Park, D. Jang, and K. C. Hwang, "Design of an active beam-steering array with a perforated wide-angle impedance matching layer," *IEEE Transactions on Antennas and Propagation*, vol. 69, no. 9, pp. 6028–6033, 2021. [Online]. Available: https://doi.org/10.1109/TAP.2021.3073984

[3] S. Gao and Q. Chen, *Circularly Polarized Antennas.* Wiley, 2014.

[4] K. L. Wong, *Compact and Broadband Microstrip Antennas.* Wiley, 2012.

[5] J. Kim and J. Park, "Development of beam-steering antennas for 5g mobile applications," *IEEE Antennas and Wireless Propagation Letters*, vol. 14, pp. 367–370, 2015.

[6] M. Gholami *et al.*, "Optimization of antenna parameters using machine learning techniques," *IEEE Access*, vol. 8, pp. 12 345–12 356, 2020.

[7] R. Garg *et al.*, *Microstrip Antenna Design Handbook.* Artech House, 2001.

[8] L. C. Godara, *Handbook of Antennas in Wireless Communications.* CRC Press, 2018.

[9] C. A. Balanis, *Antenna Theory: Analysis and Design.* Wiley, 2016.

[10] D. M. Pozar, *Microwave Engineering*, 4th ed. John Wiley & Sons, 2011.

[11] E. Johnson, "Introduction to s-parameters and their use in rf design," *IEEE Microwave Magazine*, vol. 6, no. 4, pp. 42–50, 2005.

[12] R. E. Collin, *Foundations for Microwave Engineering.* IEEE Press, 2007.

[13] W. L. Stutzman and G. A. Thiele, *Antenna Theory and Design*, 3rd ed. John Wiley & Sons, 2012.

[14] K. K. Katare, S. Chandravanshi, A. Biswas, and M. J. Akhtar, "Beam steering architectures for next-generation cellular wireless applications," in *2018 IEEE MTT-S International Microwave and RF Conference (IMaRC).* IEEE, 2018, pp. 1–3. [Online]. Available: https://doi.org/10.1109/IMaRC.2018.8877180

[15] Q. Zeng, Z. Xue, W. Ren, W. Li, and S. Yang, "Beam-steering lens antenna using two transmit arrays at x-band," in *2019 IEEE Asia-Pacific Microwave Conference (APMC).* IEEE, 2019, pp. 1212–1213. [Online]. Available: https://doi.org/10.1109/APMC46564.2019.9038766

[16] A. Bansal and R. Gupta, "A review on microstrip patch antenna and feeding techniques," *International Journal of Information Technology*, vol. 12, pp. 149–154, 2020.

[17] H. K. Varshney, M. Kumar, A. Jaiswal, R. Saxena, and K. Jaiswal, "A survey on different feeding techniques of rectangular microstrip patch antenna," *International Journal of Current Engineering and Technology*, vol. 4, no. 3, pp. 1418–1423, 2014.

[18] M. Aikawa and H. Ogawa, "Double-sided mics and their applications," *IEEE transactions on microwave theory and techniques*, vol. 37, no. 2, pp. 406–413, 1989. [Online]. Available: https://doi.org/10.1109/22.20068

[19] M. Aikawa and E. Nishiyama, "Compact mic magic-t and the integration with planar array antenna," *IEICE transactions on electronics*, vol. 95, no. 10, pp. 1560–1565, 2012.

[20] S. K. Sharma, "Design and development of some novel phased arrays and anti-jamming antennas," in *2017 IEEE radio and antenna days of the Indian ocean (RADIO).* IEEE, 2017, pp. 1–1. [Online]. Available: https://doi.org/10.23919/RADIO.2017.8242260

[21] Y. A. Litinskaya, A. Nemshon, A. Stankovsky, S. Polenga, and Y. Salomatov, "Experimental research of the antenna array with electronic and combine electronic and mechanical beam steering," in *2016 International Siberian Conference on Control and Communications (SIBCON).* IEEE, 2016, pp. 1–3. [Online]. Available: https://doi.org/10.1109/SIBCON.2016.7491862

[22] S. Mine, E. Nishiyama, and M. Aikawa, "Study on beam controllable antenna by orthogonal excitation," in *Proc. 2006 International Symposium on Antenna and Propagation, Singapore*, 2006. [Online]. Available: https://doi.org/10.34385/proc.34.1E2a-3

[23] R. Pandhare, P. Zade, and M. Abegaonkar, "Beam-steering in microstrip patch antenna array using dgs based phase shifters at 5.2 ghz," in *2015 International Conference on Information Processing (ICIP).* IEEE, 2015, pp. 239–243. [Online]. Available: https://doi.org/10.1109/INFOP.2015.7489386

[24] J. Shen and L. W. Pearson, "A design for a two-dimensional coupled oscillator beam-steering antenna array," *IEEE antennas and wireless propagation letters*, vol. 2, pp. 360–362, 2003. [Online]. Available: https://doi.org/10.1109/LAWP.2003.822201

[25] M.-Y. Li and K. Chang, "Novel low-cost beam-steering techniques using microstrip patch antenna arrays fed by dielectric image lines," *IEEE Transactions on Antennas and Propagation*, vol. 47, no. 3, pp. 453–457, 1999. [Online]. Available: https://doi.org/10.1109/8.768779

[26] K. Chang, C. T. Rodenbeck, T.-Y. Yun, and M. Li, “Broadband low cost beam-steering techniques for wireless applications,” in *IEEE Antennas and Propagation Society International Symposium (IEEE Cat. No. 02CH37313)*, vol. 2. IEEE, 2002, pp. 496–499. [Online]. Available: https://doi.org/10.1109/APS.2002.1016130

[27] M. Jusoh, M. Jamlos, M. Kamarudin, M. Salimi, F. Malek, and M. Jais, “A beam steering patch array antenna for wimax application,” in *2013 7th European conference on antennas and propagation (EuCAP)*. IEEE, 2013, pp. 924–927. [Online]. Available: https://ieeexplore.ieee.org/document/6546417

[28] C. Liu, S. Xiao, Y.-X. Guo, M.-C. Tang, Y.-Y. Bai, and B.-Z. Wang, “Circularly polarized beam-steering antenna array with butler matrix network,” *IEEE Antennas and Wireless Propagation Letters*, vol. 10, pp. 1278–1281, 2011. [Online]. Available: https://doi.org/10.1109/LAWP.2011.2176903

[29] M. A. Hossain, A. H. Murshed, M. A. Rahman, E. Nishiyama, and I. Toyoda, “A novel dual-band slot-ring array antenna using both-sided mic technology for polarization detection,” *International Journal of RF and Microwave Computer-Aided Engineering*, p. e23373, 2022. [Online]. Available: https://doi.org/10.1002/mmce.23373

[30] J. Ehmouda, Z. Briqech, and A. Amer, “Steered microstrip phased array antennas,” *World Academy of Science, Engineering and Technology*, vol. 49, pp. 319–323, 2009.

[31] M. A. Rahman, Q. D. Hossain, M. A. Hossain, M. M. Haque, E. Nishiyama, and I. Toyoda, “Design of a dual circular polarization microstrip patch array antenna,” in *2014 9th International Forum on Strategic Technology (IFOST)*. IEEE, 2014, pp. 187–190. [Online]. Available: https://doi.org/10.1109/IFOST.2014.6991101

[32] J. G. Andrews, S. Buzzi, W. Choi, S. V. Hanly, A. Lozano, A. C. Soong, and J. C. Zhang, “What will 5g be?” *IEEE Journal on selected areas in communications*, vol. 32, no. 6, pp. 1065–1082, 2014. [Online]. Available: https://doi.org/10.1109/JSAC.2014.2328098

[33] M. F. Rafdzi, S. Y. Mohamad, A. A. Ruslan, N. F. A. Malek, M. R. Islam, and A. H. A. Hashim, “Study for microstrip patch antenna for 5g networks,” in *2020 IEEE Student Conference on Research and Development (SCOReD)*. IEEE, 2020, pp. 524–528. [Online]. Available: https://doi.org/10.1109/SCOReD50371.2020.9251037

[34] N. R. Draper and H. Smith, *Applied Regression Analysis*. John Wiley & Sons, 1998.

[35] A. E. Hoerl and R. W. Kennard, “Ridge regression: Biased estimation for nonorthogonal problems,” *Technometrics*, vol. 12, no. 1, pp. 55–67, 1970.

[36] R. Tibshirani, “Regression shrinkage and selection via the lasso,” *Journal of the Royal Statistical Society: Series B*, vol. 58, no. 1, pp. 267–288, 1996.

[37] L. Breiman, “Random forests,” *Machine Learning*, vol. 45, no. 1, pp. 5–32, 2001.

[38] L. Breiman *et al.*, *Classification and Regression Trees*. Wadsworth International Group, 1984.

[39] T. Chen and C. Guestrin, "Xgboost: A scalable tree boosting system," in *Proceedings of the 22nd ACM SIGKDD International Conference on Knowledge Discovery and Data Mining*, 2016, pp. 785–794.

[40] K. P. Murphy, *Machine Learning: A Probabilistic Perspective.* MIT press, 2012.

[41] C. E. Rasmussen and C. K. Williams, *Gaussian Processes for Machine Learning.* MIT press, 2006.

[42] J. Brownlee, "Regression metrics for machine learning," https://machinelearningmastery.com/regression-metrics-for-machine-learning, accessed: 2025-01-21.

[43] I. Ogunbiyi, "Top evaluation metrics for regression problems in machine learning," https://www.freecodecamp.org/news/evaluation-metrics-for-regression-problems-machine-learning, accessed: 2025-01-21.

[44] N. Developer, "A comprehensive overview of regression evaluation metrics," https://developer.nvidia.com/blog/a-comprehensive-overview-of-regression-evaluation-metrics, accessed: 2025-01-21.

[45] R. H. Byrd, P. Lu, J. Nocedal, and C. Zhu, "A limited memory algorithm for bound constrained optimization," *SIAM Journal on Scientific Computing*, vol. 16, no. 5, pp. 1190–1208, 1995.

[46] S. G. Nash, "Preconditioned conjugate-gradient methods for large-scale bound-constrained minimization," *SIAM Journal on Numerical Analysis*, vol. 19, no. 4, pp. 985–996, 1982.

[47] D. Kraft, "On the implementation of an algorithm for large-scale equality constrained optimization," *Numerical Analysis*, vol. 28, pp. 143–167, 1988.

[48] J. H. Holland, *Adaptation in natural and artificial systems: An introductory analysis with applications to biology, control, and artificial intelligence.* University of Michigan Press, 1975.

[49] S. Kirkpatrick, C. D. Gelatt, Jr, and M. P. Vecchi, "Optimization by simulated annealing," *Science*, vol. 220, no. 4598, pp. 671–680, 1983.

[50] D. K. Sudha, D. Akshaya, N. N. Reddy, and S. V. Yadagani, "Antenna performance prediction using machine learning algorithm," in *2024 5th International Conference for Emerging Technology (INCET).* IEEE, 2024, pp. 1–6.

[51] M. A. Haque, D. Saha, S. S. Al-Bawri, L. C. Paul, M. A. Rahman, F. Alshanketi, A. Alhazmi, A. H. Rambe, M. Zakariya, and S. S. B. Hashwan, "Machine learning-based technique for resonance and directivity prediction of umts lte band quasi yagi antenna," *Heliyon*, vol. 9, no. 9, 2023.

[52] M. A. Haque, M. Zakariya, S. S. Al-Bawri, Z. Yusoff, M. Islam, D. Saha, W. M. Abdulkawi, M. A. Rahman, and L. C. Paul, "Quasi-yagi antenna design for lte applications and prediction of gain and directivity using machine learning approaches," *Alexandria Engineering Journal*, vol. 80, pp. 383–396, 2023.

[53] M. A. Haque, M. A. Rahman, S. S. Al-Bawri, K. Aljaloud, N. S. S. Singh, D. Saha, E. E. Hussin, W. M. Abdulkawi, and M. Zakariya, “Machine learning-based approach for bandwidth and frequency prediction for n77 band 5g antenna,” *Physica Scripta*, vol. 99, no. 2, p. 026005, 2024.

[54] S. S. Al-Bawri, R. A. Ananta, M. A. Haque, W. M. Abdulkawi, N. Singh, M. A. K. Jilani, L. C. Paul, and K. Aljaloud, “Machine learning technique based highly efficient slotted 4-port mimo antenna using decoupling structure for sub-thz and thz 6g band applications,” *Optical and Quantum Electronics*, vol. 56, no. 10, pp. 1–25, 2024.

[55] M. A. Haque, M. S. Ahammed, R. A. Ananta, K. Aljaloud, N. M. Jizat, W. M. Abdulkawi, K. H. Nahin, and S. S. Al-Bawri, “Broadband high gain performance mimo antenna array for 5 g mm-wave applications-based gain prediction using machine learning approach,” *Alexandria Engineering Journal*, vol. 104, pp. 665–679, 2024.

[56] R. Jain, P. Ranjan, P. Singhal, and V. V. Thakare, “Estimation of s11 values of patch antenna using various machine learning models,” in *2022 IEEE Conference on Interdisciplinary Approaches in Technology and Management for Social Innovation (IATMSI).* IEEE, 2022, pp. 1–4.

[57] J. M. JOSHIBA and D. JUDSON, “An eye bolt shape slotted microstrip patch antenna design and return loss prediction using machine learning,” *Sādhanā*, vol. 49, no. 1, p. 77, 2024.

[58] R. Jain, V. V. Thakare, and P. K. Singhal, “Design and comparative analysis of thz antenna through machine learning for 6g connectivity,” *IEEE Latin America Transactions*, vol. 22, no. 2, pp. 82–91, 2024.

[59] S. A. Babale, T. K. Geok, S. K. A. Rahim, C. P. Liew, U. Musa, M. F. Hamza, Y. A. Bakhuraisa, and L. L. Lim, “Machine learning-based optimized 3g/lte/5g planar wideband antenna with tri-bands filtering notches,” *IEEE Access*, 2024.

[60] Y. Sharma, H. H. Zhang, and H. Xin, “Machine learning techniques for optimizing design of double t-shaped monopole antenna,” *IEEE Transactions on Antennas and Propagation*, vol. 68, no. 7, pp. 5658–5664, 2020.

[61] L. Ji, Y. Zhao, W. Li, H. Zhou, and D. Han, “A hybrid machine learning method for antenna optimization,” *International Conference on Microwave and Millimeter Wave Technology*, pp. 1–6, 2023.

[62] S. R. Shakya, M. Kube, and Z. Zhou, “A comparative analysis of machine learning approach for optimizing antenna design,” *International Journal of Microwave and Wireless Technologies*, vol. 15, pp. 1–11, 2023.

[63] C.-H. Huang, A. Ali, H.-H. Tsao *et al.*, “Antenna structure prediction and optimization based on machine learning and grid search,” *IEEE Transactions on Antennas and Propagation*, pp. 1–8, 2024.

[64] M. Devnath, P. Ranjan, and R. Chowdhury, “A dual-band millimeter wave cylindrical dielectric resonator antenna using machine learning approach,” *IEEE Transactions on Antennas and Propagation*, pp. 1–6, 2024.

[65] P. Kaushik, M. Kakkar, and M. Yadav, “Unveiling novel approaches: Machine learning optimization for circularly polarized antennas tailored for 5g communication,” *IEEE Transactions on Antennas and Propagation*, pp. 1–7, 2024.

[66] D. Kaushal and R. Chandel, “Inverse artificial neural network assisted rapid multiband antenna design for multiple custom requirements,” *Arabian Journal for Science and Engineering*, vol. 49, pp. 1–12, 2024.

[67] K. Egashira, E. Nishiyama, and M. Aikawa, “Planar array antenna using both-sided mic’s feeder circuits,” *Electronics and Communications in Japan (Part I: Communications)*, vol. 87, no. 7, pp. 23–30, 2004. [Online]. Available: https://doi.org/10.1002/ecja.10179

[68] I. Bahl and P. Bhartia, *Microstrip Antennas.* Artech House, 1980.

[69] D. M. Pozar, *Microwave Engineering.* Wiley, 2005.